From the Department of Microbiology, Tumor and Cell Biology
Karolinska Institutet, Stockholm, Sweden

TOWARDS PERSONALIZED IMMUNOTHERAPY: DEVELOPMENT OF *IN VITRO* MODELS FOR IMAGING NATURAL KILLER CELL BEHAVIOR IN THE TUMOR MICROENVIRONMENT

Valentina Carannante

Karolinska Institutet

Stockholm 2022

Published by Karolinska Institutet.
Printed by Universitetsservice US-AB, 2022

ISBN 978-91-8016-502-0
Cover illustration by Chiara Zambarda and Andreas Bodén

Towards personalized immunotherapy: development of *in vitro* models for imaging natural killer cell behavior in the tumor microenvironment

THESIS FOR DOCTORAL DEGREE (Ph.D.)

By

Valentina Carannante

The thesis will be defended in public at Inghesalen in Widerströmska huset, Tomtebodavägen 18 Solna
Friday, 18th of February 2022, at 09.00

Principal Supervisor:
Björn Önfelt
Karolinska Institutet
Department of Microbiology, Tumor and Cell Biology

Co-supervisor(s):
Martin Viklund
KTH-Royal Institute of Technology
Department of Applied Physics

Andreas Lundqvist
Karolinska Institutet
Department of Oncology-Pathology

Niklas Sandström
KTH-Royal Institute of Technology
Department of Applied Physics

Opponent:
Adelheid Cerwenka
Heidelberg University, Medical Faculty Mannheim
Department of Innate Immunoscience

Examination Board:
Marcus Buggert
Karolinska Institutet
Department of Medicine

Angela Santoni
Sapienza Università di Roma
Department of Molecular Medicine

Krister Wennerberg
University of Copenhagen
Biotech Research and Innovation Center

”Amiâ un pö pulìn!”

”Và scavà e vide ca truove guagliona!”

and to a generation that with its simplicity and authenticity inspired me curiosity, wonder, and perseverance

POPULAR SCIENCE SUMMARY OF THE THESIS

The term *tumor* comes from Latin, and it means *swelling*. Our ancestors used it to describe the main macroscopic feature of this condition, which is abnormal tissue growth. Tumors can be benign or malignant. Benign tumors are confined and encapsulated in the original site of the body, and they do not represent a particular treat to our health. On the other hand, malignant tumors have self-renewal and invasive capacity, meaning that they keep growing and they can migrate into different tissues, drastically interfering with their physiological functions. Attempting to create their own nutrient supply system, malignant tumors can be highly vascularized. This feature probably inspired Hippocrates while naming them *καρκίνοι*, the Greek word for *crabs*. *Καρκίνος* then became *cancer*, the Latin word still used nowadays for malignant tumors.

Reports on how to cure cancers came long before Hippocrates, dating back to the Ancient Egypt. But it is not until late 19th and early 20th century that scientists started developing successful treatments. The discovery of radioactivity in late 19th century led to the rapid development of radiotherapy. Chemotherapy was the result of an intense research on the biological effects of chemical weapons used during the World War II. Surgical removal, radiotherapy and chemotherapy represents the traditional cancer treatments. However, already in the late 19th century some surgeons and scientists suspected that our own body might have the resources to fight tumor cells on its own, if properly stimulated. This set of resources goes under the name of immune system. Tremendous advances in the last fifty years in the field of immunology confirmed this hypothesis, and so-called *immunotherapy* is quickly replacing traditional cancer therapies nowadays.

The immune system is composed of distinct sentinel cells that patrol our body, eliminating pathogens (bacteria, viruses, etc.) and damaged tissues. Those sentinels are called *immune cells*, and they are also very efficient in recognizing, following and killing malignant cells that continuously arise in our body, limiting their potential to grow and invade other tissues. Cytotoxic T cells and Natural Killer (NK) cells are the front line in tumor recognition and killing. Cytotoxic T cells are immune cells extremely efficient in eliminating tumor cells, but they might require some time to be fully operative. On the other hand, it can take less than five minutes for an NK cell to kill a tumor cell. Their name in fact derives from their extremely fast tumor killing.

Aging and environmental factors can negatively affect the immune system. If that happens, the likelihood of tumor cells to escape the immune cell control becomes high, and malignant tumor might develop. During the tumor progression, Darwinian selective pressure favors

the development of tumor cell clones resistant to immune cell recognition. This process is called *immune evasion*. In this scenario, malignant cells create a self-protective fortress, referred to as *tumor microenvironment*, that promotes their self-renewal and growth while suppressing cytotoxic T cell and NK cell infiltration and activation. Reverting this scenario is the main goal of immunotherapy, restoring immune cell anti-tumoral activity and proliferative capacity.

Immunotherapy is nowadays considered a robust clinical approach to treat cancer, inducing durable responses and less long-term side effects compared to radiotherapy and chemotherapy. However, although some cancer patients respond very well to immunotherapy, some others do not respond at all. Today's challenge for immunotherapy is to understand the causes of patient's heterogeneity and design new therapeutic strategies to target them. Our ability to predict patient resistance and design new treatments relies on robust models that recapitulate the disease *in vitro*. Once we have those, we could test the susceptibility of specific tumors to drugs before delivering them to patients. At the same time, those models could be used to design new therapies tailored on the patient characteristics. This medical approach goes under the name of precision medicine.

Developing such models in the main aim of this thesis. We designed new methods to obtain miniaturized 3-dimensional models of solid tumors *in vitro*, using ultrasonic standing waves in a microwell chip. Ultrasonic standing waves induce cell-to-cell aggregation, favoring the formation of 3-dimensional tumor cultures, also called tumor spheroids. The microwell chip provides a platform to visualize the details of biological processes within the spheroids. We used the method to investigate NK cell suppression in tumor spheroids, and to test strategies to overcome it.

Our platforms provided new biological findings. We built up a model of NK cell recognition of Poliovirus receptor (PVR), a protein expressed in many cancer cells. PVR can induce both NK activation and inhibition, but, according to our model, its role is primarily inhibitory. This finding opened the possibility of testing multiple strategies to block PVR-NK interaction to enhance NK cell anti-tumoral activity. We demonstrated the success of the strategy in renal carcinoma spheroid models and patient-derived sarcoma spheroid models.

The work presented herein comprises the initial studies and proofs of concepts for what we envision can become a pipeline to be routinely used as a complementary tool to test therapeutic strategies in the hospitals, and to study the mechanisms of tumor progression in a research context. We believe that our method provides a solid basis towards imaging-based precision medicine for cancer patients.

SAMMANFATTNING

Ordet *tumör* kommer från latin och betyder svullnad. Våra förfäder använde det för att beskriva det huvudsakliga makroskopiska kännetecknet för detta tillstånd, nämligen onormal vävnadstillväxt. Tumörer kan vara godartade eller elakartade. Godartade tumörer är ofta inkapslade, sprider sig inte från dess ursprungliga läge och utgör inte något direkt hot mot vår hälsa. Elakartade tumörer å andra sidan kan tränga in i andra vävnader och drastiskt påverka dess fysiologiska funktion. I försök att skapa sitt eget system för näringstillförsel kan elakartade tumörer vara kraftigt vaskulariserade. Detta kännetecken inspirerade förmodligen Hippocrates när kan myntade uttrycket *καρκίνοι*, grekiska för kräfta. *Καρκίνος* blev sedan *cancer*, det latinska ordet för kräfta som än idag används för elakartade tumörer.

Rapporter om hur man botar cancer kom långt innan Hippocrates, daterade tillbaka så långt som till forntida Egypten. Men det är inte förrän sent 1800-tal och tidigt 1900-tal som forskare lyckas börja utveckla framgångsrika behandlingar. Upptäckten av radioaktivitet under sent 1800-tal ledde till en snabb utveckling av strålbehandling. Behandling med cellgifter uppstod till följd av intensiv forskning på de biologiska effekterna av kemiska vapen som användes under andra världskriget. Kirurgiskt avlägsnande, cellgifts- och strålbehandling utgör de traditionella behandlingsmetoderna för cancer. Redan på 1800-talet misstänkte dock några kirurger att vår egen kropp kan ha resurser att bekämpa cancer själv, om rätt stimulans ges. Systemet som huserar dessa resurser kallas immunförsvar. De stora framsteg som gjorts de senaste femtio åren inom immunologi bekräftar denna hypotes och så kallad *immunoterapi* ersätter nu snabbt de traditionella behandlingsmetoderna för cancer.

Immunförsvaret består av distinkta sentinelceller som patrullerar vår kropp och rensar bort patogener och skadad vävnad. Immunceller är också mycket skickliga på att känna igen, följa efter och döda de elakartade celler som kontinuerligt uppstår i vår kropp. På så sätt elimineras deras möjlighet att växa och invadera annan vävnad. Cytotoxiska T-lymfocyter och naturliga mördarceller (NK-celler efter engelskans *Natural Killer Cells*) utgör frontlinjen för immunförsvarets system för tumörigenkänning och eliminering. Cytotoxiska T-lymfocyter är immunceller som är extremt effektiva när det kommer till att eliminera tumörceller, men de kan behöva lite tid på sig för att bli fullt operativa. NK-celler kan å andra sidan döda en tumörcell på mindre än fem minuter. Faktum är att deras namn uppstod då man observerade denna extremt snabba antitumorala aktivitet.

Åldrande och miljöfaktorer kan påverka immunsystemet och minska dess antitumorala aktivitet. Om detta händer ökar sannolikheten för att tumörceller undgår immunsystemets

celler och således att tumörer kan uppstå. Under tiden som tumörer växer utsätts cellpopulationen för Darwinistiskt selektionstryck vilket gynnar cellkloner som kan undgå immunförsvarets igenkänningsmekanismer. Denna process kallas *immunflykt*. I detta scenario skapar elakartade celler ett beskyddande fort, kallat *tumörmikromiljö*, som främjar deras självförnyelse och tillväxt samtidigt som det hindrar infiltrationen och aktiveringen av Cytotoxiska T-lymfocyter och NK-celler i tumörens kärna. Att motverka denna process är det huvudsakliga målet med immunterapi och därigenom återställa immuncellernas antitumorala aktivitet och deras kapacitet att proliferera.

Immunterapi anses idag vara en robust klinisk behandlingsform som ger långvarig effekt och mindre bieffekter jämfört med strålbehandling och cellgifter. Men trots att många cancerpatienter svarar mycket bra på immunterapi, finns också de som inte svarar alls. Dagens utmaning för immunologiforskare är att förstå orsakerna till heterogeniteten hos patienter och utveckla strategier för att adressera dessa. Vår förmåga att förutspå patientsvar och utveckla nya behandlingsmetoder är beroende av robusta modeller som återskapar sjukdomen *in vitro*. Med sådana modeller kan vi testa effekten av behandlingar på specifika tumörer innan läkemedlet administreras till patienten. Detta medicinska tillvägagångssätt kallas *precisionsmedicin*.

Att utveckla sådana modeller är huvudsyftet med denna avhandling. Vi designade nya metoder för att erhålla miniatyriserade tredimensionella modeller av solida tumörer *in vitro*, med hjälp av stående ultraljudsvågor i ett mikrobrunnschip. Stående ultraljudsvågor inducerar cell-cell-aggregation, vilket gynnar bildandet av tredimensionella tumörkulturer, även kallade tumörsfäroider. Mikrobrunnschippet ger en plattform för att visualisera detaljerna i biologiska processer inom sfäroiderna. Vi använde metoden för att undersöka NK-cellsuppression i tumörsfäroider och för att testa strategier för att övervinna den. Våra plattformar gav nya biologiska fynd och insikter. Vi formulerade en modell för hur NK-celler känner av Poliovirusreceptor (PVR), ett protein som uttrycks av många cancerceller. PVR kan inducera både NK-aktivering och hämning, men enligt vår modell är dess roll i första hand hämmande. Detta fynd öppnade upp möjligheten att testa flera strategier för att blockera PVR-NK-interaktion med syftet att förbättra NK-cellernas antitumöraktivitet. Vi visade framgångsrikt strategin i sfäroidmodeller bestående av njurkarcinom samt i sarkom från patienter.

Arbetet som presenteras häri innefattar inledande studier samt konceptvalidering av vad vi tror kan bli en rutinmässigt använd kompletterande strategi för att testa behandlingsmetoder på sjukhus, och för att studera mekanismer kopplade till tumörprogression i forskningssammanhang. Vi tror att vår metod utgör en robust grund för framtida bildbaserad precisionsmedicin för cancerpatienter.

RIASSUNTO DIVULGATIVO DELLA TESI

La parola *tumore* deriva dal termine Latino *tumor*, il cui significato é *gonfiore*. Tale rigonfiamento é infatti una delle caratteristiche macroscopiche piú evidenti di questa malattia, dovuto ad una crescita anomala dei tessuti. I tumori vengono distinti in maligni e benigni. I tumori benigni sono confinati nel tessuto di origine, spesso mantenuti all'interno di una sorta di capsula tissutale che ne impedisce la migrazione in altri tessuti, nonché la loro ulteriore crescita. Date queste caratteristiche, i tumori benigni non rappresentano una particolare minaccia per la salute della persona. Diversa, invece, é la situazione nel caso di tumori maligni. I tumori maligni hanno capacitá invasiva, ovvero possono migrare in tessuti diversi da quello di origine, e proliferativa, ovvero non cessano di crescere, interferendo cosí con le funzioni fisiologiche del nostro organismo. Alcuni tumori maligni tendono a creasi un proprio rudimentale sistema vascolare per rifornirsi di nutrienti. Fu probabilmente la presenza di questi vasi sanguigni e l'aspetto del tessuto ad indurre il medico Greco Ippocrate a chiamarli *καρκίνοι*, ovvero *granchi*. *Καρκίνος* fu poi tradotto nel Latino *cancer*, e *cancro* é tuttora uno dei termini usati per indicare i tumori maligni.

Le prime descrizioni di cure contro il cancro datano fino all'Antico Egitto. Tuttavia, i primi veri successi terapeutici arrivarono solo verso la fine del 1800 e gli inizi del 1900. La scoperta della radioattivitá a fine 1800 portó al rapido sviluppo della radioterapia. La chemioterapia naque invece a seguito di un'intensa ricerca sugli effetti biologici delle armi chimiche usate durante la Seconda Guerra Mondiale. La chirugia, la radioterapia e la chemioterapia costituiscono i trattamenti traditionali contro il cancro. Tuttavia, giá a fine 1800 alcuni medici e scienziati iniziarono ad ipotizzare la presenza di risorse nel nostro organismo che, se correttamente stimolate, possono costituire una cura contro i tumori. L'insieme di queste risorse prende il nome di "sistema immunitario". Numerose scoperte, frutto di un'intensa ricerca negli ultimi cinquant'anni in questo campo, hanno confermato questa teoria. Ad oggi, l'*immunotherapia*, ovvero l'insieme di trattamenti basati sulla capacitá del sistema immunitario di riconoscere e combattere i tumori, sostituisce o accompagna le terapie tradizionali.

Il sistema immunitario é costituito da diverse cellule sentinella che controllano il nostro corpo, eliminando agenti patogeni (batteri, virus) e tessuti danneggiati. Le cellule del sistema immunitario hanno anche la funzione di riconoscere cellule che vanno incontro a trasfomazione tumorale. Una volta riconosciute, le eliminano, limitandone il potenziale pericolo per la nostra solute. I linfociti T citotossici e le cellule Natural Killer (NK) sono la nostra principale linea difensiva contro i tumori. I linfociti citotossici T sono molto

efficienti, ma richiedono del tempo prima di diventare 100% operativi, a differenza delle cellule NK che possono impiegare meno di cinque minuti ad uccidere una cellula tumorale.

L'etá avanzata e diversi fattori ambientali possono avere un impatto negativo sul sistema immunitario. Quando questo accade, le probabilitá che una cellula tumorale sfugga al controllo del sistema immunitario aumentano, portando allo sviluppo di tumori maligni. Durante la progressione della malattia, il processo di selezione naturale darwiniana favorisce lo sviluppo di cellule tumorali sempre piú resistenti al sistema immunitario, limitandone ancor piú gli effetti. Questo processo viene definito *evasione della risposta immunitaria*.

Revertire questa sistuazione é lo scopo principale dell'immunotherapia, che si pone come obbiettivo quello di ripristinare l'attivitá anti-tumorale del sistema immunitario. Tra i maggiori effetti positivi di questa terapia vi sono una risposta prolungata nel tempo e una riduzione degli effetti collaterali rispetto alle terapie tradizionali. Purtroppo la risposta al trattamento non é uguale per tutti i pazienti. Alcuni pazienti sviluppano un'ottima risposta, in altri invece terapia non ha effetti. La vera sfida della ricerca in questo settore é capire quali mecchanismi siano alla base di queste differenze tra pazienti. Una volta scoperti i meccanismi, é possibile sviluppare terapie mirate per ciascun paziente.

La possibilitá di studiare e di predirre la risposta alle cure del pazienti si fonda sulla capacitá stessa di riprodurre la malattia *in vitro*, ovvero con metodi di laboratorio. Quando questi metodi sono a disposizione, é possibile allora studiare la risposta alle cure prima ancora che la terapia venga introdotta, e sviluppare di terapie adatte a sottogruppi di pazienti. Questo approccio viene definito "medicina di precisione".

Sviluppare questi metodi é il tema principale di questa tesi. In particolare, il nostro lavoro é incentrato sullo sviluppo di piattaforme innovative per ottenere modelli tridimensionali miniaturizzati di tumori *in vitro*, e studiarne la risposta ai trattamenti immunoterapici attraverso tecniche di microscopia. I metodi sviluppati hanno contribuito a chiarire i meccanismi di riconoscimento delle cellule NK di una proteina, chiamata Poliovirus receptor (PVR). PVR é presente in molti tumori, e puó indurre sia l'attivazione che l'inibizione della risposta NK. Tuttavia, secondo i nostri studi, il ruolo di PVR é prevalentemente inibitorio. Abbiamo testato strategie per ridurre l'attivitá inibitoria di PVR, ottenendo un miglioramento dell'attivitá anti-tumorale delle cellule NK.

Lo svilippo di queste piattaforme é solo al suo inizio. La nostra visione é continuare a implementare i nostri metodi, per poterli in futuro utilizzare come strumenti per testare trattemenți negli ospedali, e per studiare meccanismi biologici nei laboratori. In

conclusione, crediamo che la nostra ricerca ponga delle solide basi verso lo sviluppo di una medicina di precisione basata su tecniche di microscopia per la cura dei tumori.

ABSTRACT

Tremendous advances in the tumor immunology field have transformed immunotherapy from a promising approach to a standard clinical practice. However, a subset of cancer patients is non-responsive to immunotherapy. More research is therefore needed to understand the mechanisms underlying tumor resistance to immunotherapeutic treatments. The aim of this doctoral work was to develop new tools to study the mechanisms of cancer immunosurveillance and to test immunotherapeutic treatments *in vitro*. In this thesis, I describe the methods developed, and I discuss the main biological findings obtained by using these methods.

The thesis is organized as follows. A short historical background of immunotherapy is provided in **Chapter 1**. **Chapter 2** describes the principles of NK cell-mediated cancer immunosurveillance, and provides an overview on rare cancers, mainly focusing on sarcoma. The research aims are listed in **Chapter 3**. In **Chapter 4**, I describe the cell culture methods and cell analysis techniques relevant for my doctoral work. In **Chapter 5**, I describe the methods we developed to culture tumor spheroids *in vitro* using ultrasonic standing waves in microwell chips, focusing on the theory, design, and applications. **Chapter 6** and **Chapter 7** focus on the biological findings obtained using our platform in combination with traditional immunological methods, followed by future implementations discussed in **Chapter 8**. The constituent papers are provided at the end of the thesis.

In **Paper I**, we combined the use of the microwell chip, ultrasonic standing waves and a protein-repellent polymer coating to enable the production of spheroids from multiple cell types. In absence of cell adhesion to the chip, spheroids could be collected and further analyzed by off-the-chip techniques.

In **Paper II**, we designed a novel multichambered microwell chip to perform multiplexed fluorescence screening of two- or three-dimensional cell cultures. The platform allows the direct assessment of drug or immune cell cytotoxic efficacy, making it a promising tool for individualized cytotoxicity tests for personalized medicine.

In **Paper III**, we investigate the function of PVR receptors in NK cells interacting with renal carcinoma spheroids, and the impact of PVR in NK cell-based cellular immunotherapy. We demonstrated that variations in PVR expression are primarily recognized by the inhibitory receptor TIGIT, while DNAM-1 strongly contributes to NK cell activation mainly through PVR-independent mechanisms. We performed NK cell-based cytotoxicity assays against renal carcinoma spheroids in the microwell chip. Anti-TIGIT treatment was effective only for $TIGIT^{high}$ NK cells both when used as

monotherapy or in combination with other drugs, suggesting that only a fraction of patients might respond to anti-TIGIT therapy.

In **Paper IV**, a similar approach was used with primary sarcomas. We cultured patient-derived sarcoma spheroids and tested NK cell-based immunotherapy in the microwell chip, either alone or in combination with antibody therapy, and we identified promising treatment combinations.

In **Paper V**, we applied the use of expansion microscopy to visualize NK cells infiltrating renal carcinoma spheroids. In conclusion, our multi-disciplinary work shows the development of new imaging-based platform and its use to study the mechanisms of NK cell-mediated tumor surveillance and for personalized therapy.

LIST OF SCIENTIFIC PAPERS

I. K. Olofsson, **V. Carannante**, M. Ohlin, T. Frisk, K. Kushiro, M. Takai, A. Lundqvist, B. Önfelt and M. Wiklund. "Acoustic formation of multicellular tumor spheroids enabling on-chip functional and structural imaging", *Lab on a Chip*, 18, 2466-2476, (2018)

II. N. Sandström*, **V. Carannante***, K. Olofsson, P. A. Sandoz, E. Moussaud-Lamodière, B. Seashore-Ludlow, H. Van Ooijen, Q. Verron, T. Frisk, M. Takai, M. Wiklund, P. Östling and B. Önfelt. "Miniaturized and multiplexed high-content screening of drug and immune sensitivity in a novel multichambered microwell chip", *manuscript under revision*

III. **V. Carannante**, K. Olofsson, N. Sandström, A. Kathleen Wagner, P. Sandoz, J. Fontana, D. Toullec, G. Turyasingura, B. Hell, H. Van Ooijen, A. Lundqvist, M. Wiklund, B. Önfelt. "TIGIT dominates NK cell recognition of PVR-levels on tumor cells leading to donor dependent responses to checkpoint blockade", *manuscript under submission*

IV. **V. Carannante**, S.Y. Neo, K Olofsson, L. Sanchez-Rivera, J. Fontana, D. Toullec, N. Sandström, N. Dziedzic, M. Wiklund, F. Haglund, A. Lunqvist, B. Önfelt." Evaluation of combinatorial treatments boosting natural killer cell cytotoxicity against patient-derived sarcoma spheroids", *manuscript*

V. S.J. Edwards, **V. Carannante**, K. Kuhnigk, H. Ring,T. Tararuk, F. Hallböök, H. Blom, B. Önfelt and H. Brismar. "High-resolution imaging of tumor spheroids and organoids enabled by expansion Microscopy", Frontiers in Molecular Bioscience, 7, 2020

**both authors contributed equally*

SCIENTIFIC PAPERS NOT INCLUDED IN THE THESIS

I. E. Fogelqvist, M. Kördel, **V. Carannante**, B. Önfelt and H. Hertz. ”Laboratory cryo x-ray microscopy for 3D cell imaging”. *Scientific Reports* **7**, 13433 (2017)

II. A. K. Wagner, U. Gehrmann, S. Hiltbrunne, **V. Carannante**, T. T. Luu TT, T. I. Näslund, et al. ”Soluble and exosome-bound α-galactosylceramide mediate preferential proliferation of educated NK cells with increased anti-tumor capacity”. *Cancers* . 2021;13(2).

III. K. Olofsson, **V. Carannante**, M. Takai, B. Önfelt, M. Wiklund. ”Ultrasound-based ccaffold-free core-shell multicellular tumor spheroid formation. Vol. 12, Micromachines . 2021.

IV. K. Olofsson, **V. Carannante**, M. Takai, B. Önfelt, M. Wiklund. ”Single cell organization and cell cycle characterization of DNA stained multicellular tumor spheroids”. Scientific Reports. 2021;11(1):17076.

CONTENTS

LIST OF ABBREVIATIONS

2D	2-dimensional
3D	3-dimensional
ADCC	Antibody-depended cellular cytotoxicity
ALL	Acute lymphoblastoid leukemia
AML	Acute myeloid leukemia
APC	Antigen presenting cells
ATM	Ataxia-telangiectasia mutated protein
ATR	Ataxia-telangiectasia and Rad3-related protein
AU	Arbitrary unit
CCD	Charge-coupled devices
CCL	C-C motif chemokine ligand
CD	Cluster of differentiation
CMOS	Complementary metal oxide semiconductors
CTL	Cytotoxic T lymphocyte
CTLA-4	Cytotoxic T lymphocyte associated protein 4
CXCL	C-X-C motif chemokine ligand
CXCR	C-X-C chemokine receptor
DAMP	Damage-associated molecular patterns
DC	Dendritic cell
DNAM-1	DNAX accessory molecule 1
ECM	Extracellular matrix
EGF	Epidermal growth factor
EGFR	Epidermal growth factor receptor
ER	Endoplasmatic reticulum
FasL	Fas ligand

FBS	Fetal bovine serum
FDA	Food and Drug Administration
FCS	Fetal calf serum
G-CSF	Granulocyte colony-stimulating factor
GEMM	Genetically engineered mouse models
GFP	Green fluorescent protein
GIST	Gastrointestinal stromal tumors
GM-CSF	Granulocyte macrophage colony-stimulating factor
HCMV	Human cytomegalovirus
HLA	Human leucocyte antigen
HSC	Hepatic stellate cells
ICI	Immune checkpoint inhibitor
IDO	Indoleamine-2,3-dioxygenase
Ig	Immunoglobin
IL	Interleukin
INF-ɣ	Interferon ɣ
IP-10	Interferon ɣ-inducible protein 10
ITP	Idiopathic thrombocytopenic purpura
KIR	Killer cell immunoglobulin-like receptor
KO	Knock-out
LAD	Leukocytes adhesion deficiency
LAG3	Lymphocyte-activation gene 3
LED	Light-emitting diodes
LFA-1	Lymphocyte function-associated antigen 1
MPNST	Malignant peripheral nerve sheath
MSI	Microsatellite instability

NA	Numerical aperture
NCRs	Natural cytotoxicity receptors
Necl	Nectin-like protein
NK	Natural killer
NSCLC	Non-small cell lung cancer
PD-1	Programmed cell death protein 1
PD-L1	Programmed death ligand 1
PDGF	Platelet-derived growth factor
PDGFR	Platelet-derived growth factor receptor
PDMS	Polydimethylsiloxane
PDX	Patient-derived tumor xenografts
PGE2	Prostaglandin E2
PKC	Protein kinase C
PSF	Point spread function
PTM	Photomultiplier
PVR	Poliovirus receptor
RFP	Red fluorescent protein
RI	Refractive index
SDF-1α	Stromal cell-derived factor-1 α
siRNA	Small interfering RNA
SNP	Single nucleotide polymorphism
TA	Tumor antigen
TACTILE	T cell activation increased late expression
TCR	T cell receptor
TGF-β	Transforming growth factor β
TIGIT	T cell immunoglobulin and ITIM domain

Tim-3	T cell immunoglobulin and mucin-domain containing-3
TliSA	T lineage-specific activation antigen
TMB	Tumor mutational burden
TMRM	Tetramethylrhodamine methyl ester
TNF-α	Tumor necrosis factor α
UPS	Undifferentiated pleiomorphic sarcoma
USW	Ultrasonic standing waves
VEGF	Vascular endothelial growth factor
WHO	World Health Organization
WUCAM	Washington University cell adhesion molecule
WT	Wild-type
β2-m	β2-Microglobulin

1 AN OVERVIEW OF CANCER IMMUNOLOGY

Cancer is the second leading cause of death worldwide, accounting for approximately 10 million deaths in 2020[1,2]. The disease arises from a gradual accumulation of DNA mutations, that leads to uncontrolled cell proliferation and aberrant tissue growth. Eventually, cancer cells leave the tissue of origin and spread to other organs, a process referred to as "metastasizing"[3]. According to the World Health Organization report, one third of cancer deaths are caused by behavioral and dietary factors[4]. Those include tobacco and alcohol use, low intake of fruits and vegetables, high body weight and scarce physical activity. The other two thirds of cancer deaths are due to cancerogenic substances and radiations exposure, hormones, infectious agents, chronic inflammation, immune suppression, and aging[4,5]. All these factors indirectly impair the immune system, or are directly related to its dysfunction. The immune system is a complex network of tissue-resident and circulating immune cells, signaling molecules and physical barriers aimed to protect our body from danger. The immune system is also a key mediator of tissue development and regeneration. Immune cells play a major role in cancer surveillance, as they can eliminate malignant cells that continuously arise in our body[6,7]. This notion constitutes the rationale of cancer immunotherapy, defined as a large set of therapeutical strategies aimed at using or improving the immune cell activity against tumors.

1.1 THE ORIGIN OF CANCER IMMUNOTHERAPY

The origin of cancer immunotherapy can be traced back to 1891, with the publication of "Contribution to the knowledge of sarcoma" by William B. Coley [8]. W. B. Coley was a medical surgeon in the Bone Sarcoma Unit at the Memorial Hospital in New York[9]. At that time, he was facing the enormous difficulties of treating sarcomas, heterogeneous family of bone and soft-tissue cancers still today characterized by very poor prognosis[10].

He himself wrote about sarcoma: "*The large proportion of cases in which fatal and often speedy recurrence follows operation, is sufficient to make the surgeon almost lose faith in his art in the treatment of this dread disease. There are certain types of sarcoma that seem almost hopeless from the start, and when surgical skill, if called upon, only proves how utterly powerless it is. Is there nothing else that can be done to stay the progress of this disease?"*[8].

To find the answer, he collected and studied the clinical history of 44 sarcoma patients, from both published and unpublished cases. He found multiple reports of spontaneous tumor regression, and even complete recovery, in cancer patients that have undergone *erysipelas*[11–

[13]. "*Erysipelas"* is the old definition of the *Streptococcus pyogenes* skin infection[8], and its etiology[12] was discovered just couples of years before W. B. Coley's work. W. B. Coley made the conclusion that a bacterial infection could somehow cure the cancer in some patients.

"Nature often gives us hints to her profoundest secrets, and it is possible that she has given us a hint which, if we will but follow, may lead us on to the solution of this difficult problem". To follow the lead, W. B. Coley injected a mixture of *Streptococcus pyogenes* into two sarcoma patients, obtaining tumor shrinkage[8]. Later, he refined the composition of the inoculation, combining heat-inactivated *Streptococcus pyogenes* with *Serratia marcescens*[14], a mixture known as "Coley's toxins". He treated approximately 1000 patients with inoperable malignant tumors with Coley's toxins, achieving complete remission in 10% of the patients[9].

At that time, W. B. Coley was not aware of the mechanisms of action of the Coley's toxins. He hypothesized that: 1) the bacteria could have a "*direct destructive action*" on the tumor, 2) fever induced by the infection could have a direct impact on tumor cell viability, 3) sarcoma could have a bacterial origin, therefore the combination of *Streptococcus pyogenes* with *Serratia marcescens* could antagonize the proliferation of the bacteria responsible for the tumor growth. Today, we know that those responses were the results of the ongoing infection, which caused inflammation and boosted the immune system of the patients, leading to the immune-mediated tumor "rejection".

Despite the promising results, Coley's treatment faced resistance within the scientific community at the time. The main reasons for such resistance were the risk of causing serious infections in patients and the lack of mechanisms of action, combined with poorly documented patient follow-ups, inconsistent methods of administration and batch-to-batch variation in the Coley's toxin composition[9].

Other factors also contributed to deflect the attention from Coley's results. In 1895, Wilhelm C. Röntgen published the discovery of X-rays[15], which just few months later were applied as medical treatment by Emil H. Grubbé[16,17]. Between 1899 and 1901, Friedrich Giesel, Henri Becquerel, Pierre and Marie Curie reported the necrotic effects of radiation[18–22], reinforcing the idea of their use in cancer treatment. Cancer radiotherapy quickly gained enthusiasm among physicians. Therefore, skepticism towards Coley's practice together with the advent of radiotherapy quickly buried Coley's legacy, as well as research into the mechanisms behind the patient's response to Coley's toxin.

Lloyd J.Old and colleagues tried an approach similar to Coley's in 1959. They injected the Bacillus Calmette-Guérin[23], also known as the tuberculosis vaccine, in mice challenged with

tumors. They observed 70-75% of tumor regression compared to non-inoculated mice[24]. Following this experiment, many physicians started treating multiple cancers with tuberculosis vaccine between 1973-1976[25–29]. Tuberculosis vaccine is still used today for the treatment of non-muscle invasive bladder cancer.

At that time, more knowledge was available compared to Coley's days. Physicians and scientists were aware that our own body defenses could be involved in the tumor regression in response to Bacillus Calmette-Guérin injection. But the mechanisms and the cells involved were still unknown. In fact, Paul Ehrlich, German physician and Nobel prize-winner in 1908, proposed the idea that the immune system could be involved in the control of carcinomas in 1909[30,31]. In 1915, James B. Murphy and John, J. Morton hypothesized the presence of "natural" and "induced lymphocytes" that could target tumor cells and therefore could be a "necessary factor in cancer immunity"[32]. Still, it took almost forty years before the theory of immunological control of tumors could be firmly reproposed.

Frank M. Burnet, Australian virologist and Nobel prize winner in 1960, was one of the main supporters of this theory. He wrote in 1954: "A slightly more hopeful [therapeutic] approach, which, however, is so dependent on the body's own resources that it has never been seriously propounded, is the immunological one. […] It is by no means inconceivable that small accumulations of tumor cells may develop and because of their possession of new antigenic potentialities provoke an effective immunological reaction, with regression of the tumor and no clinical hint of its existence"[33].

In the 1950s, great advances in the study of hypersensitivity and graft rejections (transplantation) boosted the immunological research, providing new ideas that eventually became the Thomas and Burnet's theory of immunological surveillance. In fact, inspired by Lewis Thomas hypothesis on the role of cellular immunity in early sensing and eliminating neoplastic cells, F. M Burnet presented the theory of immunological surveillance in his work "Immunological surveillance of neoplasia" in 1971[34,35]. According to the theory, the majority of tumor transformed cells presented some characteristics, or "antigens", that made them different from the normal cells they derive from; those antigens could be recognized as "non-self" by thymus-dependent lymphocytes (T cells), which would therefore mediate an immune response against tumors under appropriate conditions[34].

F. M. Burnet and L. Thomas's theory had multiple clinical evidence[34,35]. First, higher incidence of tumors was observed in pediatric and geriatric individuals, where the immune system is generally less efficient compared to other age-categories. Second, the development of cancers was frequent in patients affected by immunodeficiency or treated with immunosuppressive drugs, for instance following heart and kidney transplantation.

Last, the literature supported the involvement of the immune system in the spontaneous tumor regression[34,35].

This theory became even more accepted with the discovery of cytotoxic T cells[36,37] and natural killer (NK) cells[38,39], the two immune cell subsets involved in the control of tumor. In fact, both cytotoxic T cells and NK cells can eliminate tumor cells. Together, the discovery of the role of cytokines in promoting immune response against tumors[40–43] led up to the standard use of immunomodulators for the therapy of some cancer types, such as melanoma and renal cell carcinoma.

These discoveries set the foundations of the modern cancer immunotherapy. For the past 30 years, deciphering the mechanisms of cancer immunological surveillance has been one of the main priorities of immunologists. The effort led up to the Nobel prize winning discovery of the immune checkpoint inhibitors by Tasuku Honjo and James P. Allison[44,45]. Immune checkpoints are "molecular brakes" that turn off the immune cell functions, including their anti-tumoral activity. Using immune checkpoint inhibitors, those brakes are removed, and immune cells can keep fighting against tumor cells. Immune checkpoint inhibitors revolutionized the practice of tumor treatment, and immunotherapy is now the primary therapy for multiple cancer types[46].

T. Honjo and J. P. Allison were awarded the Nobel prize in 2018, 127 years after the publication of "Contribution to the knowledge of sarcoma" by W. B. Coley. During the years, W. B. Coley's work has been revaluated and he is today recognized as the "Father of Immunotherapy". In 1982, L. Thomas wrote: "*what would happen if you were to remove the putative defence mechanism of cellular immunity in human beings? Would this affect either the incidence or clinical course of cancer?*". Now, we know that the answer is yes. The mechanisms behind the tumor immune surveillance will be described in details in the next chapters.

2 INTRODUCTION

2.1 PRINCIPLES OF IMMUNE CELL RECOGNITION OF CANCER

Cancer immunosurveillance is orchestrated by the combined action of innate and adaptive immunity. Innate immunity constitutes the first line of defense, acting within a few minutes from the recognition of dangerous signals. Innate immune cells sense danger in the form of damage-associated molecular patterns (DAMPs) and stress-induced ligands. Those are usually present in the tumor microenvironment. Natural Killer cells (NK), macrophages, dendritic cells (DCs), neutrophils, eosinophils, basophils, mast cells and innate lymphoid cells are typical examples of innate immune cells. Once activated, innate immune cells rapidly kill and phagocyte tumor cells[47]. Phagocytosis is mainly performed by macrophages and dendritic cells, also called "antigen-presenting cells" (APCs). APCs display tumor antigens on the surface through HLA class I and HLA class II molecules. The antigen presentation is a key step for bringing adaptive immunity into play. Adaptive immunity is so called because its two major components, T cells and B cells, go through receptor rearrangement following the antigen exposure. This process of "adaptation" to the antigen leads to the expansion of highly selective and long-lasting protection.

The antigen presentation occurs in the lymph nodes. Following activation, APCs acquire the ability to leave the tumor site and migrate to the lymph nodes. There, they induce T cell priming and activation. Those two steps ensure the proliferation of antigen specific T cells, which develop a cytotoxic machinery and start producing cytokines. At this point, T cells also acquire the ability to leave the lymph nodes and migrate to tissues. Chemotactic factors produced by innate cells and fibroblasts direct T cell recruitment to the tumor site, where $CD8^+$ cytotoxic T cells can directly kill tumor cells, and $CD4^+$ T cells can help other effector cells in eliminating the tumor[47].

In some cases, this process does not function as it should, and immune cells lose the ability to efficiently fight cancer. The set of mechanisms involved in this process goes under the name of cancer "immune escape" or "immune evasion"[7,48].

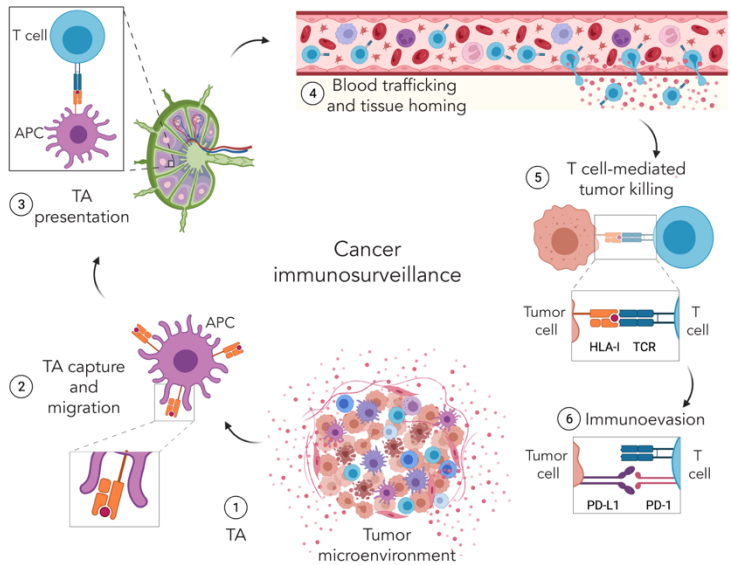

Figure 2.1: The main steps of immune cell recognition of cancer cells: tumor antigens (TAs) in the tumor microenvironment (1) are captured by antigen presenting cells (APCs), which expose the TA on Human Leukocyte Antigen class I and class II proteins (only HLA class I is shown here) (2). APCs leave the tissue and migrate into the lymph nodes, where they perform the antigen presentation (3). During this process, T cell clones that recognize TA through the T cell receptor (TCR) get activated. Activated T cell clones enter the blood stream, and they are recruited to the inflamed tissue by chemokines and protein expressed by the endothelium (4). In the tumor tissue, T cells recognize and eliminate tumor cells (5). In fact, tumor cells express TA on their HLA class I, which is recognized by the TCR (5). Selective pressure induces the proliferation of tumor cells resistant to T cell recognition, for instance tumor cells with low HLA class I expression (6). The set of events leading to impaired immune cell recognition and activity against tumor cells goes under the name of immune evasion.

2.2 CANCER IMMUNE EVASION

During tumor progression, malignant cells acquire new characteristics to elude immune recognition, a process referred to as "immune evasion"[6,7]. The main features of this process are: 1) the creation of non-permissive environment (changes in the extracellular matrix composition, aberrant angiogenesis and formation of hypoxic areas) that impairs lymphocytes migration and survival; 2) down-regulation of activating signals, affecting the ability of immune cells to recognize tumor cells; 3) differentiation and recruitment of regulatory immune cell subsets, which are aimed to stop the inflammation; 4) up-regulation of immune-checkpoint inhibitors and soluble immune-suppressive mediators, that render tumor-infiltrated effector cells functionally inert[47,49–52].

Immune checkpoints comprise different signals that physiologically control the quality and duration of the immune response, to maintain self-tolerance and minimize tissue damages during the inflammation[53]. The most studied immune checkpoint molecules are CTLA-4, PD-1, Tim-3, LAG-3 and TIGIT[53,54]. Immune checkpoint inhibitors (ICIs) have emerged as a robust clinical approach to treat cancer by restoring T cell effector functions and proliferative capacity, leading to the approval of antibodies specific for CTLA-4, PD-1 or PD-L1 for treatment of melanoma, renal cell carcinoma, Hodgkin lymphoma, head and neck squamous carcinoma, urothelial carcinoma, hepatocellular carcinoma, gastric and gastroesophageal cancer and non-small cell lung cancer[55,56]. However, only a subset of patients is responsive to the therapy[52], suggesting that different immune-suppression mechanisms might be involved in the tumor progression of each individual.

One common strategy to evade T-cell recognition is the down-regulation, or complete loss of expression, of HLA class I molecules by transformed cells[6]. However, HLA-I down-modulation constitutes an activating signal for NK cells, which are innate lymphocytes able to perform cell-mediated cytotoxicity against transformed cells and enhance pro-inflammatory responses[57]. Therefore, new therapeutic strategies boosting NK cell activity might be valid alternatives for patients that do not respond to T cell therapies.

Unfortunately, consistent data explaining the mechanisms of NK cell infiltration and activity within solid tumors are lacking, partly since NK cells represent a small lymphocyte population, difficult to isolate from patient-derived tumor tissues. In additions, possible tumor-driven changes in their phenotype might render their identification even more tricky[58].

Our ability to design efficient NK-based therapy requires broad knowledge on NK cell behavior in tumor environments and reliable drug-screening methods that closely reproduce such environments *in vitro*. In the next sections, I will go through current knowledge of NK cell-based anti-tumor activity, highlighting recent developments of *in vitro* systems to study NK interactions with solid tumors.

2.3 NATURAL KILLER CELLS

2.3.1 An overview of NK cell functions

NK cells are innate lymphocytes that promote immunity and tissue homeostasis[59]. They can be identified by the expression of T-bet/Eomes transcription factors and the cell surface marker NKp46[60]. NK cells are particularly effective in detecting and eliminating virus-infected and tumor transformed cells. Fast activation is one of the key features of NK

cells, which contributed to their discovery. In 1975, R. Kiessling, E. Klein and H. Wigzell reported their identification of "naturally occurring lymphocytes" able to "spontaneously kill" mouse Moloney leukemia cells[38,39]. The term "spontaneously" referred to their ability to perform cytotoxicity within an hour, without requiring prior exposure to the same tumor cells[38,39]. Today, we know that NK cells can kill tumor cells within a few minutes of exposure. Rapid effector functions and lack of prior sensitization markedly distinguishes NK cells from T cells, that require 6 hours (with co-stimulation) up to 30 hours (in the absence of co-stimulation) to be fully activated [61]. Cell-mediated cytotoxicity and release of pro-inflammatory cytokines are the most well-known NK cell effector functions[62]. However, multiple NK cells subsets with both distinct and convergent functions have been reported since their discovery, which will be described in the next sections.

2.3.2 NK cell distribution and subsets

NK cells are divided into circulating and tissue-resident cells. Circulating NK cells, also called "conventional" NK cells, represent 5-15% of peripheral blood mononuclear cells. They constantly travel between spleen, lymph nodes and inflamed tissues using blood and lymphatic vessels[63]. Tissue-resident NK cells NK cells can be found in the liver, lung, adipose tissue, and uterus during pregnancy[64].

Two main NK cell subsets have been characterized in humans: $CD56^{Bright}$ $CD16^{-}$ and $CD56^{Dim}$ $CD16^{+}$[65]. $CD56^{Bright}$ $CD16^{-}$ NK cells are preferentially distributed in lymph nodes, tonsils, and uterus, and they show strong cytokine production[66,67]. $CD56^{Dim}$ $CD16^{+}$ cells represent approximately 90% of circulating NK cells in blood and spleen, and their main features are cytotoxic activity and cytokine production[68]. NK cytolytic activity is mediated by both release of perforin/granzyme granules and death receptor activation[69]. Cytokines produced by NK cells comprise pro-inflammatory mediators, such as interferon γ (IFN-γ) and tumor necrosis factor-α (TFN-α), and immunosuppressive mediators, such as interleukin (IL)-10. NK cells also secrete growth factors, such as granulocyte macrophage colony-stimulating factor (GM-CSF) and granulocyte colony-stimulating factor (G-CSF)[70]. NK cells are also able to produce several chemokines, including CCL2, CCL3, CCL4 and CCL5[71]. Chemokines are necessary for the recruitment of immune cells into the inflamed tissue[71], while cytokines orchestrate the crosstalk between NK, macrophages and DCs, shaping the strength and the quality of T cell priming[72]. Therefore, NK cells also participate to the activation of the adaptive immunity. In turn, the adaptive immunity provides factors essential for specialized NK cell functions.

A clear example of NK-adaptive immunity crosstalk is the activation of the antibody-depended cellular cytotoxicity (ADCC). ADCC is a potent type of cell-mediated

cytotoxicity that relies on antibody crosslinking on the target[67]. Its activation proceeds as following: at early phase of immune responses, NK cells produce IFN-γ, a potent activator of macrophages and the promoter of Th1 response. IFN-γ induces the switch of immunoglobulin isotype towards IgG in B cells. NK cells express the IgG receptor, called FcγRIIIa receptor or CD16a. At late phases of the immune responses and during antigen re-challenge, IgG immunoglobulins binds the target, which now could be recognized by NK cells via CD16. Such recognition induces a strong release of granzyme and perforin, that ultimately kills the target cells.

The NK cell activities described so far are mainly pro-inflammatory. However, NK cells also play a role in tissue homeostasis[64]. Such a role is well-exemplified by decidual NK cells (dNK). dNK cells are poorly cytotoxic tissue-resident NK cells. They are found in pregnant endometrial tissue to orchestrate placenta development. First, dNK cells produce angiogenic factors to re-model the uterine arterial system [73,74]. Secondly, they control extra-villous trophoblast cell invasion of spiral arteries, releasing interleukin-8 (IL-8) and interferon-inducible protein-10 (IP-10)[75]. Both steps are crucial for ensuring the positive outcome of pregnancy[76].

NK cells exist also in the adult liver and adipose tissues. After liver damage, NK cells collaborate with macrophages and hepatic stellate cells (HSCs) in the resolution of fibrosis[77]. In addition, cytotoxic NK cells kill HSCs, specifically discerning between quiescent and activated HSCs[78]. In adipose tissue, NK can sustain a local Th1 response and contribute to obesity-associated metabolic disease[79].

As a part of anti-inflammatory activity, NK cells are also involved in the prevention of autoimmunity, being able to kill immature DCs[80] and activated T cells[81,82]. In this our work, we have primarily focused on the role of conventional NK cells in cancer immune surveillance. Therefore, the features of conventional NK cells will be mainly discussed in this thesis.

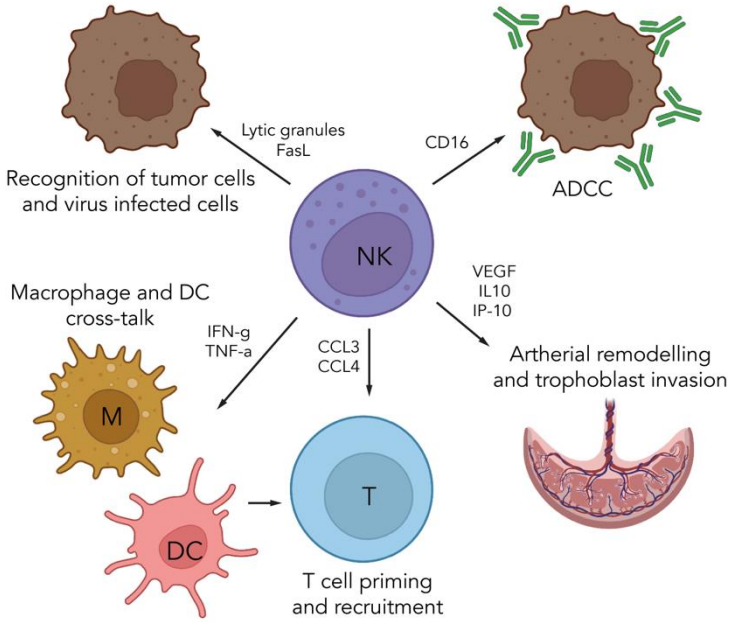

Figure 4.2: Few examples of NK cell functions.

2.3.3 NK cell trafficking and migration into solid tumors

NK cells primarily develop in the bone marrow, where the chemokine SDF-1α retains them in the parenchyma[60,83]. During NK maturation, SDF-1α receptor (CXCR4) is partially desensitized on NK cells[83]. This, together with the upregulation of $S1P_5$ receptor, drives NK cell mobilization from the bone marrow into systemic circulation[83–85]. At steady state, NK cells circulate from the blood into secondary lymphoid organs, where their turnover is about 2 weeks[86]. Trafficking into lymph nodes is mainly mediated by two lymph node homing receptors: CCR7[87], and L-selectin (also called CD62L)[67,88].

According to their differential distribution, $CD56^{Bright}$ NK express high levels of CCR7 and L-selectin, while both receptors are absent on $CD56^{Dim}$[89,90]. $CD56^{Dim}$ present high levels of CXCR1, CX3CR1 and Chem23, chemokine receptors that drive $CD56^{Dim}$ recruitment into inflamed tissues in response to CXCL8, Fractaline and Chemerin, respectively[70,88,91].

Migration into peripheral tissues is assisted by additional adhesion proteins, which recognize molecules induced on endothelial cells during inflammation. Such proteins are low-affinity ligands for E-selectin and P-selectin, that promote leukocyte rolling on the vascular bed, and high-affinity integrins that mediate firm adhesion to endothelial cells and

subsequent trans-endothelial migration[67]. In addition to the mechanisms descried above, NK cell subsets can respond to a variety of inflammatory cytokines via additional receptors[67,92].

Even though the tumor microenvironment is a highly inflamed tissue, the NK cell migration into tumor sites is still quite controversial. NK cells are enriched in non-small cell lung carcinoma (NSCLC) [93,94], gastrointestinal sarcoma[95], colorectal carcinoma[95] and in lung metastases of renal cell carcinoma [96], where their infiltration correlate with good prognosis. In NSCLC, NK cells mainly localize in the connective tissue, specifically in the invasive margins of the tumor[94,97], and intratumorally in the fibrous septa[94]. Interesting, NK cell infiltrating breast tumors[98] and NSCLC[94] are mainly $CD56^{Bright}$, and the same NK subset is enriched in the peritoneal effusions of patients with ovarian carcinoma[99]. Other studies describe poor NK cell infiltration in melanoma[95,100], hepatocellular carcinoma[95], breast cancer[95], colorectal carcinoma[101] and renal cell carcinoma[102,103]. In this context, down-regulation of chemerin gene expression reduces the infiltration of $CD56^{Dim}$ NK cells in prostate, breast and lung adenocarcinoma, and colon adenoma[104]. Interestingly, certain chemokines involved in NK trafficking also promote cell proliferation and angiogenesis[105]. For instance, transformed cells express CXCL8 receptors, and high concentrations of CXCL8 have been detected in both solid and hematological cancers, correlating to increased tumor growth, aberrant angiogenesis, and metastasis[105].

These observations suggest that NK cell infiltration within primary tumors and metastasis varies depending on the tissue involved and the intrinsic characteristic of the tumor environment, possibly differing at different stages of tumor progression. In fact, transformed cells might develop features that inhibit NK cell migration to escape immune surveillance. It is therefore questionable whether the accumulation of $CD56^{Bright}$ cells to the tumor site is the result of a selective $CD56^{Bright}$ NK cell recruitment or lack of $CD56^{Dim}$ specific chemokines, or a combination of the two factors. In addition, it is not clear whether tumor infiltrating-NK are recruited from the blood, or they are specialized tissue-resident cells. Addressing these questions might clarify the mechanisms behind differential NK cell distribution in different types of tumors and their susceptibility to NK cell activity.

2.3.4 NK cell activation

NK cells can perform cytolytic activity within a few minutes from the recognition of a dangerous signal. This is because they dispose of cytolytic machinery in their cytoplasm, which can be quickly released in the proper conditions. Such artillery could be dangerous if timing and target recognition are not regulated. Thus, a dynamic system of inhibitory and activating signals balances NK cell activation and prevent NK cell-mediated autoimmunity[62].This system mainly relies on NK cell surface receptors that discriminate

between healthy and unhealthy cells[62]. Thus, tumor cells become susceptible to NK cell destruction because of increased expression of NK activating ligands, decreased expression of NK inhibitory ligands, or a combination of these two events[106].

Ligands for NK cell activating receptors are usually poorly expressed by normal cells but are upregulated by unhealthy cells. The main activating receptors are CD16, NKG2D and the natural cytotoxicity receptors (NCRs) NKp30, NKp44 and NKp46. Their activation triggers the release of cytolytic granules and the production of pro-inflammatory cytokines[107]. The NK response is potentiated when multiple activating receptors and co-receptors are simultaneously engaged. DNAM-1, CD2 and 2B4 are examples of co-stimulatory molecules that are unable to trigger NK cell on their own but increase the efficiency of NCRs and NKG2D signaling[108–111]. Additional co-stimulatory signals are cytokines, especially IL-2, IL-15, IL-12 and IL-18[112]. Activating and co-activating receptors can signal through immune-receptor tyrosine-based activation motifs (ITAM)-containing subunits (CD16, NKp46, NKp44), the DAP-10 or CD3ζ-associated adaptors (NKG2D, NKp30) and other intracellular pathways (DNAM-1, CD2 and 2B4).

On the other hand, downstream signaling of inhibitory receptors mainly relies on the recruitment of tyrosine phosphatases by immunoreceptor tyrosine-based inhibitory motifs (ITIM) in their cytoplasmatic tails[113]. Such phosphatases dephosphorylate mediators of activating receptor downstream signaling. The main NK cell inhibitory receptors are inhibitory KIRs (Killer cell Ig-like Receptors), CD94/NKG2A (C-type Lectin superfamily glycoproteins)[107] and TIGIT[114,115]. Inhibitory KIRs are encoded by KIR polygenic and polymorphic locus that includes both activating and inhibitory variants. Two KIRs haplotypes have been characterized in humans, A and B, differing in the amount of inhibitory and activating KIRs, respectively[116]. KIR receptors recognize the classical HLA class I molecules (HLA-A, HLA-B, HLA-C). One exception is represented by KIR2DL5, which binds the Poliovirus receptor (PVR)[117]. CD94/NKG2A binds to non-classical HLA class I (HLA-E)[118].

Classical HLA class I molecules are expressed by all nucleated cells to allow immune cells to discriminate between self and non-self[119]. Classical HLA class I binds to TCR and NK cell inhibitory receptors in trimolecular complex consisting of polymorphic heavy chain (HC), self or foreign peptide antigen, and the nonpolymorphic β2-microglobulin (β2-m) light chain[119]. HLA-E is a molecular sensor of classical HLA class I expression. In fact, the correct expression of HLA-E requires its binding to a nonameric peptide derived from the ER-leader sequence of most classical HLA class I molecules. If the synthesis of classical HLA class I is proceeding normally, the ER-leader sequence binds to HLA-E, ensuring HLA-E stability at the cell surface. Conversely, defects of intracellular HLA-A, B, C

synthesis and assembly cause a direct perturbation of HLA-E expression[120]. Such defects are usually caused by viral-infection, tumor transformation or stress-responses[121]. Therefore, inhibitory KIRs and CD94/NKG2A represent a double checkpoint used by NK to sense HLA class I levels and eliminate target cells with reduced expression. This mechanism is defined as the "missing-self hypothesis"[122]. Since HLA class I molecules are ubiquitously expressed, NK cells constantly undergo a process of education that finely tunes their responsiveness, optimizing their ability to mount an immune response while maintaining tolerance to self[123,124].

2.3.5 NK cell education

NK cells constantly undergo a process of education that finely tunes their responsiveness, optimizing their ability to mount an immune response while maintaining tolerance to self[123,124]. NK education is dynamically shaped by a combination of inhibitory and activating inputs from cell surface receptors and cytokines, accompanied by a physical change of the localization of the signaling machinery[123,125,126]. For instance, engagement of inhibitory KIRs by self-HLA class I ligands promotes the subsequent ability to mount a response against HLA-class I deficient cells (educated NK), while NK become anergic in the absence of such input (uneducated NK)[127]. A plethora of receptors and cytokines have been associated to NK cell education, complicating the efforts to understand the molecular mechanisms behind it[123,128]. In addition, a recently identified inhibitory receptor, TIGIT, has been shown to cooperate with it activating counterpart, DNAM-1, in shaping NK cell education in mouse[129]. These receptors will be described later in this chapter.

2.3.6 Cancer evasion from NK cell recognition

Tumors evades the immune responses shifting the balance from activating to inhibitory stimuli[6,52]. For instance, presence of a non-permissive microenvironment, usually highly hypoxic[130] and acidic[131], affect NK cell survival and activity in the tumors[131–136]. Tumor cells and fibroblasts cooperate in producing soluble factors that directly suppress NK cells, such as TGF-β[137], IDO[138] and/or PGE2[139].

Another common strategy to inhibit NK cell tumor recognition is affecting the expression of NK receptors and/or their corresponding ligands in the tumor microenvironment[140–142]. PVR is an NK cell ligand commonly over-expressed during tumor progression[143–149]. PVR binds to four NK cell receptors: DNAM-1[150,151], TIGIT[114,115], CD96[152,153] and KIR2DL5[117,154]. DNAM-1 induces NK cell activation [110,150], while TIGIT and KIR2DL5 induce inhibition[114,115,155].The role of CD96 is not completely defined in human NK cells. It may be clear that the system built to recognize PVR is quite complex, and shift in the

expression of PVR or its receptor might affect the equilibrium between NK cell activation and inhibition. A significant part of this thesis focuses on studying the mechanisms of PVR recognition and their impact on NK cell-mediated tumor surveillance.

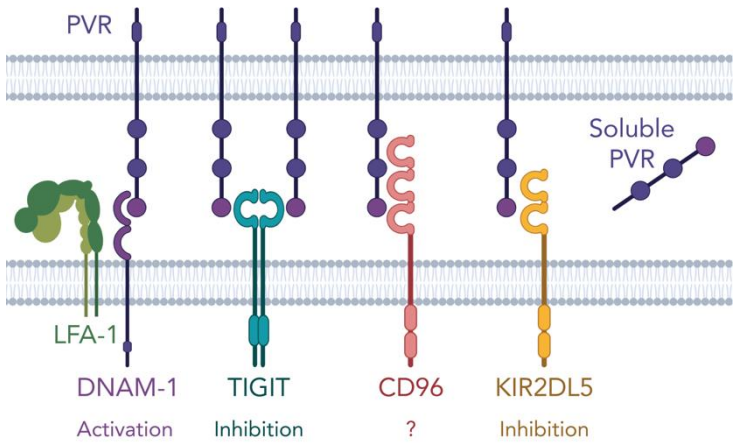

Figure 2.3: Schematic illustration of PVR recognition in NK cells

2.4 NK RECOGNITION OF POLIOVIRUS RECEPTOR

2.4.1 Poliovirus receptor

PVR carries out multiple biological functions. Accordingly, a plethora of names has been assigned to it. Those include Nectin-like molecule 5 (NECL5 or Necl-5)[156], Cluster of Differentiation 155 (CD155)[157], Poliovirus Sensitivity gene (PVS)[158] and Tumor-Associated Glycoprotein E4 (TAGE4)[159].

The first indirect description of PVR dates back to 1985, when P. Nobis et al. isolated the monoclonal antibody D171, which blocked the entry of three poliovirus serotypes in permissive cells[160]. P. Nobis et al. suggested the presence of an integral membrane protein functioning as "poliovirus receptor", lately isolated and identified through molecular cloning[161]. Interesting, despite the high variety of monoclonal antibodies available today, D171 is still the most used antibody for blocking PVR in functional assays.

PVR is a Nectin-like (Necl) molecule, composed by three extracellular Ig-like loops, a single transmembrane domain and a cytoplasmatic tail. Necl family comprises five Ca^{2+}-independent cell adhesion proteins. The term "Nectin-like" comes from the fact that Necl and nectins have similar extracellular domains. Different from nectins, Necls

intracellular domains lack the binding site for afadin, a cytoplasmatic protein that connects nectins to the cytoskeletal machinery and regulate cell motility.

Most of the Necl proteins undergo multiple splicing events, and PVR is no exception. Alternative splicing events give rise to four PVR mRNA isoforms: PVRα, PVRβ, PVRγ and PVRδ[162]. PVRβ and PVRγ lack the transmembrane domain sequence, therefore they are expressed as soluble proteins[162]. Accordingly, PVR can be found in the blood serum and cerebrospinal fluid[163,164]. PVRα and PVRδ isoforms encode for transmembrane proteins, but only PVRα contains ITIM domains in the cytoplasmatic tail. Soluble PVR corresponds to the extracellular region of transmembrane PVR. Therefore, the different isoforms can compete with each other to bind their targets[162].

In adult tissues, membrane bound PVR is physiologically expressed in liver, pancreas, placenta, lung, brain, heart, kidney, and leukocytes[162,163]. The highest expression of PVR is detected in the liver, which is probably also the main source of serological PVR[163]. B. Baury et al. analyzed the relative expression of PVRα, PVRβ and PVRγ in the adult tissues.[163] They showed that PVRα is the most abundant mRNA isoform, accounting for almost 40% of the total PVR transcripts. The percentage increases to 60% in the brain and in the heart[163]. The remaining percentage is equally splitted between PVRβ and PVRγ[163]. Importantly, the PVRδ isoform was not measured in the study, and its contribution is still unknown. Membrane-bound PVR is the most studied PVR isoform, due to its ability to transduce intracellular signals. Indeed, PVRα, but not PVRδ, contains ITIM domains in the cytoplasmatic tail[165].

2.4.1.1 The role of PVR in cell adhesion and proliferation

PVR can initiate the formation of adherent junctions and regulate cell proliferation. Structural similarity between Necl and nectins allows homophilic and heterophilic interaction. Accordingly, membrane-bound PVR can bind to Nectin-3 expressed on adjacent cells [156,166,167]. PVR-Nectin-3 trans-interaction occurs at early stages of cell-to-cell contact, it is transient, and it rapidly induces PVR internalization via clathrin-dependent endocytosis[166]. Nectin-3 retained on the cell surface recruits cadherins, eventually establishing adherent junctions[166]. This sequence of events has a direct impact on cell proliferation. PVR intracellular tail is linked to sprouty2, a negative modulator of Raf/MEK/ERK pathway[168,169]. The interaction with PVR prevents Sprouty2 activation [168]. However, when PVR is internalized, Sprouty2 is released from PVR and phosphorylated. It subsequently translocates into the cytoplasm and represses Raf-MEK-ERK signaling,

turning off cell division[168,169].The system of Nectin-3/PVR trans-interaction represents a fine-tuned mechanism of contact inhibition of cell growth.

2.4.1.2 The role of PVR in cell migration

PVR stimulation with either D171 monoclonal antibody, poliovirus, or PVR receptors induces the phosphorylation of PVR intracellular domains. Specifically, Src kinases phosphorylate ITIM domains, with subsequent recruitment of SHP-2 phosphatases. This signaling inhibits cell adhesion and induces cell motility [170]. PVR contributes to cell directional movement by interacting with PDGF-Rβ (Platelet-derived growth factor-receptor β) and integrin $\alpha_v\beta_3$ *in cis*. Platelet-derived growth factor (PDGF) is produced during inflammation. It binds to PDGF-R expressed by fibroblasts and drives their recruitment to the inflamed tissues. During this process, PVR, integrin $\alpha_v\beta_3$ and PDGFRβ synergistically drive reorganization of the actin cytoskeleton and effectively induce directional movement[171,172].

Sequential expression of PECAM-1, PVR and CD99 on endothelial cells regulates the trans-endothelial migration of monocytes[173,174]. Interestingly, monocytes also express PVR physically associated with CD44, the receptor of hyaluronan[157]. However, the biological relevance of CD44 and PVR co-expression in monocytes has not been investigated.

2.4.1.3 The role of PVR in tumor progression

The hallmarks of cancer include abnormal cell proliferation, uncontrolled cell migration and immune evasion[175]. Since PVR controls each of these functions, it is not surprising that PVR dysregulation is often observed in cancers. PVR overexpression positively correlates with proliferation rate[148,176], invasiveness[146,149,176] and angiogenesis[148] *in vitro*. This has been proved with numerous human tumor cell lines, such as glioma[146,147,177], pancreatic carcinoma[148], lung adenocarcinoma[176], colorectal carcinoma[145], ovarian carcinoma[164], cervical carcinoma[164], endometrial carcinoma[164], melanoma cells[149,178] and acute myeloid leukemia[144]. In addition, high concentration of soluble PVR can be detected in supernatants from gastric, breast, prostate, and melanoma cell lines[163,164].

Immunohistochemical analysis of a broad panel of surgically resected tumor tissues has confirmed the observations *in vitro*. In fact, PVR is overexpressed in cancerous tissue compared to the healthy counterpart in colorectal adenoma[145], adenocarcarcinoma[145], glioblastoma[146,147], pancreatic carcinoma[146,148,179], renal cell carcinoma[146], prostate carcinoma[146], lung carcinoma[143], cutaneous melanoma[149] and acute myeloid leukemia[144]. In line with that, increased levels of PVR were detected in sera of patients affected by lung,

esophageal, gastric, colorectal, bile-duct, pancreatic, breast, ovarian, endometrial cancer[164]. Importantly, PVR overexpression positively correlates with tumor burden and metastatic progression[143,144,149], while it negatively correlates with lymphocyte infiltration[148], disease-free survival rate[143,148] and ICI response[180,181]. Hepatocellular carcinoma seems to represent an exception to this trend, as low levels of PVR are associated with tumor progression and relapse[182,183]. Similarly, MYNC oncogene is a poor prognostic factor in neuroblastoma patients, and it inversely correlates with PVR expression[184]. These findings suggest that modulation of PVR could lead to different outcomes depending on the cancer type.

2.4.1.4 Modulation of PVR expression during drug treatments and viral infections

Insights of PVR regulation comes again from cancer patients and viruses. Chemotherapeutic drugs used in clinical trials comprise DNA intercalants (daunorubicin, doxorubicin, melphalan), proteasome inhibitors (bortemozib) and microtubule inhibitors (vincristine). These drugs induce cytotoxic stress. It has been shown that activation of ATR-ATM DNA damage response following DNA intercalants therapy up-regulates PVR in multiple myeloma patients [185,186]. Similar findings have been shown for proteasome inhibitors treatment[186,187]. Similarly, vincristine treatment increases PVR expression in multiple myeloma cells via p38-mediated activation of E2F1 transcription factor[188]. In light of these findings, it seems that cell-stress could be one of the factors inducing PVR over-expression in the tumor microenvironment. It might be also important to define whether the PVR overexpression measured in the histological samples results from the cancer progression or the previous therapeutic treatments. Interestingly, DNA damage response[189] is also involved in modulating PVR expression during HIV infection, helping the virus to circumvent immune responses. A similar strategy might be used by tumor cell for evading NK and T cell responses.

PVR recognition by NK and T cells is mediated by four PVR receptors: DNAM-1, TIGIT, CD96 and KIR2DL5. The features of each receptor will be covered in the next sections.

2.4.2 DNAM-1

DNAM-1 is a type 1 transmembrane protein belonging to the Ig supergene family. In humans, it is constitutively expressed in conventional T cells, γδ T cells, NK cells, NKT cells, monocytes, DCs, mast cells, eosinophils, platelets and in a small subset of B cells[150,190]. DNAM-1 was described for the first time in 1985. The authors called it "T lineage-specific activation antigen" (TLiSA), for being involved in the differentiation of human $CD8^+$ cytotoxic T cells (CTL) *in vitro*[191]. Few years later, its function in platelet

activation was also identified[192]. The identification of DX11 monoclonal antibody led to its re-discovery ten years later with the new designation "DNAX accessory molecule-1" (DNAM-1)[150], as an "intercellular adhesion molecule" that promotes $CD8^+$ T cell and NK cell-mediated cytotoxicity, as well as TNF-α, IFN-γ and GM-CSF secretion[110,150]. Subsequent work revealed that DNAM-1 plays an important role in tumor immunosurveillance, being involved in recognition and killing of multiple cancer types, such as melanoma[193,194], rhabdomyosarcoma[195], Ewing's sarcoma[196], hepatocellular carcinoma[197], ovarian carcinoma[198,199], colorectal carcinoma[200], neuroblastoma[201,202] and myeloma cells[203]. DNAM-1 also promotes NK cell interactions with dendritic cells[204] and elimination of human cytomegalovirus (HCMV)-infected DCs[205]. In monocytes, DNAM-1 regulates trans-endothelial migration via its interaction with PVR expressed at endothelial junctions[173,174]. Due to its pro-inflammatory functions, DNAM-1 is commonly defined as an activating or co-activating immunoreceptor. Importantly, DNAM-1 can also interact with Nectin-2, but the binding affinity to Nectin-2 is lower compared to PVR[206,207].

2.4.2.1 DNAM-1 signaling pathway

DNAM-1 intracellular signaling is only partially understood to date. It does not rely on ITAMs or ITAM-bearing adapters as the majority of activating immune receptors, but on serine, tyrosine and asparagine-containing motifs situated in its intracellular domains[208,209]. Such motifs become phosphorylated during DNAM-1 activation. For instance, Protein kinase C (PKC)-mediated phosphorylation of Ser329 promotes the association of DNAM-1 to LFA-1. This event requires prior TCR engagement or cytokine stimulation in resting T cells, while LFA-1 and DNAM-1 have been found to be associated also in resting NK cells [210].

DNAM-1-mediated cytolytic signaling is dependent on the phosphorylation of tyrosine in position 319 (Y319 in mice, Y322 in humans) and asparagine in position 321 (N321) [209]. In fact, phosphorylated Y319 and N322 act as binding site for the adaptor protein Grb2. The recruitment of Grb2 activates Vav-1, PI3K, and PLC-ɣ1, which initiate Erk, Akt, and calcium flux pathways [209]. Activated Akt induce the degradation of FOXO-1, a negative regulator of NK cell effector funtions[211]. It remains to be proven whether the same steps are required for DNAM-1 signaling in human NK cells.

The cytoplasmic domain of DNAM-1 contains binding motifs for human discs large (hDlg), a member of the MAGUK family[212]. These proteins function as molecular scaffolds, linking membrane receptors to the cytoskeleton. hD1g has been shown tobe involved in the synapse formation in Jurkat T lymphocytes[213]. In addition, members of MAGUK family participate in the activation of JNK and the NF-κB signaling pathway[212]. These observations suggest a

possible involvement of MAGUK family in DNAM-1 down-stream signaling, as well as DNAM-1/LFA-1 clustering at the immune synapse. However, further evidence to prove these functions is needed.

DNAM-1 is often defined as "co-activating" receptor. This term derives from the fact that triggering DNAM-1 alone does not induce degranulation and cytokine secretion in resting NK cells. In fact, resting NK cells require the co-engagement of DNAM-1 with NKG2D to produce IFN-ɣ and TNF-α[214]. Similarly, DNAM-1 needs to be co-activated with 2B4 to induce cytotoxic granule release[214]. In resting NK cells, co-engagement between DNAM-1 and 2B4 induces the tyrosine phosphorylation of SLP-76 at two different sites. SLP-76 is an adaptor protein that requires the phosphorylation of both sites to be functional[215]. Therefore, SLP-76 seems to be involved in the synergistic effect of DNAM-1 and 2B4 in resting NK cells. SLP-76 is an adaptor protein[215]. These considerations are valid for resting NK cells. Once NK cells have been pre-activated with IL-2, DNAM-1 alone can induce NK cell effector functions without the engagement of other receptors[214,216]. Therefore, the data available so far indicate that DNAM-1 requires a second signal to trigger NK cell activity, either in the form of cytokines or additional NK receptors.

2.4.2.2 The role of DNAM-1 and LFA-1 association

DNAM-1 and LFA-1 can be physically associated on NK cells at steady state, while pre-activation is required for T cells. LFA-1 is central mediator of immune cell adhesion to target cells and formation of immune synapses[217]. LFA-1 is a β2 integrin composed of two subunits, CD11a and CD18[218]. In immunoprecipitation assays, DNAM-1 co-immunoprecipitates using both anti-CD11a and anti-CD18 antibodies[216]. The extracellular domains of LFA-1 can exchange between two conformational states, defined as "open" and "close"[219]. During activation, LFA-1^{close} switch into LFA-1^{open} conformation, which presents an extended structure with increased affinity for it ligands[219]. DNAM-1/LFA-1 association has important biological consequences, as observed in patients affected by leukocytes adhesion deficiency (LAD) syndrome. LAD patients lack the expression of CD18, and their lymphocytes show profound defects in DNAM-1 mediated cytotoxicity, which can be restored by genetically introducing LFA-1[216].

The importance of DNAM-1/LFA-1 association has also been observed in models of ligand-receptor engagement *in vitro*. *C. Fauriat et al.* induced the expression of multiple NK cell ligands in drosophila Schneider 2 (S2) cells.The aim was to study which NK receptors, engaged either alone or in combination, are required for cytokine and chemokine production. S2 cells expressing ICAM-1 and PVR triggered IFN-γ production in resting NK

cells, while PVR alone had small effect, indicating the synergistic activity of DNAM-1 and LFA-1[110]. Using the same system, *Y. Bryceson et al.* showed that DNAM-1/PVR interaction can induce LFA-1^{open} conformation in NK cells[109], even without ICAM-1 binding. *M. Enqvist et al.* showed that LFA-1^{open} and DNAM-1 co-localize at the immune synapse in educated NK cells[220]. Interesting, these last expreriments were carried out using S2 cell expressing ICAM-1, ULBP-1 and CD48, but not PVR. Therefore, it seems that both DNAM-1 and LFA-1 can be partially independent from their respective ligands, as long as one of their ligands is expressed on the target cells. These data further suggest the association of DNAM-1 and LFA-1 at the plasma membrane.

2.4.2.3 The association of DNAM-1 with NK cell education

Different DNAM-1 expression patterns have been observed on NK cells depending on their differentiation and education status. The highest expression of DNAM-1 is observed on terminally differentiated memory-like NK cells[220]. Independently from their differentiation, educated NK cells display more DNAM-1 compared to the uneducated counterpart[221,222]. Furthermore, DNAM-1 expression positively correlates with the magnitude of NK cell response[222]. To date, no other activating receptors or adhesion molecules have been associated with NK cell education, except for LFA-1.

Educated and non-educated NK cells regulates the balance between the open and closed forms of LFA-1 differently[220,223]. The simultaneous regulation of DNAM-1 expression and LFA-1 conformations might represent an important checkpoint control for the immune synapse formation. DNAM-1 association with NK education has been observed also in mouse models[224]. However, the requirement of DNAM-1 expression for NK cell education has not been proven yet.

2.4.2.4 DNAM-1 and cancer

Modulation of DNAM-1 expression is observed in the tumor microenvironment, where DNAM-1 can be down-regulated by ligand exposure. For instance, interaction with membrane bound PVR induces a rapid DNAM-1 internalization in tumor infiltrating NK cells in ovarian cancer[225] and melanoma[226]. An inverse correlation between Nectin-2 and DNAM-1 expression was also found in acute myeloid leukemia patients[227]. In patients with gastric carcinoma[228], colorectal carcinoma[200] and neuroblastoma[202], circulating NK cells reduce the levels of DNAM-1 via mechanism involving TGF-β1 signalling[202,228]. Cutaneous T cell lymphoma patients showed high levels of soluble DNAM-1 in the serum, negatively correlating with the frequency of DNAM-1^{+} NK cells, suggesting that shedding might also occur[229]. In all the previous settings, DNAM-1 down-modulation was linked to NK cell

functional impairment and disease progression. Loss of DNAM-1 expression has been also associated with impaired response to immune checkpoint therapy[181,226,230,231].

Ligand-independent regulation of DNAM-1 has been recently described by *M. Weulersse et al.*[231] . Specifically, the transcription factor Eomes is partially responsible for the down-regulation of DNAM-1 in $CD8^+$ T cells and NK cells, even in the absence of DNAM-1/ligand interaction[231]. Eomes-dependent DNAM-1 loss causes a decrease of LFA-1 activation via reduction of the open conformation, impairing $CD8^+$ T cells and NK cell functions even in the absence of PVR and Nectin-2[231]. *Li et al*. recently demonstrated that the number melanoma lung metastasis increases after DNAM-1 blockade even in PVR-deficient mice[232].

Independently from the presence of the absence of its ligands, DNAM-1 promotes the immune cell recognition of cancers.

2.4.2.5 DNAM-1 and autoimmune diseases

A nonsynonymous single nucleotide polymorphism (SNP) in DNAM-1 encoding gene, called Rs763361 or Gly307Ser polymorphism, has been associated to multiple autoimmune diseases, such as rheumatoid arthritis[233–235], multiple sclerosis[236], systemic lupus erythematosus[237], psoriasis[238], systemic sclerosis[239], autoimmune thyroid disease and type I diabetes[240,241]. The substitution of glycine into serine occurs in the cytoplasmatic tail of DNAM-1, possibly inducing defect in its intracellular signaling[240]. These data show the importance of DNAM-1 regulation for maintaining tissue homeostasis.

2.4.3 TIGIT

TIGIT was discovered in 2009 during the independent work of three research teams[114,115,242]. Its discovery is the result of two different computational strategies: *X. Yu et al.* and *N. Stanietsky et al*. performed a bioinformatic screening for ITIMs-bearing proteins, to identify new inhibitory receptors[114,115]. This search led to the identification of a protein specifically expressed in T cells and NK cells, which they called "TIGIT" (for 'T cell immunoglobulin and ITIM domain')[115]. *K. S. Boles et al.* followed another lead. They were looking at amino acid alignment of Nectins, Necl and their receptors to study their interaction at the cell surface, when they also performed sequence alignment using the NCBI cDNA database. They found an additional "candidate receptor" that aligned with Nectin-1-4, PVR, DNAM-1 and CD96. They named it "WUCAM" (Washington University Cell Adhesion Molecule)[242]. WUCAM and TIGIT referred to the same molecule, and the term TIGIT was consequently maintained.

According to its immunoregulatory role, TIGIT inhibits T cell and NK cell effector functions with both direct and indirect mechanisms[114,115,243,244]. For instance, TIGIT expressed on T cells can bind to PVR expressed on DCs. This event leads to abundant secretion of IL-10 by DCs, which also reduce the production of pro-inflammatory cytokines[115]. The direct interaction of TIGIT with PVR expressed on tumor cells inhibits degranulation and cytokine production in both T cells and NK cells[114,243–245].

TIGIT also interact with proteins belonging to the Nectin family, such as Nectin-2 and Nectin-3 (with lower affinity compared to PVR) and Nectin-4 (with similar affinity as PVR)[246].

A lot of effort has focused on increasing the understanding of TIGIT regulation and functions in the last decade. Nowadays, TIGIT is fully considered an immune checkpoint, and multiple pharma companies are currently investing resources in developing therapeutic strategies to block TIGIT functions. More than 40 currently ongoing clinical trials are aimed to target the TIGIT pathway[247].

2.4.3.1 TIGIT signaling pathway

Despite its recent discovery, a clearer understanding of TIGIT intracellular signaling is available compared to DNAM-1. TIGIT consists of an extracellular immunoglobulin variable (IgV) domain, a type-I transmembrane domain, and a cytoplasmatic tail bearing an ITT-like motif and a classical ITIM motif[115]. Studies in primary NK cells and immortalized YTS cells have shown that PVR engagement induces the phosphorylation of TIGIT ITT-like motif[244]. This step is mediated by Src-family kinases Fyn and Lck, and it is required for the association of TIGIT with adaptor proteins [244]. TIGIT uses two distinct adaptors, Grb2 and β-arrestin 2, to propagate the signal intracellularly. Specifically, Grb2 and β-arrestin modulate cytotoxicity and cytokine secretion, respectively[244,248]. Grb2 recruits SHIP1, which suppresses PI3K and MAPK downstream effectors, causing the inhibition of granule polarization[244]. On the other hand, the activation of β-arrestin 2 leads to the suppression of the NK-κB pathway[248,249]. NK-κB resides in the cytosol bound to IκBα. The association with IκBα prevents NK-κB translocation into the nucleus. The stability of IκBα is under the control of ubiquitin E6 ligase TRAF6. Specifically, TRAF6 autoubiquitination is required to initiate a series of signals that leads to IκBα degradation[250,251]. TIGIT association with β-arrestin 2 leads to the SHIP1-mediated inhibition of TRAF6, terminating IκBα degradation and, consequently, NK-κB activation[248].

Experimental observations suggest that tyrosine-independent mechanisms are also involved in TIGIT signalling, however a clear picture of how they work is not available yet[243,244].

2.4.3.2 TIGIT in cancer

TIGIT is preferentially expressed on NK cells, peripheral regulatory $CD4^+$ T cells, memory T cells and follicular helper $CD4^+$ T cells [114,115,242,252]. It can be further upregulated after *in vitro* stimulation, as well as de novo induced in naïve $CD45RA^+$ $CD4^+$ T cells[106,115,242]. TIGIT is also present on effector $CD8^+$ T cells and NKT cells, but at lower levels compared to NK cells[115,252].

Elevated TIGIT levels are found in tumor-infiltrated lymphocytes (TILs) isolated from multiple solid cancer, such as NSCLC, pancreatic cancer[253], colorectal carcinoma[254], gastric cancer[255], follicular lymphoma[256] and melanoma[226,257,258] Circulating $TIGIT^+$ lymphocytes have been also isolated in patients affected by hematological cancers[259–261], correlating with poor prognosis.

TIGIT impairs the immunosurveillance by inducing effector T cell exhaustion and enhancing Treg immunosuppressive activities. Accordingly, TIGIT up-regulation in the tumor microenvironment affects all different T cell subsets ($CD4^+$ [256,261], $CD8^+$ [254–257,259,260] and Treg [262,263]) and correlates with the expression of co-inhibitory receptors, such as PD-1[255–261], CTLA-4[258] and Tim-3[257].

Although its inhibitory role on NK cell activity has been proven[114,243,244], the relevance of TIGIT in NK cell-mediated anti-tumor immune surveillance is less clear. In this context, high-levels of TIGIT were observed on circulating and tumor-infiltrating NK cells in gastrointestinal cancer patients[252] and colon cancer patients[264], respectively. However, slight down-regulation of TIGIT expression was observed in tumor-infiltrating NK cells compared non-tumoral NK cells in melanoma and hepatocellular carcinoma patients[226,265].

Bacteria and viruses can shape the NK cell recognition of tumors, and TIGIT seems to be involved in this process. For instance, the protein Fap2 of *Fusobacterium nucleatum*, an anaerobic Gram-negative bacterium often enriched in colon adenocarcinoma, directly binds to TIGIT and impairs NK cytotoxic activity[266]. In addition, adaptive NK cells are insensitive to MDSC-mediated suppression *in vitro* due to reduced levels of TIGIT compared to conventional NK[267].

These findings strongly suggest that TIGIT might be critical for NK cell-mediated tumor surveillance. Interesting, TIGIT expression on NK cells shows a wide variation among individuals and NK cell subsets[252]. This opens the possibility to study TIGIT modulation in correlation with individual response to NK cell treatment, as well as to select specific NK cell subsets better suited for tumor therapy.

2.4.3.3 Anti-TIGIT therapy

The percentage of NK cells positive for granzyme A/B and perforin staining is higher in $TIGIT^+$ compared to $TIGIT^-$ cells in both healthy individuals and cancer patients [226]. Still, $TIGIT^+$ NK cells degranulate less against PVR-positive target cells. It seems therefore that TIGIT might represent a checkpoint control for NK cells characterized by high cytotoxic potential. This rationale led to the development of anti-TIGIT antibodies for cancer therapy.

TIGIT blockade as single agent has shown limited results in clinical trials[268,269]. According to *J. M Chauvin et al.* and *H. Jin et al.*, the expression of DNAM-1 is essential to maintain the efficacy of TIGIT blockade[226,270]. IL-15 stimulation has been proven to partially restore the activity of DNAM-1 and the efficacy of anti-TIGIT blockade[226]. However, the effect does not seem be TIGIT-specific, as the absence of DNAM-1 affects also anti-PD-1 therapy[231]. Therefore, maintaining high levels of DNAM-1 expression might be required for the efficacy of any immunocheckpoint inhibitor, not only anti-TIGIT antibody.

TIGIT blockade has been shown to enhance T-cell anti-tumor functions in combination with other checkpoint inhibitors[255–261].CITYSCAPE is an ongoing clinical trial testing the efficacy of anti-TIGIT and anti-PD-L1 antibodies in combination in patients affected by metastatic NSCLC[271]. The results shown in phase II are promising[272].

Despite the high interest of scientists and pharmaceutical companies in TIGIT, the mechanisms regulating TIGIT expression in the tumor microenvironment are still missing, together with factors predicting which patients might actually benefit from anti-TIGIT therapy. Better understanding the involvement of TIGIT in NK cell-mediated tumor surveillance is one of the key focus areas of this thesis.

2.4.4 CD96

CD96 was identified in 1992, using an antibody produced against IL-2-dependent human T cell lines[152]. The authors named the antigen "TACTILE", standing for "T cell activation, increased late expression", as cell surface levels peak between 6 to 9 days after activation[152,273].

CD96 is expressed on $CD4^+$ and $CD8^+$ T cells, γδ T cells, NK cells and small subsets of B cells[152,153,197]. In addition, CD96 transcript can be found in fetal brain, kidney, thymus and spleen, as well as in adult secondary lymphoid organs, colon, ovary and kidney[273]. CD96 transcription levels show high variation between individuals, especially in lymphocytes[273]. CD96 recognizes also Nectin-1, but with lower affinity compared to PVR[274].

2.4.4.1 CD96 structure

CD96 is a single-pass transmembrane glycoprotein[152]. The extracellular region comprises three-Ig like extracellular domains: the first domain is required for PVR binding, while the second domain defines the magnitude of binding[152,153,273]. Alternative splicing of CD96 mRNA generates two variants, namely V1 and V2[273]. V2 variant mediates a stronger PVR-binding and it predominates in tissues compared to V1[273]. It is interesting to note that CD96 alternative splicing takes place only in humans, not in mice.

2.4.4.2 CD96 in human diseases

In humans, mutations in the third Ig-like domain or genetic disruption of CD96 correlate with the manifestation of the C syndrome (Opitz trigonocephaly), a rare disorder characterized by trigonocephaly, psychomotor retardation and other body malformations[275]. Significant increase of CD96 has been observed in hematopoietic stem cells from ITP bone marrow (Idiopathic Thrombocytopenic Purpura)[276], in acute myeloid leukemia (AML), T-cell acute lymphoblastic leukemia (T-ALL)[273] and myelodysplastic syndrome[277]. The extracellular protein structure, together with the expression pattern, suggests CD96 involvement in cell-to-cell adhesion during tissue development and immune responses. However, a systematic and unified description of CD96 function is still missing.

2.4.4.3 Role of CD96 in human NK cells

According to *A. Fuchs et al.*, CD96 alone triggers human NK cell cytotoxicity in redirected lysis assay[153]. A few years later, *Stanietsky et al.* reached a different conclusion, showing that CD96 boosts NK redirected killing only in combination with other stimuli, while CD96 alone has no effect[114]. In addition, CD96/PVR interaction promotes cell adhesion in NK92 cell line, quickly followed by CD96 down-regulation[153]. Although these observations point to an activating/co-activating receptor function, *in vitro* neutralizing experiments did not reveal any effect of CD96 in NK-mediated killing of myeloma cell lines[203]. Therefore, direct proof of CD96-PVR binding and activating signaling is still missing in human NK cells. Similarly, not much is known about CD96 function in other cell types. While its role is still unclear in humans, multiple evidence showed the immune suppressing role of CD96 in mouse models[278–281].

2.4.4.4 CD96 signaling pathway

Despite being discovered 30 years ago, the downstream signaling of CD96 has not been characterized yet. CD96 cytoplasmic tail contains a single ITIM-domain, suggesting an inhibitory function. However, in humans, but not in mice, this sequence partially overlaps

with a short YXXM rich motif. YXXM rich motifs are found in both inhibitory (i.e. CTLA-4) and activating receptors (i.e. CD28), alternatively binding to protein phosphatases or kinases[282]. Defining the signaling machinery associated to CD96 might clarify some aspects of its function.

2.4.5 KIR2DL5

KIR2DL5 (CD158f) is an inhibitory receptor belonging to the human KIR family[154,155]. It is clonally expressed in a small fraction of $CD56^{Dim}$ NK and T cells[154,155], and only in some individuals[154]. Specifically, the KIR2DL5 gene is restricted to the B haplotype[283]. Allelic polymorphisms[284], promoter variants[285], alternative splicing events[154] and epigenetic silencing[286] further increase the variation of KIR2DL5 expression among individuals.

KIR2DL5 engagement leads to the phosphorylation of ITIM domains, which recruit the tyrosine phosphatases SHP-1 and SHP-2[155,287]. However, only SHP-2-dependent pathway has been shown to reduce NK cell cytotoxicity upon KIR2DL5 triggering[288].

The KIR2DL5 gene has been associated to ankylosing spondylitis[289–291], SLE[292] and sporadic dermal neurofibroma[293]. However, knowledge on KIR2DL5 physiological functions and its impact on human diseases remain scarce. In fact, KIR2DL5 remained an orphan receptor for almost twenty years. The discovery of PVR as KIR2DL5 ligands in 2019 opens for new possibilities to understand the biological functions of KIR2DL5[117].

2.5 RARE CANCERS

According to the Surveillance of Rare Cancer in Europe (RARECARE), rare cancers are classified as cancers occurring with an incidence lower than 6 cases out of 100 000 individuals per year[294]. To put things into perspective, the two most common cancers are lung cancer (in men) and breast cancer (in women), and their incidence in developed countries corresponds to 39 cases per 100 000 individuals and 59 cases per 100 000 individuals, respectively[1]. However, the totality of rare cancers accounts for 20-25% of all cancers in Europe and USA[295,296], and they are the most common malignancies in children and adolescents[296]. Therefore, despite being perceived as uncommon, the burden of rare cancers is quite substantial in human societies.

Rare cancers include highly heterogeneous tumor types, different in term of tissue location, age and sex incidence, and survival rates. However, when analyzed in their totality, the 5-years survival is lower for rare cancers compared to common cancers in all age and sex categories [296]. These data indicate that more effort is needed to better prevent and cure them.

Rare cancer heterogeneity definitely represents a limit for research. Low availability of patients to enroll in clinical trials, scarcity of primary tumor material, and lack of *in vitro* models recapitulating the clinical features of the original tumors are the main challenges faced in rare cancer research. These factors limit the development of new therapeutic approaches aimed to improve the patient's survival. Establishing new methods to study rare cancers *in vitro* is one of the subjects of this thesis, with a particular focus on sarcomas.

2.5.1 Sarcomas

Sarcomas are rare tumors[295]. They are prevalent in children and adolescents, accounting for 18% of all pediatric cancer-related deaths[297]. Sarcomas originate from mesenchymal tissues, such as adipose, muscle, fibrous, cartilage, nervous, and vascular tissues, or bone. Since these tissues are distributed throughout the human body, sarcomas can occur in almost all organs[298]. Depending on the anatomical site of origin, sarcomas are divided into two main categories: soft-tissue sarcomas and bone sarcomas[298,299]. Such classification is very broad, and large heterogeneity can be found within each category. The WHO classification is more representative of the sarcoma heterogeneity, listing more than 180 sarcomas subtypes based on their morphology and genetic mutations[300–302]. Such diversity, together with small patient numbers, directly translates into low statistical significance in clinical trials and undermines the development of cutting-edge therapies[298]. As results, sarcoma treatment did not significantly change over the last decades[299].

2.5.1.1 Therapy of sarcomas

The first line treatment of sarcomas is surgical resection, which can be accompanied with chemotherapy and/or radiotherapy depending on the sarcoma subtype and grade[10,303]. Chemotherapy is performed before and/or after surgical treatment in the case of advanced sarcomas or aggressive sarcomas subtypes with high risk of recurrency[10,303,304]. Chemotherapeutic treatments include doxorubicin, cisplatin, methotrexate, ifosfamide gemcitabine, docetaxel, dacarbazine as single agents or in combination (i.e. doxorubicin with ifosfamide, doxorubicin with dacarbazine)[10,305]. Similarly, radiotherapy is performed before or after surgery for high-grade sarcomas.

Advanced grade leiomyosarcomas and liposarcomas not responding to first line chemotherapy are treated with eribulin, an inhibitor of microtubule polymerization, or with trabectedin, a DNA-intercalating drug that inhibits the cell cycle progression[303,306]. Target therapy is used for the treatment of soft-tissue sarcomas. For instance, gastrointestinal stromal tumors (GIST) are sarcomas that frequently present mutations in Kit and PDGFR[10]. Accordingly, imatinib, an inhibitor of PDGFR and Kit pathways[307], is used as first line

therapy for GIST[308]. B-RAF inhibitors are used for BRAF-mutated GISTs non-responding to imatinib. In addition, other soft-tissue sarcomas (with the exception of liposarcomas) can be treated with pazopanib as second-line therapy[306]. Pazopanib is a broad-range inhibitor of VEGF and PDGF receptors and it blocks angiogenesis and tumor growth[309]. Denosumab is a monoclonal antibody specific for RANK ligand and it is used for first line treatment of giant cell tumor of bone, a bone sarcoma subtype[304].

Inherent or acquired resistance to chemotherapy and target therapy is frequent among sarcoma patients[10,308,310], and immunotherapy could represent an alternative for these cases. Historically, the first form of immunotherapy was experimented on sarcoma patients[8]. Despite that, the introduction of immunotherapy in sarcoma care is falling behind. There are many reasons for that. First, the mentioned rarity of some sarcoma subtypes making it difficult to enroll patients in clinical trials is still a big obstacle for the introduction of any type of treatment in sarcomas. Second, most sarcomas fall into the definition of "cold tumors", defined as non-inflamed tumors with scarce immune cell infiltration[311]. As low immune cell infiltration is a negative prognostic factor for immune checkpoint blockade[312], sarcomas were generally considered as not ideal targets for ICIs. Third, during the histological assessment of immune checkpoint expression, wide interpatient variability and differences among subtypes are usually observed[313–315]. Given the high heterogeneity of sarcomas, variation within subtypes and patients should be expected in terms of response to immunotherapy[316].

Recently, more efforts have been directed into better classifying which sarcomas are suitable for immunotherapy. T cell infiltration was observed in a subgroup of soft-tissue sarcomas, specifically myxofibrosarcoma, undifferentiated pleiomorphic sarcoma (UPS), dedifferentiated liposarcoma, epithelioid sarcoma and angiosarcomas, also characterized by high expression of immune checkpoints[313–315] . Angiosarcomas show high tumor mutational burden (TMB)[317], which has been proposed as a positive prognostic factor for immune checkpoint blockade[318]. Accordingly, durable response following pembrolizumab treatment were observed in UPS and dedifferentiated liposarcoma in a phase II study[319]. High-rate response to ICIs was also observed in angiosarcoma patients in clinical trials and case reports[317,320,321]. Response to ICIs has been reported also for alveolar soft part sarcoma[322,323], Kaposi's sarcoma[324], chordoma[325] and malignant peripheral nerve sheath tumor (MPNST)[326]. Still, no immunotherapeutic treatment is currently approved for sarcomas. Even though more knowledge is slowly accumulating, better understanding of sarcomas' pathogenesis and response to drugs is needed to improve patient survival. However, the field also suffers from the scarcity of *in vitro* models for pre-clinical research.

2.5.1.2 Impact of sarcoma heterogeneity on basic and translational research

Sarcoma heterogeneity and scarcity of primary material affect basic research and preclinical studies. For instance, a very limited number of sarcoma cell lines is commercially available[295,327]. Within the few cell lines established, the majority are Ewing´s sarcomas and osteosarcomas, which are aggressive but quite rare sarcoma subtypes[295,304,327]. On the other hand, more common sarcomas, such as undifferentiated pleiomorphic sarcomas, liposarcoma and leiomyosarcoma, are underrepresented in the cell banks[327]. Beyond that, most of the available sarcoma cell lines date back to 1950s and 1960s and lack the patient history, impacting the clinical relevance of the results.

Genetically engineered mouse models (GEMMs) can be extremely useful to understand the mechanisms of carcinogenesis and cancer development, providing a platform to identify genes and molecular pathways initiating and driving the pathology[328]. Regarding sarcomagenesis, GEMMs have helped understanding which genetic mutations that are responsible of the high prevalence of osteosarcoma in hereditary disorders such as Li-Fraumeni syndrome (TP53), hereditary retinoblastoma (RB1), and Rothmund-Thomson syndrome (RECQL4)[329]. Similarly, GEMMs carrying mutations in the p53 pathway confirmed the involvement of this oncosuppressor in the development of sporadic sarcoma[330]. Dysregulation of p53 accompanied with mutations in Rb, Pax3, or K-ras led to development of osteosarcoma, rhabdomyosarcoma and undifferentiated pleomorphic sarcoma respectively, recapitulating the pathogenesis observed in humans[331–333]. GEMMs have been also useful in proving the role of chromosomal rearrangements in the development of synovial sarcoma and liposarcoma[334,335].

Despite that GEMMs models have proven useful for systematic studies of how individual genes and mutations impact sarcomagenesis, these models present several limitations. First, GEMMs are available only for few sarcoma subtypes. Second, the models themselves have demonstrated that sporadic sarcoma is a multi-hit disease, where cooperative interaction between mutations is responsible for its clinical appearance. Such heterogeneity and complexity can hardly be reproduced in GEMMs, due to constraints in the number of mutations that can be introduced and the available time to follow the disease.

Given the limitation of GEMMs, patient-derived tumor xenografts (PDX) are becoming the favored preclinical animal model for sarcomas. The PDX approach means engrafting patient-derived tumor tissue in mice either subcutaneously or orthotopically[336]. Orthotopic PDX-models are usually preferred, as the tumor is implanted in the same anatomic site as the primary tumor originated from; this is done to mimic the microenvironment of the primary location and to reproduce similar pattern of metastatic dissemination into secondary

tissues. As the key aspects of PDX-model are the preservation of the architecture, heterogeneity, and metastatic behavior of the individual patient's tumor, they are currently used to understand sarcoma proliferation, metastasis, chemo-resistance and for personalized clinical decision making[337,338]. Several orthotopic PDX-models have been developed for different sarcoma subtypes, such as liposarcoma, osteosarcoma, rhabdomyosarcoma, undifferentiated pleomorphic sarcoma, Erwing's sarcoma, leiomyosarcoma and synovial sarcoma[339]. Still, many sarcoma subtypes are underrepresented. The factors contributing to the various engraftment success rate between sarcoma subtypes are still unknown, as the field suffers from non-standardized methodology and inconsistent criterion of data analysis and reporting[338].

One well-known reason for engraftment failure among different tumors is acute transplant rejection caused by the host immune sytem[338]. Therefore, PDX models need to be established in immunocompromised mice, such as *Scid*, *NS* and *NSG* mouse strains. In addition, PDX-tumors tend to gradually replace the human stroma with the murine counterpart, altering the original environment. The lack of functional immune system and changes in the stroma composition stroma are the main limits of the PDX-models. In fact, they undermine the use of PDX-models in drug testing, excluding large categories of oncological treatments, such as immunotherapy and target therapy[340].

Large breed dogs represent a high-value translational model due to the spontaneous development of the tumor (i.e., non-genetically modified animals) in an immunocompetent organism. However, their use is limited to osteosarcoma.

Better models to study the molecular drivers of sarcomas and the efficacy of treatments are needed to broaden the knowledge of sarcomas and translate the finding into improved patient survival.

2.6 PRECISION MEDICINE

2.6.1 Tumor-centered vs patient-centered treatment

Traditionally, the therapy for cancer patients is decided based on which treatment is most effective for a particular tumor type. This strategy is called "tumor type-centered" approach[340]. For instance, leiomyosarcomas often do not respond to ifosfamide, while the combination of gemcitabine and docetaxel has been proven to be effective. On the other hand, ifosfamide shows good efficacy in synovial sarcomas. Therefore, in standard sarcoma care, the combination of gemcitabine and docetaxel is used for leiomyosarcomas, while ifosfamide for synovial sarcomas.

However, treatment response is much more complex than that. Individuals have different genetic backgrounds that influence the predisposition to cancer as well as the response to therapy. Age, sex, diet, exposure to environmental factors and socio-economic status are additional elements that impact cancer prognosis and therapy[341,342]. The tumor itself is under the constant pressure of Darwinian selection and Lamarckian induction, which favor the proliferation of tumor subclones resistant to immune surveillance and treatments, adding further heterogeneity[343,344]. Considering that, the "tumor type-centered" approach seems to be a too simplistic approach.

In an attempt to consider interpatient variability during the treatment decision-making, cancer therapy is moving from the "tumor type-centered" approach to a "patient-centered approach". Such approach goes also under the name of "precision medicine". The term "precision medicine" was introduced by the National Research Cancer (US) Committee in 2012 to indicate a medical treatment "tailored to the individual characteristics of patients"[345]. This approach aims to identify subpopulations of patients that differ in disease susceptibility, prognosis and response to therapy, and to develop strategies of prevention and treatment adapted to the specific characteristics of the particular subpopulation[345].

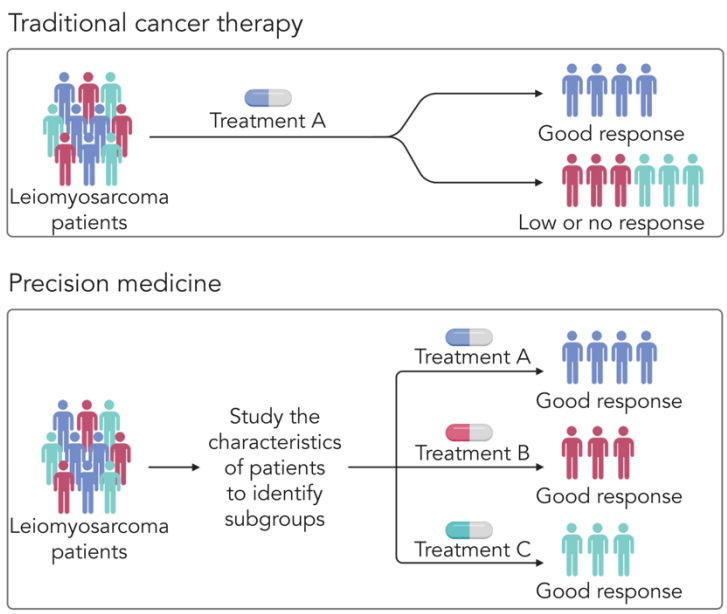

Figure 2.4: A schematic overview of traditional cancer therapy versus precision medicine.

2.6.2 Precision medicine today

Precision medicine is already a reality in multiple cancer types. For example, the selection of treatment for non-small cell lung cancer is based on the identification of molecular drivers, such as EGFR mutation, ALK translocation, and BRAF mutations. Patients carrying EGFR mutations, which leads to the overactivation of the EGFR pathway, are treated with EGFR tyrosine kinase inhibitors. In case of chromosomal translocation in ALK, crizotinib is used instead. BRAF and MEK inhibitors can be administered in case of BRAF-V600 mutation, while ICIs are preferred in the absence of the previous mutations[346]. Therefore, within the same type of cancers, multiple approaches are available depending on the characteristics of the patient. Other types of cancers that are treated with similar approaches include acute myeloid leukemia (Philadelphia chromosome translocation), melanoma (BRAF-V600 mutation), breast cancers (BRCA-1/2 mutations), renal carcinoma (VHL loss) and GIST sarcomas (Kit mutation). Multiple reports showed the superior efficacy of the "patient-driven approach" compared to the "tumor-driven approach"[340]. Currently, precision medicine relies on biomarkers that precisely and accurately identify subpopulations of patients. Nowadays, the strategies to identify novel biomarkers includes histology, genetic and epigenetic analysis, transcriptomic, proteomic, metabolomic and microbiome analysis, alone or in combination[340,347,348]. Each of these sectors has progressed rapidly in terms of instrumentation, analysis, data sharing, standardization, and cost effectiveness[348,349]. This rapid expansion opens to the possibility of new biomarkers discovery, which will hopefully translate into better patient care. However, at the state of the art, predictive biomarkers are not available or still uncertain for multiple cancer treatments.

2.6.3 Precision medicine for immunotherapy

One treatment category that is rapidly moving forward but still lags behind in terms of predictive biomarkers is immunotherapy. According to the "tumor-centered approach", cancer types better responding to immunotherapy have been identified. For instance, anti-PD-L1 response rate as singe agent is 40%-70% for Merkel cell carcinoma, Hodgkin lymphoma and melanoma, while the response rates go down to 15%-25% for other cancer types[350]. This data not only show heterogeneity of response depending on the tumor type, but also highlight the fact that immunotherapy is still not effective in many cancer patients, even the ones carrying so called "responsive tumors". Personalized medicine approaches are trying to identify the mechanisms of primary and acquired resistance occurring in non-responders, to better select the patients to enroll for immunotherapeutic treatments and possibly develop new strategies to overcome resistance.

One of the first proposed predictive biomarkers for ICIs therapy is PD-L1 expression in the tumor. Although the levels of PD-L1 expression have been shown to correlate with successful ICI treatment in some studies[351–353], other studies has shown that it was predictive only in a small percentage of cases[354], and benefits have been observed also in PD-L1 negative tumors[355]. These contrasting results might be due to differences among the tumor types, or to different criteria applied during the analysis. For instance, the analysis of PD-L1 expression has been limited to the tumor cells in some papers, while its expression on tumor-infiltrating immune cells has been considered in others. The evaluation is even more difficult when the metastasis and primary tumor show different levels of PD-L1 expression. Therefore, PD-L1 expression as predictive biomarker needs further investigation and consensus about how to characterize the expression.

Another recently proposed biomarker is the tumor mutational burden (TMB), indicating the total number of mutations occurring in a tumor. Following the rationale that TMB can correlate with neoantigen load, which is one of the factors defining the immunogenicity of tumors[356,357], high TMB has been proposed as predictive biomarker for ICI therapy. After the publication of promising data using this strategy[358], FDA approved the use of pembrolizumab for multiple tumors with high TMB ($\geq$ 10 mutations/megabase of DNA) after the failure of prior therapies[359]. However, part of the scientific community criticized the choice of a universal cut-off value for a wide range of tumor histologies[358,360,361]. In addition, a recent publication reported no predictive value of TMB [362]. Again, it is important to notice that multiple technical factors can affect the evaluation of TMB and its significance in predicting patient response. Nowadays, the detection of high microsatellite instability (MSI) to predict immunotherapy response has gained more consensus compared to high TMB[363,364]. T cell infiltration[365], gut microbiome[366,367] diversity, PBRM1 loss-of-function mutations[368] have also shown to correlate with patient response, although their evaluation needs further investigations.

More research is needed to better predict the response of cancer patients to immunotherapy. The challenge is certainly very difficult, and this is not surprising. The immune system is one of the most variable components across individuals, having a great impact in shaping people heterogeneity. Variations in the immune system of different individuals are partially inborn, and partially shaped during the lifetime by the exposure to pathogens and other environmental factors. Such diversity definitely influences tumor progression and therapy response. The possibility of dissecting the reasons for a patient to better perform immunosurveillance under restimulation requires the development of robust *in vitro* systems for tumor immunological studies.

3 RESEARCH AIMS

Since immunotherapy became a standard clinical practice, multiple cases of innate and acquired resistance have been reported, pointing out that more research is needed to understand individual response to treatment. Various platforms to study the tumor microenvironment *in vitro* are available nowadays, namely 3D cultures. However, the implementation of such methods in the immunology field is lagging. One possible reason among many is that a limited number of 3D culture systems can simultaneously provide high-throughput screening, high-resolution analysis and compatibility with both live cell imaging and other traditional immunological techniques.

The main aim of our projects is to provide a platform for 3D cell cultures and deep-tissue imaging suitable for basic and translational immunology research.

Our research focused on the following specific aims:

1. Developing a microwell chip to study immunotherapy *in vitro* with the following characteristics:
    a. It should be compatible with 2D and 3D cell cultures, both from cell lines and primary cells
    b. It should allow sample preparation, live cell imaging and high-resolution imaging directly in the chip
    c. It should allow to combine high-throughput screening and high-resolution analysis in the same experiment
    d. It should allow non-imaging-based analysis off-the-chip, such as DNA, RNA and protein analysis
2. Applying the use of the microwell chip to basic immunological research, such as understanding the hierarchy and dynamics of PVR receptors in NK cells, both at steady state and in the tumor microenvironment
3. Applying the use of the microwell chip to test personalized strategies for immunotherapy, both as single agent or in combinatorial therapy

Our research is the result of a multidisciplinary approach based on the tight collaboration between biotechnologists, physical engineers and medical doctors based at Karolinska University, KTH Royal Institute of Technology and Karolinska Hospital.

4 MATERIALS AND METHODS

4.1 CELL CULTURE

The following sections cover the theory and the methods available for culturing cells of human origin *in vitro*.

4.1.1 Requirements for cells to grow *in vitro*

Our ability to describe biological processes relies on the existence, and continuous improvement, of *in vitro* systems that accurately and precisely reproduce the events taking place in our body. Culturing cells in laboratories is one of the most basic and widespread tools that researchers dispose to study biological mechanisms. Cells are obtained from tissues or body fluids and placed in conditions that favor their maintenance outside the body. Different methods are available for isolating cells. The most common include tissue dissociation, either enzymatic or mechanical, followed by filtration, and standard centrifugation of body fluids. If the research focuses on a particular cell lineage, cell sorting can be performed prior to cell culture.

The optimal conditions for cell culture might vary depending on the cell types, however most cells require physiological pH (pH=7.4), osmotic pressure and temperature (t=37° C), adequate levels of oxygen ($[O_2]$=21%, although this value varies greatly across human tissues), nutrients and growth factors. *In vitro*, such factors are guaranteed by cell culture media and cell incubators. Cell culture media are buffer solutions containing salts, sugar, amino acids and vitamins, ensuring correct pH, osmotic pressure and nutrients. Depending on the cell type, cell culture media can be further supplemented with animal serum. The sera most commonly used for human research are pooled male AB human serum, fetal bovine serum (FBS) and fetal calf serum (FCS). Serum is rich in carbohydrates, growth factors, proteins, lipids and electrolytes, which help sustaining cell proliferation and long-term culture. Additional recombinant growth factors can be added to the culture to achieve proliferation, differentiation, and maturation of specific cell lineages. For instance, interleukin-15 (IL-15) is used to achieve NK cell proliferation and maturation in Paper II, III and IV. Oxygen levels, temperature and additional pH control are maintained by cell incubators.

Cell cultures are usually distinguished in “primary cultures” and “cell lines”. “Primary cultures” refers to the culture of cells isolated from the original tissue or body fluids and placed into an *in vitro* system. The shorter the is time between cell isolation and their use,

the lower the risk is of introducing artificial artifacts, and the higher the possibility is to accurately reproduce the mechanisms occurring *in vivo*. Therefore, primary cultures are considered the method of choice for studying many biological mechanisms. However, obtaining primary cell cultures is not easy, as it relies on 1) access to human primary material, 2) enough tissue/body fluids to set-up a culture, 3) good communication with surgeons and pathologists to ensure good preservation of the specimen, and 4) fast processing from the surgical excision to the culture set up. Depending on the application and tissue availability, primary cells might not be used immediately, but instead kept for long-term cultures. In that case, continuous cell proliferation is needed. Healthy cells and low-grade tumor cells undergo senescence processes during cell division, that ultimately lead to cell apoptosis. Therefore, healthy cells and low-grade tumor cells need to be artificially manipulated to become "immortalized". Examples of artificial manipulation to force cellular self-renewal *in vitro* are transfection with viral genes promoting cell cycle progression (SV40 T-antigen, adenoviral genes E1A and E1B, HPV E6/E7 genes), induction of TERT enzyme expression (hTERT) and induction of spontaneous mutations by long-term passaging. On the other hand, stem cells and high-grade tumor cells do not need artificial manipulation to sustain proliferation. Stem cells have unlimited capacity to self-renew before becoming committing to a certain differentiation path (once they do that, they also lose their stem cell status). Tumor cells usually carry mutations in the genes controlling cell proliferation, senescence and apoptosis, which make them self-renewing for long-term even *in vitro*. Cells that have been maintained in cell culture for long-term and have undergone multiple sub-cultures are defined cell lines. Examples of *finite cell lines* are cultures of fibroblasts, which can double up to 70 times before undergoing apoptosis. Human cervical cancer cells HeLa are a good example of a *continuous cell line*, isolated in 1951 and still largely used for multiple research applications.

As they do in our body, different cell types show heterogeneous behaviors *in vitro*. Some cells are maintained simply floating in the cell culture media, and they are commonly defined "suspension cell cultures". Lymphocytes are typical examples of cells growing in suspension, which reflects their behavior in the blood stream. However, cells obtained from most tissues grow as "adherent cells". As the name indicates, adherent cells need to attach to a proper substrate to function properly. Typical examples of adherent cells are those with epithelial, mesenchymal and neuronal origin. The tendency to adhere to a substrate is directly linked to the cell function in the original tissue, and it is caused by the expression of adhesion molecules on the cell surface. For instance, adhesion molecules and extracellular matrix (EMC) are the main drivers of cell polarity and specialization in the epithelium, as well as differentiation and migration in mesenchymal tissues. There are

different ways to recreate substrates for adherent cells *in vitro*, and the choice of which one to use depends on the research application.

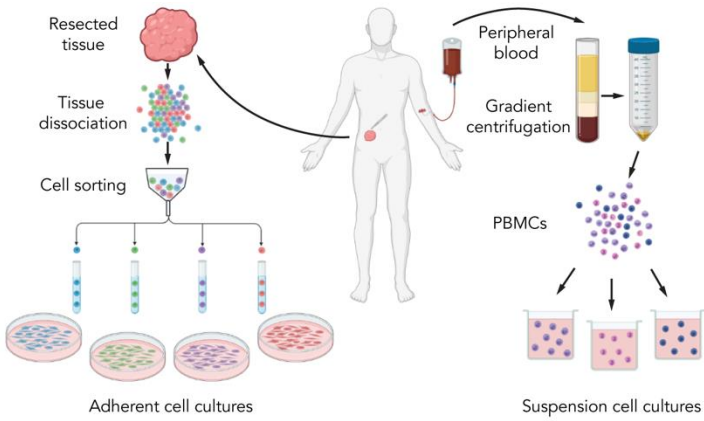

Figure 4.1: A typical workflow to obtain adherent and suspension cell cultures. Left panel: adherent cell cultures can be obtained from resected tissues, after enzymatic or mechanical dissociation. Cell sorting can be performed to separate different cell lineages. Adherent cells are cultured in petri dishes or tissue flasks. Right panel: cell suspensions are typically obtained from peripheral blood after a procedure called gradient centrifugation, which separates the blood into different components, such as plasma and platelets, peripheral blood mononuclear cells (PBMCs), and erythrocytes. PBMCs can either undergo an additional step of cell selection or being directly cultured as suspension cells.

4.1.2 2-dimensional and 3-dimensional cell cultures

Historically, glass surfaces were the first substrates used for cell cultures. Glass presents some advantages: 1) it is transparent, allowing to check the status of cells by conventional microscopes, 2) it is inert and impermeable, therefore it does not interact with cells and compounds, 3) it can be sterilized by autoclaving or chemical products, ensuring an environment free from contamination, as well as the possibility to re-use the same surface. However, not all cell types adhere to glass. Solutions to overcome this problem include oxygen plasma treatment and coating. These steps enhance cell adhesion to glass by 1) increasing the number of electrostatic interactions occurring between glass surface and cell membrane, and 2) activating integrins and other ECM receptors, simulating *in vivo* interactions with the extracellular space.

While glass is still used with imaging, cell cultures are mainly carried out on plastic surfaces nowadays. Specifically, oxygen plasma-treated polystyrene surfaces in combination with serum-supplemented culture media efficiently support cell adhesion. ECM coating can still

be applied for cells that adhere weakly directly to plastic. The main advantages of plastic are that is cheap to produce and disposable. Even if being disposable has negative implications for the environment, it improves the safety of laboratory employees, reducing the risk of direct exposure to hazardous compounds (chemotherapeutic drugs, cell labeling dyes, strong immunomodulators) while cleaning and re-using the materials. Polystyrene is also transparent, allowing cell imaging. Multiple shapes and dimensions of plastic surfaces are available for cell culture, such as multi-well plate, petri dishes and T-flasks. Other materials that have been demonstrated to be suitable for adherent cell growth include polydimethylsiloxane (PDMS)[369], cyclo-olefin polymer (COP)[370], polymethyl-methacrylate (PMMA)[371] and polycarbonate (PC)[372], which are especially used in the microfluidic field.

Independently from the material used, cells that adhere to the previously mentioned substrates tend to distribute as monolayers. Due to this behavior, they are commonly defined 2-dimensional (2D) cultures. 2D cultures are frequently used in research since they are easy to handle, not expensive and well compatible with wide range of assays. However, they are far from being representative of the original tissue. The function of a cell in a tissue is strictly dependent on its position in relation to the EMC and surrounding cells[373,374]. The composition of the ECM, cell-to-cell adhesion and mechanical stress contribute to cell proliferation, differentiation and migration[375–378]. Gas exchange and nutrient availability determine the fate of cells in tissues, shaping their metabolic program, migration and entry into apoptosis/necrosis[379–381]. Chemotactic gradients modulate the direction and dynamics of cell migration[382]. This combination of biomechanical and biochemical cues has significant implications for tumor progression, immunosurveillance and drug response[50,383]. Therefore, the possibility of reproducing them *in vitro* is essential for developing anti-tumoral strategies. Since 2D cultures show multiple limitations in this regard[384], other strategies for 3-dimensional (3D) cultures have been developed.

As the name indicates, 3D cultures aim to recreate the 3-dimensional architecture and chemical properties of tissues *in vitro*. They are characterized by multi-layered cellular composition, ECM deposition and gradients of pH, gases, and soluble factors. Therefore, they are superior for studying the mechanisms of tissue development and regeneration, as well as the properties of the solid tumor microenvironment, such as immune cell infiltration, tumor cell migration, drug efficacy and immune cell activity in hypoxic and necrotic regions, as well as immune cell and tumor metabolism[384–387].

A wide variety of techniques have been developed and optimized for routine use of 3D cultures in research. 3D cultures are commonly categorized into scaffold-based and scaffold-free cultures. In scaffold-based 3D cultures, a substrate is provided to simulate the properties of ECM and promote cell adhesion[388–394]. Such substrates are hydrogels or

porous implants that can be obtained from animals (e.g., fibrous gelatin, collagen, Matrigel, chitosan, hyaluronic acid, silk fibroin), plants (e.g., alginate) or synthetic production (polyethylene glycol, polylactic acid, poly-ε-caprolactone, polyurethans)[394–396]. Hydrogels of animal and plant origin have some limitations, such as batch-to-batch variability, susceptibility to fast cell degradation, and immunogenicity, therefore synthetic hydrogels are nowadays preferred[394–396]. Porous inserts are biodegradable and biocompatible scaffolds characterized by high surface area, capillary networks and specific pore size that support cell differentiation and vascularization. They are mainly applied in bone and myocardial tissue regeneration[397].

Scaffold-free 3D cultures relies on the formation of multicellular aggregates, such as cellular spheroids and organoids, promoting the adhesion of cells to other cells rather than to a substate. In fact, cell adhesion to any substrate is usually prevented in scaffold-free 3D cultures, while favoring cell-to-cell interaction and cell-driven ECM production is favoured[398]. Spheroids and organoids can be obtained passively using low-adhesion plates (e.g., agarose hydrogels and coating, poly-HEMA coating, micropatterned surface and ultra-low attachment plates) and gravitational forces (e.g., the hanging drop method), or actively, directly manipulating cell positioning. In the last case, acoustic, magnetic, and centrifugal forces can be used to increase the number of cell collisions and facilitate cell interaction[399–403]. While the term "spheroids" refers to unstructured cellular aggregates, the term "organoids" usually refers to 3D cultures composed of multiple cell types with specific localization and functions, resembling the composition and the organization of the original tissue[404]. Scaffold-free 3D cultures are low-cost and they guarantee high levels of reproducibility[384]. Their main applications include studies of solid tumor models, immune cell-solid tumor interaction and drug screening. However, most scaffold-free 3D cultures rely on 96-well or 384-well plates.

Figure 4.2: Illustrations of scaffold-based (left panel) and scaffold-free (right panel) 3D cultures.

4.2 ANALYSIS OF CELL PHENOTYPE, LOCALIZATION AND BEHAVIOR

Multiple methods of cell analysis have been developed during the years, and many are under development now. So far, the main strategies to understand immunosurveillance *in vitro* include:

1. Analysis of cell phenotype: the phenotype makes it possible to distinguish one cell type from another (red blood cell/lymphocyte, epithelial cell/mesenchymal cell) and provides information regarding the status of a cell (live/dead, naïve/activated/exhausted, healthy/tumoral)
2. Analysis of spatial distribution of cells: the localization of a cell is intrinsically connected to its biological function and interaction with other cells, and it also influences the efficacy of therapeutic treatments
3. Analysis of cell function: if cell phenotype and topology give us clues, functional assays can directly show the role of cells in heathy and pathological conditions

Phenotype, localization, and function can be analyzed at different levels, from gene expression to cell morphology and dynamics. The next chapters will cover the main techniques used in this doctoral work.

4.2.1 Principles of light interaction with samples

Most of the methods used in this thesis take advantages of, and try to deal with, the properties of light interaction with matter. Therefore, an introduction to such properties will be covered in this section. When a specimen is illuminated, incident light can be absorbed, scattered, or refracted, depending on its optical properties. When light is properly collected, these phenomena can provide information of the biological composition of a sample. For instance, the denser the granules of cells, the more the light is scattered from its original path. While many interactions occur already in unlabeled samples, treatments with dyes and fluorophores further increase the possibility of detecting biological variations. Fluorophores are small compounds, or functional groups within a molecule, that absorb and emit light at specific wavelengths. During the excitation phase, illumination with a specific wavelength (excitation wavelength) shifts the electrons of the fluorophore into a higher energy level. Such shift is transient, and the electrons quickly return to their energetic ground state. During this transition, energy absorbed in the excitation phase is emitted in the form of fluorescence (emission wavelength) and non-radiative transitions (mainly vibrational relaxation). Due to quick non-radiative energy dissipation in the excited state, the emission wavelength is usually longer than the excitation wavelength, and the energy difference is called Stokes shift. Fluorophores are commonly available for research applications in the form of fluorescent organic dyes, fluorophore-conjugated antibodies, fluorescent proteins

and quantum dots[405]. In addition, some biological samples, as well as drugs, are characterized by auto-fluorescence, which allow their discrimination even without the addition of dyes. Typical examples of auto-fluorescent biological components are hemoglobin, collagen fibers, and the tyrosine kinase inhibitor sunitinib.

Another important light behavior to consider is refraction. Light changes its speed and direction when travelling through the interface of two media with different refractive indices, and this phenomenon is called refraction. Each medium is characterized by a refractive index value, which describes how fast light moves in the medium. Specifically, the refractive index of the medium (n) corresponds to the ratio between the speed of light in vacuum (c) and thee speed of light in the medium (v).

$$n = \frac{c}{v}$$

Light sources used to guarantee adequate and specific sample illumination include lamps (mercury or xenon arc lamps, metal halide lamp, tungsten lamp)[406], light-emitting diodes (LEDs)[407] and lasers (argon-ion, krypton-ion, helium-neon, helium-cadmium, laser diodes and solid-state lasers)[408]. Similarly, different types of detectors collect the information from the sample, such as photomultipliers tubes (PMT), charge-coupled devices (CCD), complementary metal oxide semiconductors (CMOS), or "simply" our eyes. Such detectors have different features (dynamic range, quantum efficiency, linearity, signal-to-noise ratio, bandwidth), making them suitable for different applications.

Light can be used as a powerful tool for collecting biological information, and the following techniques are just a few examples of how this phenomenon can be exploited for research purposes.

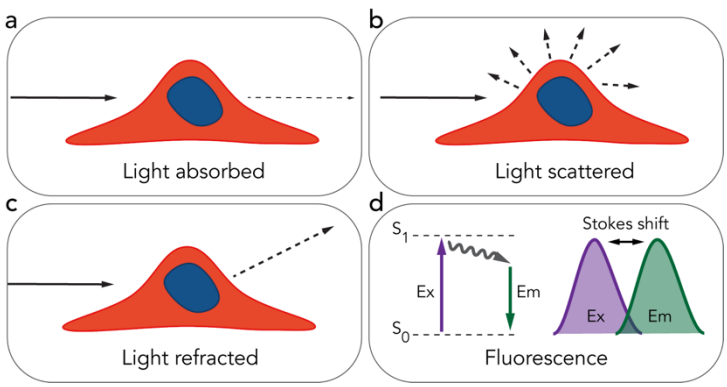

Figure 4.3: a-c. Light interacting with matter, such as cells, can be absorbed (**a.**), scattered in multiple and random directions (**b.**), or refracted in a predictable way (**c.**). **d.** Illustration of the main principles of fluorescence. The excitation wavelength (purple arrow) moves the electrons of the fluorophore from the ground energy state (S_0) to a higher energy level (S1). The energy gained is quickly released in the form of non-radiative energy dissipation (gray arrow) and emission wavelength (green arrow). The energy difference between the excitation and the emission wavelength is called Stokes shift.

4.2.2 Flow cytometry

Flow cytometry provides rapid, quantitative and multi-parametric single cell analysis, that allows characterization of cell phenotype and function (standard flow cytometry instruments) and physically sorting cells of interest (fluorescence activated cell sorting (FACS) instruments). Applications of standard flow cytometry include identification of cell types based on lineage markers, quantitative expression of membrane-bound, intracellular and intranuclear molecules, and analysis of cell proliferation and other functions. Flow cytometers can detect cells and particles within 0,2-150 μm in diameter, although specialized systems can allow detection outside this range. Flow cytometers are schematically composed by a fluidic system, an optical system, and electronics. The fluidic system consists of pressurized sheath fluid that, in combination with the sample fluid, transport cells from the sample tube through the instrument to a waste collection at the end. The cell suspension is injected in the system through a capillary, and differential pressure between the sample fluid and the sheath fluid causes hydrodynamic focusing, which aligns cells in the flow cell. Single cells are excited by the laser beams in the flow cell, also called interrogation points, and the emitted light is collected by detectors. The optical system is composed of lasers for excitation, detectors, and dichroic filters. The lasers are the excitation source. The detectors, usually PMTs, collect and amplify the emitted light. Dichroic filters allow the discrimination of the excitation light and detection of the desired signal. Finally, the electronics convert the optical signal into a digital signal. In a typical flow cytometry experiment, thousands of cells per second pass through the interrogation points, even if only one cell at the time is analyzed. The outputs are forward scatter (cell size), side scatter (cell granularity) and a wide range of fluorescent signals. Cell size is estimated measuring the magnitude of the laser light scattered by the cell in the forward direction. Granularity is estimated collecting the light scattered by dense intracellular vesicles on the side, using a detector located at 90° from the laser's path. The number of lasers, detectors and filter combinations determines how many parameters can be studied. The most recent configurations of commercially available flow cytometers can discriminate more than 30 different emitting fluorophores. It is therefore clear that the multi-parametric power of flow cytometry mostly derives from the ability to collect and differentiate a wide range of

fluorophores. Therefore, staining with fluorescent dyes and conjugated antibodies is usually performed prior to flow cytometry acquisition. In the presence of multi-color staining, fluorescence spillover into multiple detectors occurs, and spectral unmixing is performed to guarantee the attribution of detected signals to the right fluorophores. This process goes also under the name of signal compensation[408–410].

The main advantages of flow cytometry are being high-throughput and providing quantitative multi-parametric analysis of single cells. For these reasons, flow cytometry is widely used for studying tumor immunosurveillance, allowing to capture features of multiple cells in parallel without requiring prior physical cell separation. Typical assays include proliferation assays of both immune cells and tumor cells, the characterization composition and status of immune cells infiltrating the tumor, and analysis of functional parameters. Specifically for NK cells, functionality is indirectly derived by qualitative and quantitative assessment of cytokine production and granule content (IFN-ɣ, TNF-α, CCL3, perforin, granzyme B) and granule release (CD107a degranulation assay) in cell resting or stimulated by tumor cells or other signals. NK cell cytotoxicity can also be directly analyzed quantifying tumor cell death using live-dead discrimination dyes and designing proper cell gating strategies during the post-processing analysis. Additionally, the last developments in the field allow the quantification of soluble factors using antigen-capturing beads. However, flow cytometry lacks spatial and temporal resolution. Mechanical or enzymatic tissue dissociation is required prior to flow cytometry acquisition, as only cells dispersed in suspension can be analyzed. This passage takes away the spatial information of the original sample. Additionally, it can affect the cell behavior and expression profile, introducing technical artifacts. Such risk can be reduced by using mild dissociation agents and decreasing the time between the dissociation and the flow cytometry acquisition. Lastly, flow cytometry analysis is not optimal for following biological events over time since cells are lost at the end of the assay. For instance, the dynamics of NK cell killing of tumor cells over time can only be assessed by preparing multiple NK-tumor co-cultures, and analyzing each of them at different time, with technical variability affecting the robustness of the assay. Therefore, it is preferable to use flow cytometry for a single-timepoint experiment and use microscopy when spatial information and dynamics are part of the biological question.

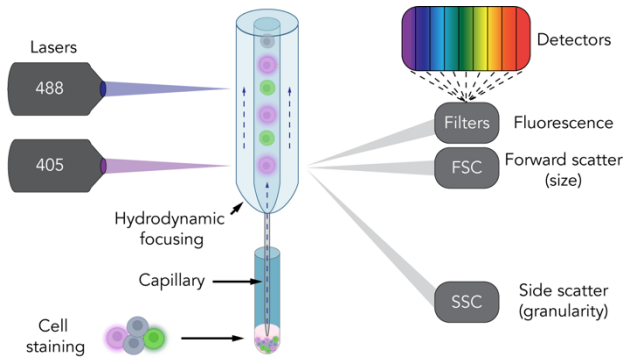

Figure 4.4. An overview of the main components of flow cytometry. Cells are usually stained in a tube, which is then placed in contact with the flow cytometry capillary. The cell suspension is aspirated through the capillary, and the differential pressure between the sheath fluid and the sample fluid creates hydrodynamic focusing. One cell at the time is illuminated by the lasers. Forward scatter detector measures light transmitted, proportional to the cell size. The side scatter detector measures light scattering, an indicator of cell granularity. Fluorescence emitted by the fluorophores passes through optical filters, which redirect the signal to the detectors.

4.2.3 Light microscopy

The term light microscopy includes a wide range of techniques that use light and optics to create magnified images of objects. Since the publication of *Micrographia* by Robert Hooke in 1665[411], light microscopy has contributed to countless biological discoveries over the years. Development of new techniques, and continuous improvement of old ones, keeps providing a deeper understanding of biological mechanisms. Depending on the application, many types of microscopes are available for biological research, each characterized by specific designs. Illumination is provided by a light source and directed to the sample by a series of mirrors and lenses. Then, the light is collected by the objective and redirected to an ocular or detectors, where it is converted to an image. In a transmission microscope, the sample is illuminated and viewed from opposite sides (Figure 4.5a). In epifluorescence microscopes, both the illumination and detection light passes through the same objective. Objectives are available with different magnifications (1.25x to 150x), NA (0.04 to 1.7), correction for optical aberrations (achromat, plan, apochromat) and immersion medium (air, water, glycerol, oil). Two different microscope configurations are available, namely up-right (Fig.4.5b) and inverted (Fig.4.5c). The two differ in the disposition of objectives in relation to the sample. In up-right microscopes, the objectives are placed above the sample, and the opposite is valid for the inverted microscopes. In addition to such basic features, each microscopy technique presents its own implementations, setup, and specific applications.

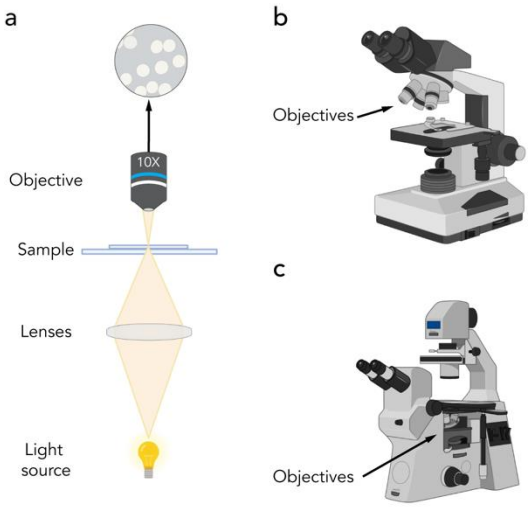

Figure 4.5: a. An overview of the main components of a transmission microscope. A source generates light that is redirected to the sample through a series of lenses. The objective captures the light emitted by the samples. Differences in the amount of light absorbed by the sample and the medium generate a brightfield image. **b.** An example of up-right microscopes, where the objectives are positioned above the sample. **c.** An example of inverted microscope, where the objectives are positioned below the sample.

The concept of refractive index was briefly mentioned in the introduction of this chapter. The refractive index value has important implications in imaging, influencing the resolution of optical microscopes. Resolution is commonly used to describe the ability to distinguish two closely-spaced emitting points in an image generated by an optical system. The image of an emitting point in the objective focal plane shows a specific light distribution, also known as Point Spread Function (PSF) (Fig.4.6a). The size and shape of the PSF correlates to the resolving power of an optical system: a smaller PSF corresponds to higher resolution. According to the Rayleigh criterion, the minimal distance between two optically separable points in a light microscope is:

$$r_{xy} = \frac{0.61\lambda}{NA}$$

$$r_z = \frac{2\lambda}{NA^2}$$

where r_{xy} and r_z are lateral and axial distances, respectively, and λ is the emission wavelength. *NA* is the numerical aperture of the objective, and it describes the capacity of the objectives to collect light[405,412]. Specifically:

$$NA = n \sin(a)$$

where *n* is the refractive index, and *a* is half the angular aperture of the objective. Therefore, the higher the refractive index of the immersion medium of the objective, the higher the capacity of collecting information, and the higher the resolving power of the optical system. On top of these consideration, the sample itself can contain multiple sources of optical imperfections, also called aberrations. The most common one is spherical aberrations, which can be caused by refractive index mismatch between the objective immersion medium and the sample embedding medium (Fig.4.6b). Spherical aberrations affect the shape of the PSF, causing considerable loss of resolution. Since spherical aberrations increase deeper into the sample, refractive index mismatch affects our ability to retrieve correct information especially while imaging thick samples [405,412]. The combination of the optical system and the sample preparation ultimately defines the quality of the imaging data. In the next chapters, we will examine the specific imaging techniques relevant for the thesis: brightfield microscopy, widefield fluorescence microscopy, confocal microscopy, and light-sheet microscopy.

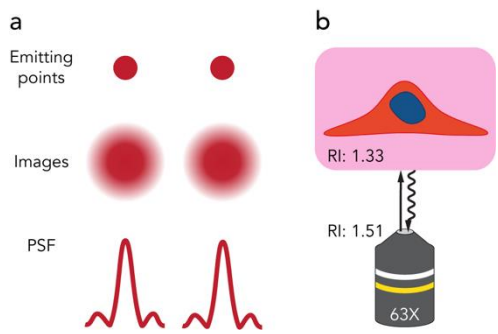

Figure 4.6: a. Illustration of two emitting points, such as two fluorescent proteins in a biological sample, and their image in an optical system. The blurriness can be mathematically expressed by the Point Spread Function (PSF), which defines the resolution capacity of optical systems. **b.** A schematic example of refractive index mis-match between the objective immersion medium (in this example, an oil objective) and the sample embedding medium (in this example, cell culture medium). RI: refractive index.

4.2.3.1 Brightfield microscopy

Brightfield microscopy is one of the most popular imaging techniques, available in almost any laboratory. Its principles have been partially described in the previous sections. White light from an halogen lamp is directed to the specimen, which absorbs part of the signal. The degree of adsorption depends on the composition of the sample. This process reduces the intensity of the light that reaches the objective, forming shades and dark patterns that are translated into an image. In basic microscopes, the task of detection is usually assigned to human eyes looking through the eyepieces. More advanced microscopes are also equipped with brightfield illumination, which can be detected both by the eyepieces and

cameras/PMTs. Despite being considered a quite basic techniques, brightfield imaging provides enormous biological information. Cell size, shape and granularity allows identification of cell types without the use of additional dyes. For instance, erythrocytes can be detected for their typical biconcave shape, since light propagates better through their center due to the absence of nucleus. Similarly, melanocytes can be spotted in the epithelium because of the light absorbing properties of melanin, and necrotic spheroids can be discerned by healthy ones due to their darker core. Unfortunately, brightfield imaging per se has low contrast. To improve contrast, the specimens can be pre-treated with fixatives and dyes. Sample staining combined with brightfield imaging allows the visualization of cellular subcomponents and extracellular matrix for instance. Typical staining used for this purpose are hematoxylin/eosin staining (acid-basic components), periodic acid-Schiff staining (complex carbohydrates), Van Gieson's staining (connective tissue), Giemsa staining (blood components), etc. This method constitutes the foundation of histology, which contributed to understand cell functions and tissue organization, and it is still nowadays an important diagnostic tool. There are also other methods that improve the contrast, which are worth mentioning as they usually complement standard brightfield microscopes and more advanced microscopes. Those are differential interference contrast (DIC) and phase contrast microscopy. Many biological components do not absorb light, but they can slow it down because of variations of their refractive index or thickness compared to the surrounding components. Those variations are not visible with brightfield imaging, but they can be captured using DIC and phase contrast imaging.

4.2.3.2 Widefield fluorescence microscopy

Widefield fluorescence microscopy takes advantages of fluorescence to improve the contrast, allowing the discrimination of multiple biological components. Strong sample illumination is usually provided by LED lamps or arc burner lamps, such as mercury and xenon arc lamps. Before reaching the sample, light passes through an excitation filter or a dichroic beam splitter that select the proper excitation wavelength. Most fluorescence microscopes use the epifluorescence strategy where the excitation light illuminates the sample through the objective, which also collects the light emitted by the fluorophores. The emitted light passes through an emission filter, which selects the emission wavelength of the fluorophore of interest. The signal is then detected by a CCD or CMOS camera, which transforms the signal into a digital image. Most fluorescence microscopes combine detection of transmitted light (by brightfield, phase contrast or DIC) with fluorescence, allowing multi-parametric analysis of the specimen. The number of fluorophores detectable depends on the combination of excitation and emission filters, however most of the filter combinations available do not allow more than 4 to 5 different colors. The image acquisition

is usually fast, making it possible to capture the details of biological processes over time. For this reason, widefield fluorescence microscopy is widely used for live imaging. In addition, the technique is very photon efficient, allowing the detection of dim samples.

In widefield imaging, the light source illuminates the entire specimens, and the detectors receive transmitted and emitted light from the entire field of view. This results in the detection of background signal, which decreases resolution and contrast, and significantly limits the possibility of performing 3D imaging. To represent details of the sample more accurately, deconvolution can be performed. Deconvolution is a post-processing analysis that uses the PSF for reassigning the proper signal to the correct emitting point. It is based on the concept that, if we can describe how emitting points are mis-shaped by the lenses (and that we do with the PSF), we can use the same description (the PSF) to recreate the real object. This process in quite elaborate, and small distortions in the PSF can seriously affect data interpretation. Therefore, when the biological question requires high-resolution 3D imaging for being answered, confocal or light sheet microscopy should be considered instead.

4.2.3.3 Confocal microscopy

Confocal microscopy shares a few features with widefield fluorescence microscopy, such as epifluorescence illumination, use of fluorescence to improve contrast, possibility of being complemented with brightfield/phase contrast/DIC, and possibility to perform live imaging when equipped with a proper incubation system. However, confocal microscopy differs significantly from widefield techniques in the illumination used for the excitation. The light source is a laser, which is responsible for creating a point-scanning illumination. The excitation light travels through the excitation filters, before being focused onto the specimen by the objective. The objective collects the emitted fluorescent light, which passes through the emission filters and a pinhole before reaching the detectors. The pinhole excludes a significant part of fluorescence emitted by points above or below the focal plane. The diameter of the pinhole can be adjusted: while a small pinhole should be used for higher axial resolution, larger sizes can be used when signal is too low. The confocal design allows imaging selected *xy* regions within the sample (through point-scanning) and exclude the background signal (through the pinhole). These features dramatically improve the signal-to-noise ratio compared to widefield fluorescence microscopy and allow high axial resolution. In addition, the theoretical lateral resolution of the confocal system is slightly improved compared to widefield fluorescence microscopy, corresponding to:

$$r_{xy} = \frac{0.90\lambda}{2n(\sin \alpha)} = \frac{0.45\lambda}{NA}$$

To achieve optimal performance, highly sensitive photon detectors are used, such as PMTs. In the most recent versions of confocal microscopes, the filter sets and traditional PMTs have been replace with multichannel PMTs to allow multispectral imaging, increasing the number of colors that can be detected in a single experiment. Due to the aforementioned properties, confocal microscopy is the gold-standard method for multicolor high-resolution 3D imaging. However, confocal microscopy has few drawbacks, such as 1) the limited number of channels (colors) that can be imaged in parallel; 2) the exposure to high intensity laser irradiation can cause photobleaching and phototoxicity, which are particularly problematic for long-term imaging; 3) confocal 3D imaging is inherently slow, being sub-optimal for capturing fast biological processes; 4) high-NA objectives have short working distances, therefore optical sectioning at high resolution can be achieved only up to a few hundred μm from the coverslip. To overcome these issues, other techniques are rapidly expanding for 3D live cell imaging, and one of these is light sheet microscopy.

4.2.3.4 Light sheet microscopy

Light sheet microscopy is an imaging technique particularly suited for live imaging of thick samples, due to reduced phototoxicity, photobleaching and fast acquisitions. Phototoxicity and photobleaching are the main limitations of the previously mentioned epifluorescence techniques. For instance, in confocal microscopes, the signal is still generated from out-of-focus planes, even if it is filtered out from detection to collect only information from the focal plane. This problem is inherent to the design of epifluorescence systems, where a single objective is used for both illumination and detection. Instead, in light sheet microscopy, the excitation and emission paths are decoupled. Two objectives placed at 90° from each other are separately used for illuminating the sample and detecting the signal. The illumination objective focuses a sheet of light (a few micrometers thick) to the focal plane of interest, and the detection objective collects light from the excited focal plane. Using this design, only the focal plane of interest is illuminated, reducing both photobleaching and phototoxicity. In addition, since the whole focal plane is illuminated, the acquisition is dramatically faster than point-scanning confocal imaging. The collection of emitted light is detected by standard widefield detectors, such as CCD or CMOS cameras[413,414]. The light sheet axial resolution is defined by the thickness of the light sheet and the objective NA. Thick samples which cause large light scatter are challenging to image even in light sheet systems. In those cases, light sheet microscopy can be performed using multi-view acquisition, i.e., imaging the sample from multiple angles and combining the information during post-processing[413]. These features make light sheet microscopy

widely used for imaging fast biological events occurring in thick samples, such as cell division in tumor spheroids[415], embryogenesis of *Drosophila melanogaster*[416] (common fruit fly) and *Danio rerio*[417] (zebrafish), and neurodevelopment of *Caenorhabditis elegans*[418] (nematode). Like every technique, also light sheet microscopy presents its own disadvantages. The preparation is quite laborious and not compatible with high throughput analysis. The sample is commonly embedded in hydrogel in order to be maintained in a vertical orientation during imaging. Typical mounting hydrogels are 1.5% agarose, although collagen and Matrigel can be used for specific applications. The agarose-embedded sample is then maintained in a chamber filled with cell culture medium to provide nutrients and stable culture conditions during long-term imaging. The embedding medium can be used alone or supported by fluorinated ethylene propylene (FEP) capillaries. 1.5% agarose and FEP tubes refractive indexes match the refractive index of water, which minimizes refractive index mismatch along the light path. For the same reason, water dipping objectives are commonly used. The embedding procedure can be quite laborious, and it can affect sample viability. In addition, some embedding media are not compatible with all cell types. Finally, a typical light sheet microscopy experiment generates massive amount of data, which are time consuming to transfer and process, and requiring high computational and storage capacity. Eventually, the speed gained during imaging can be easily lost during the post-processing phase.

In conclusion, light microscopy is an invaluable tool for gathering information regarding the spatial distribution of cells and molecules, as well as the temporal aspect of biological processes. Even if multi-parametric analysis can be performed, the currently available microscopes do not exceed the simultaneous discrimination of 5-colors, still far from the 30-colors acquisition of flow cytometers. Therefore, combining multiple techniques might be needed to understand biological processes. High-content imaging requires efficient and automated analysis. Improvements in this direction have led to the development of automated fluorescence and confocal imaging systems, such as Incucyte and ImageXpress, but further upgrades are needed to combine high-throughput analysis and high-resolution detection.

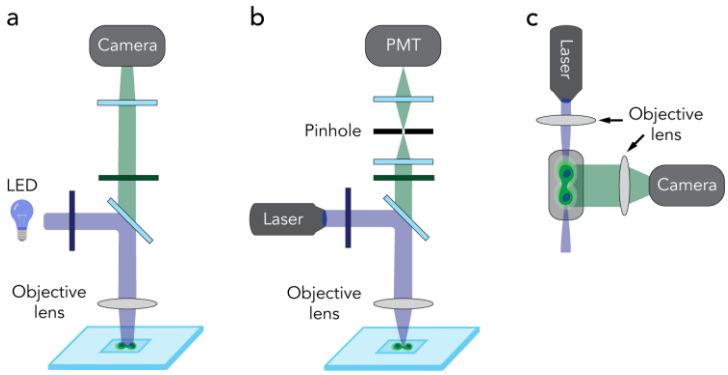

Figure 4.7: a-c. A schematic comparison between the light paths of a fluorescence widefield microscope (**a.**), a confocal microscope (**b.**) and a light sheet microscope (**c.**).

4.3 SAMPLE PREPARATION

Sample preparation refers to the sequence of steps preceding the analysis of the sample. We have briefly mentioned the importance of not introducing experimental artifacts, as they can negatively affect the data interpretation. Even if artifacts can occur while performing flow cytometry or imaging, most of them are associated to improper sample preparation. Sample preparation differs depending on the application. A single cell suspension is needed for flow cytometry, therefore adherent cells or tumor spheroids should be treated with enzymatic solution, such as trypsin-EDTA, accutase, collagenase or accumax, before proceeding with sample staining. Sample staining for flow cytometry consists of incubating single cell suspension with fluorophore-conjugated antibodies specific for the markers of interest, or fluorescent dyes. The incubation is rather short (usually no more than half-hour), carried out at low temperature and in the presence of FBS or bovine serum albumin to reduce the background signal. Sample fixation can be performed if more than a few hours elapse between the sample preparation and data acquisition. In addition, sample fixation combined with permeabilization is performed for intracellular staining. In case of cytokine quantification, pre-treatment with monensin or brefeldin A is recommended to prevent cytokine secretion during the assay and consequent underestimation of their levels[419].

Similar protocols are used before imaging the sample, with a few adjustments. For instance, tissue dissociation is not performed, as gathering spatial information is the scope of the assays. Fixation, permeabilization and staining follows the same steps as in flow cytometry, however the incubation time varies depending on the thickness of the sample. The thicker the sample, the longer the time needed to ensure complete and homogeneous distribution of

reagents. To facilitate the reagent penetration through thick specimens, it is common to perform tissue staining at room temperature or 37°C.

4.3.1 Tissue clearing

We have previously discussed how illumination patterns and detection strategies can improve optical resolution. However, none of the techniques mentioned completely solve the problem of light scattering and refraction within the sample. These phenomena dramatically reduce the amount of light collected by the detectors and is particularly evident in thick biological samples. Multiple biological components, such as lipids and dense protein structures, have high refractive index. Tissue clearing partially solves this issue by reducing the refractive index mismatch across the specimen. The procedure consists of dehydrating the sample and exposing it to solvents, or aqueous solutions, with high refractive index. Specifically, sample dehydration can be performed with methanol or tetrahydrofurane (THF), which remove water and clear lipids. This step can be followed by treatments with high-refractive index solvents, such as benzylbenzoate/methylsalicilate (Spatleholz method), benzylalcohol/benzylbenzoate (BABB method), dichloromethane/dibenzylether (3DISCO), dichloromethane/dibenzylheter (iDISCO). Since these solvents are quite toxic and can induce tissue shrinkage and loss of fluorescence, aqueous solutions are usually preferred, such as glycerol, iohexol (Omnipaque, Histodenz), thiodiethanol (TDE), fructose/thioglycerol/urea (FRUIT method) or formamide-formamide/PEG (ClearT and ClearT2 method). Other clearing techniques merge dehydration and lipid removal in a single step. For instance, CUBIC protocol uses of high levels of detergent (Triton X-100) to remove lipids, and urea with glycerol to partially denaturate hydrophobic regions of proteins that contributes to light scattering. The CLARITY protocol instead consists of embedding the sample directly in hydrogels, followed by a long incubation with detergents (SDS) and immersion in clearing solutions such as TDE and Histodenz. At the end of the tissue clearing process, the specimens are almost transparent, and the quality of 3D imaging is dramatically improved. Protocol optimization and the development of new methods is rapidly expanding its use to multiple research applications, such as spheroids, organoids and primary tissues[420,421].

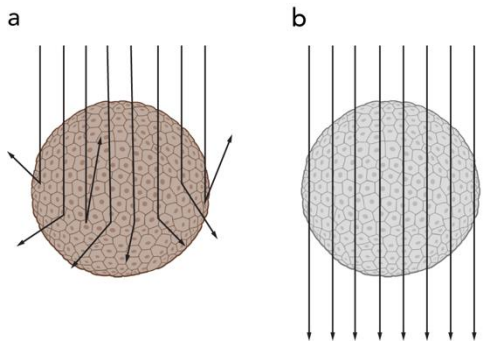

Figure 4.8: a. A schematic illustration of the effect of light scattering and refraction, which reduce both the excitation and emission signal through thick samples. **b.** Tissue clearing removes biological components with high refractive index and reduces the overall refractive index mis-match along the light path. The sample is now homogeneously illuminated, and the emission light can be properly collected by the objective lenses.

4.3.2 Tissue expansion

Expansion microscopy is another strategy available to improve the detailed visualization of biological samples. It is primarily a type of sample preparation that combines tissue clearing with physical tissue swelling. In other words, the sample itself is enlarged before imaging, providing both physical and optical magnification. The passages to obtain tissue expansion includes conventional fixation, permeabilization and staining of the specimen, followed by Acryloyl-X SE treatment and hydrogel embedding (usually polyacrylate-co-acrylamide). Acryloyl-X SE reacts with the amines and facilitates the linkage of biomolecules to the hydrogel. This step is followed by hydrogel polymerization. Exposure to high-temperature and detergent, or proteinase K, induces protein denaturation and homogenizes the composition of the hydrogel-embedded sample. The hydrogel-embedded sample is then placed in water, where it undergoes ~ 4.5 x linear isotropic expansion. This method improves the resolution by physically by magnifying the sample and simultaneously making it transparent[422]. In iterative expansion microscopy (iExM), the procedure is repeated in multiple rounds, leading to ~ 20 x linear expansion[423]. One disadvantage of this method is the loss of signal consequent to reduced fluorophore concentration, which is proportional to the volumetric expansion (~ 90 x in a standard expansion protocol). Part of the signal is also lost during the hydrogel polymerization and denaturation. To overcome this issue, alternative methods have been developed where tissue staining follows hydrogel polymerization and denaturation. Still, not every molecule efficiently binds to the hydrogel, and it is not trivial to effectively quantify the degree of expansion obtained in each experiment[424,425]. These factors limit the use of tissue expansion to a few applications, and further method development is needed to fully exploit its advantages.

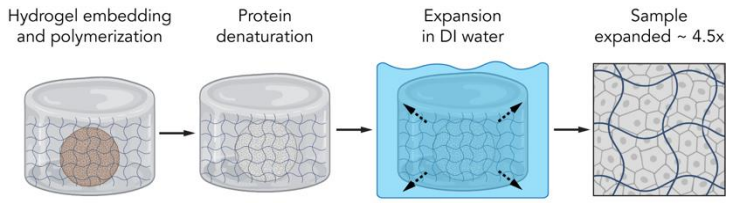

Figure 4.9: Illustration of the main steps of tissue expansion protocol.

5 DEVELOPMENT OF IMAGING-BASED METHODS FOR STUDYING CANCER IMMUNOSURVEILLANCE

Historically, the discovery of many immune cell types followed the observation of their functions. The impact of immune cell activity is connected to their localization. For instance, tumor surveillance by cytotoxic lymphocytes is dependent on their ability to reach and infiltrate the tumor tissue. Dynamics is also an essential parameter for immune cell function. Immune cell response is tightly regulated, and fully activated lymphocytes might gain an exhausted status with time. Lastly, the phenotypic analysis at single cell level is needed to link a function with a cell type. Phenotypic analysis also represents an essential tool for isolating the cell subsets of interest and use them for cancer therapy. In the following chapters, we will discuss several *in vitro* methods developed in our laboratories for studying localization, dynamics, and phenotype of NK cells in the tumor microenvironment.

5.1 MICROWELL CHIP DESIGN

Studying cell dynamics and location *in vitro* requires cell culture platforms compatible with live cell imaging and cell tracking. Most cells have migratory behavior that brings them outside the objective field of view during long-term imaging (Fig.5.1a) in conventional cell culture substrates. A strategy to facilitate cell tracking over time is confining the sample within a well. If the well dimensions fit the objective field-of-view, all the events occurring can easily be recorded without changing the sample positions or losing track of cells migrating outside the area of interest (Fig.5.1b).

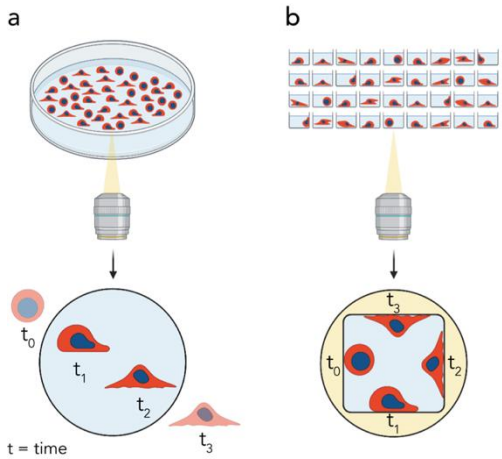

Figure 5.1: a. Live cell imaging in a standard cell culture plate. Events happening before (t0) a migrating cell enters, or after (t3) it exits the field of view (circle) are lost unless multiple positions are recorded. **b.** An example of live cells in microwells that fit the objective field of view. This strategy allows all the events in a well to be captured without moving the sample stage, shortening both imaging and post-processing time.

Our group have developed microwell chips optimized for cell culture and high-resolution live cell imaging, matching well design with biocompatibility and imaging requirements. The microwell chips consist of a thin glass layer, a silicon layer and a PDMS frame (Fig.5.2a). The borosilicate glass layer forms the bottom surface of the microwells, and it is as thick as a #1.5H coverslip (175 μm), making the chip compatible with high-resolution imaging. The microwell walls are made of silicon, which is bonded to the glass layer (Fig.5.2b). The PDMS frame provides the division of the microwell arrays in chambers (Fig.5.2a). Different shapes and number of wells can be etched in the silicon layer, depending on the application. For the work presented in this thesis, we produced two microwell chip designs: a single chambered (Fig.5.2c) and a multichambered microwell chip (Fig.5.2d). The single chambered chip contains a single array of 10x10 wells (Fig.5.2c), while the multichambered chip contains 16 arrays of 6x6 wells (576 wells in total) (Fig.5.2d). In both designs, each well is characterized by a bottom area of each well that is approximately 350 × 350 μm^2 and a depth of 300 μm (Fig.5.2b, 5.2e). The bottom area and the distance between wells make it possible to image an entire single well with a20x magnification objective, while nine wells can be simultaneously imaged with a 10x magnification objective (Fig.5.2e). The chip is also compatible with higher magnification objectives, such as 40x and 63x. Each well has a total volume capacity of 34 nL (Fig.5.2b). Such volume would evaporate quickly under standard cell culture conditions. Therefore, an additional liquid reservoir is provided by the PDMS frame bonded to the silicon layer. In the multichambered microwell chip, each chamber contains 58 μl of cell culture medium (Fig.5.2a). To maintain sterile conditions and reduce cell medium evaporation, a coverslip can be placed on top of the PDMS frame (Fig.5.2f). PDMS is permeable to gas such as O_2 and CO_2, allowing cell viability when gas exchange is prevented by the coverslip (Fig.5.2f).

The PDMS frame also provides physical separation between the 16 chambers in the multichambered microwell chip. The chip can be placed in a custom-made holder compatible with standard microscope stage inserts (Fig.5.2g). The single chambered and multichambered microwell chips not only differs in terms of number of microwells, but also in the number of conditions allowed to be tested in a single experiment. The single chambered microwell chip contains 100 wells all sharing the same liquid reservoir. This design allows a single cell culture condition but provides 100 replicates. In the multichambered microwell chip, 16 conditions can be tested simultaneously, and 36 replicates are available for each condition (Fig.5.2c, 5.2d).

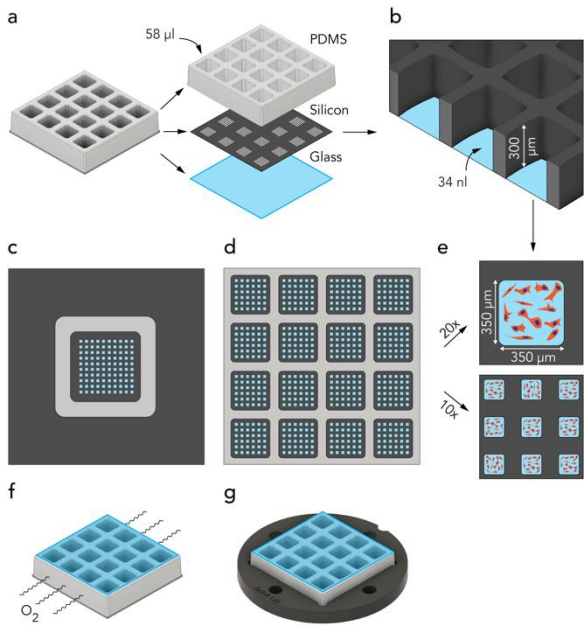

Figure 5.2: a. An illustration of the multichambered microwell chip composed of a glass bottom layer, a middle layer of silicon and PDMS on top. **b.** The silicon layer and glass layer are bonded together to provide the walls and the bottom of the microwells, respectively. **c, d.** A schematic representation of the single chambered microwell chip (**c.**) and multichambered microwell chip (**d.**). **e.** A single microwell (on top) or nine microwells (at the bottom) fit a standard 20x or a 10x objective field of view, respectively. **f.** PDMS is gas-permeable, therefore a coverslip can be placed on top of the PDMS to maintain sterility and prevent medium evaporation without compromising gas exchange. **g.** The microwell chip is placed in a costume-made chip holder fitting standard microscope stage inserts.

One of the main advantages of the microwell chip is that all the experimental phases (cell culture, staining and imaging) can be performed in the chip, which drastically reduces the risk of losing and/or affecting the sample integrity (Fig.5.3). Low-volume requirement facilitate to set-up cell culture when primary material is scarce. Other advantages are

compatibility with high-resolution imaging, live cell imaging and cell tracking. Finally, the chip can undergo multiple rounds of cleaning and sterilization, thus permitting it to be reused.

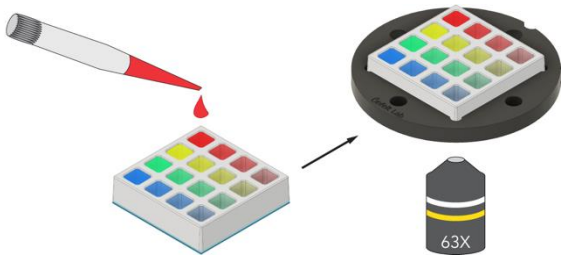

Figure 5.3: Cell culture, addition of treatments, staining and imaging can be performed in the microwell chip without moving the samples.

5.2 ULTRASONIC STANDING WAVE-INDUCED SPHEROID FORMATION IN MICROWELL CHIPS

Another advantage of the microwell chip is that each well can be used as an acoustic resonator. This property can be exploited to manipulate cell-to-cell interactions with ultrasound. Ultrasound is acoustic waves with frequency higher than 20 Hz. It has many biological applications, such as diagnostic tools (ultrasound imaging) and medical treatments (high-intensity focused ultrasounds). When the chip is exposed to ultrasounds, ultrasonic standing waves (USWs) are generated within each microwell. This phenomenon creates a pressure node and anti-nodes, where the waves reach zero and maximum amplitude, respectively. At the right frequency, the pressure node localizes in the central position of the microwell (Fig.5.4a), while the pressure anti-nodes are found at the well walls. When single tumor cells that are dispersed in cell culture medium are exposed to USWs, they are forced to the pressure nodes, i.e., focused to the central position of each well (Fig.5.4b). This phenomenon is called acoustic trapping and it can be used to induce an initial cell aggregation and cell-to-cell interaction (Fig.5.4c). Protein adhesion and ECM deposition following cell aggregation leads to the formation of stable tumor spheroids (Fig.5.4d). Therefore, ultrasonic standing waves can be used to induce spheroid cultures in the microwell chip. This method goes under the name of USW-induced spheroid formation, and it has been extensively used in papers I, II, III and IV.

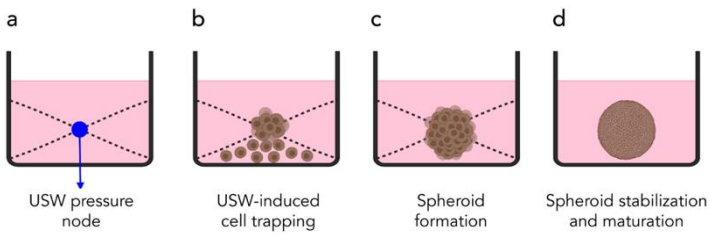

Figure 5.4: a. Ultrasonic standing waves (USW) generated in a silicon well. In the pressure node the amplitude is zero. **b, c.** Cells in suspension aggregates at the USW pressure node (**b.**), leading to the formation of a single spheroid in each well (**c.**). **d.** Once USWs are turned off, the spheroid settles, and assumes characteristics that are cell line dependent.

Ultrasound actuation is performed in a standard cell culture incubator using a custom-made USW set-up (Fig5.5). The USW device is composed of a ring transducer connected to a signal generator and amplifier. The microwell chip is placed on top of the piezoceramic plate, corresponding to the inner part of the ring transducer, and exposed to 2.47 ± 0.05 MHz central frequency and 15 V_{pp} amplitude for 24 hours. Within this time frame, cells firmly aggregate in the center of each well, generating one spheroid per well. Then the microwell chip is displaced from the USW transducer and maintained in the incubator for long-term culture or directly used in the microscope for live imaging.

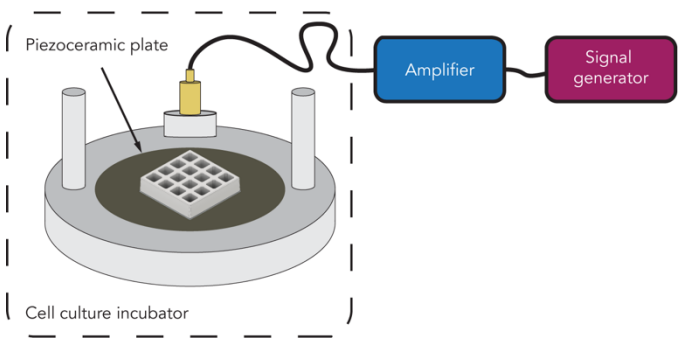

Figure 5.5: A schematic representation of the USW set-up.

In the first version of this method, the architecture and stability of the spheroid depended on the propensity of the cells to adhere to the glass bottom of the microwells once the USWs were turned off (Fig.5.6a). For instance, HepG2 hepatocellular carcinoma cells grew as hemi-spheroids anchored at the bottom of the wells (Fig.5.6a, 5.6b), and A498 and ACHN

renal carcinoma cells and LUTC-2 anaplastic thyroid carcinoma cells tended to spread on the glass bottom, quickly re-establishing 2-dimensional culture conditions (Fig.5.6a, 5.6c). The versatility of the USW-induced spheroid formation was improved in paper I, applying a thin layer of protein repellent coating to the well surfaces (Fig.5.6d). We used a biocompatible polymer (poly MPC-co-MPTSSi-co-MPTMSi) exhibiting long-term stability in aqueous solutions and good optical properties. The coating prevented cell adhesion to the glass, enabling the production of un-anchored, uniformly sized, and stable spheroids, without sacrificing the image quality (Fig.5.6e). The restrictions related to the cell type were abrogated, increasing the spectrum of possible applications. Furthermore, spheroids could now be collected and further analyzed by different techniques, such as flow cytometry (Fig.5.6f).

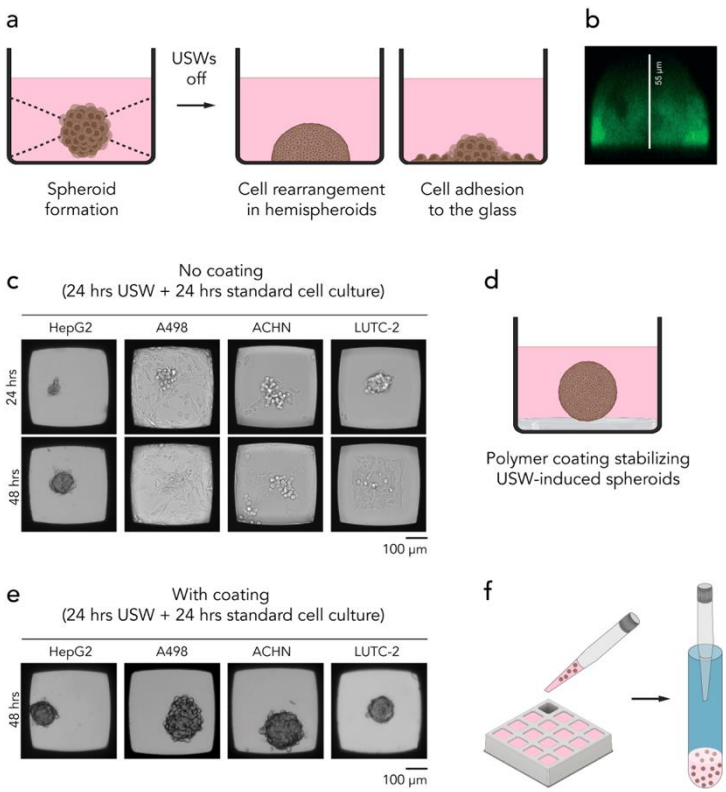

Figure 5.6: a. Most cell lines form spheroids once exposed to USWs, but some rearrange in hemispheroids or spread across the glass bottom when USWs are turned off. **b.** A typical HepG2 hemispheroid in a microwell. In

green: calcein green AM viability dye. **c.** Images of multiple cell lines exposed to USWs for 24 hours (upper panel) and left in culture without USWs for additional 24 hours (lower panel). In the absence of coating, cells quickly adhere to the glass bottom and re-establish 2D cultures. **d.** Strategy of applying a protein repellent coating to prevent cell adhesion to the microwells to maintain the 3D conformation stable over time. **e.** The efficacy of the coating strategy demonstrated with HepG2, A498, ACHN and LUTC-2 cell lines, which kept growing as spheroids once USWs were turned off. **f.** In the absence of cell adhesion to the glass bottom, spheroids can be collected from each chamber for further analysis.

5.3 BIOCOMPATIBILITY OF MICROWELL CHIPS AND ULTRASONIC STANDING WAVES

The standard workflow of cell culture in the miniaturized device consists of harvesting cells from standard cell culture flasks and plating them in the chip either as monolayers or USW-induced spheroids. The number of cells plated depends on the characteristics of the cell type (size and proliferation rate) and the culture conditions. On average, ~10-20 cells per microwell were cultured as monolayer, while ~250-500 cells per microwell were used for spheroid formation. In paper II, we demonstrated that the distribution of cells across multiple microwells and chambers was homogeneous, counting the number of A498 renal carcinoma cell nuclei in each microwell (Fig.5.7a-5.7c). Similarly, the area of USW-induced A498 spheroids was even across multiple microwells and chambers (Fig.5.7d, 5.7e). Since TMRM is a viability dye, these experiments also proved that cells were equally viable across the chip.

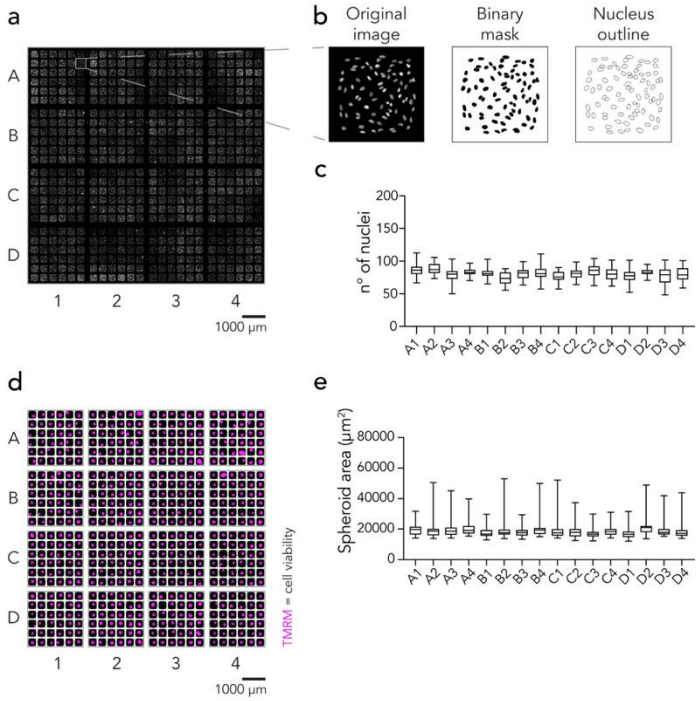

Figure 5.7: a. Nuclear staining in A498 cells after being maintained in culture overnight in the multichambered microwell chip (in grey: DAPI staining). **b.** Strategy used to count cell nuclei. From left to right: an example of a DAPI image from a single well, the corresponding binary mask, and nuclei outlines. A watershed algorithm was applied to separate adjacent nuclei. Automatic nuclei count was performed with ImageJ software. A similar post-processing workflow was used to calculate the area of spheroids. **c.** Numbers of cell nuclei in the wells for the individual chambers. Statistical analysis revealed no significant differences in nuclei number between wells and chambers. **d.** USW-induced A498 spheroids in the multichambered microwell chip after 48 hours culture (in magenta: TMRM viability dye). **e.** Spheroid area in the wells for the individual chambers. No significant differences were detected across microwells and chambers.

Long-term viability of both cellular monolayers and USW-induced spheroids in the microwell chip was further demonstrated in paper I, paper II, III and IV by both flow cytometry and microscopy. Those experiments consisted of both 24 hours and 48 hour of cell culture followed by live cell imaging up to 72 hours, and involved multiple cell lines, such as A498, NCHI-1975, HCC827, Kuramochi and OVCAR8 cells, as well as primary cell cultures. Thus, the microwell chip and the USW method fulfilled the requirements of homogeneous cell distribution, biocompatibility, and versatility. Next, we tested their performance in multiple biological applications.

5.4 APPLICATIONS OF MICROWELL CHIPS AND ULTRASONIC STANDING WAVES

5.4.1 High-resolution imaging of cellular monolayers and spheroids

Tissue culture plates are usually made of polystyrene, which is not an ideal material for high-resolution imaging. In addition, plates for spheroid culture are commonly coated with thick hydrogels, which further reduce the image quality. The combination of a glass bottom plate, cell confinement, and thin hydrogel makes the microwell chip ideal for high-quality deep tissue imaging. The applications are shown in paper I and II. In paper II, both culture and immunostaining of RFP^{+}-A498 renal carcinoma monolayers were performed directly in the multichambered microwell chip. Serial dilutions of primary and secondary antibodies were simultaneously tested to achieve optimal visualization of microtubules. Fixed dye concentrations were used to stain nuclei and actin filaments. Pre-screening with 10x objective was performed to evaluate the signal-to-noise ratio of each primary and secondary antibody combination (Fig.5.8). This step was followed by high-resolution imaging of the tubulin filaments in the chamber characterized by the best staining index. These data demonstrated the possibility of performing multicolor staining, fast screening and high-resolution imaging in the same experiment.

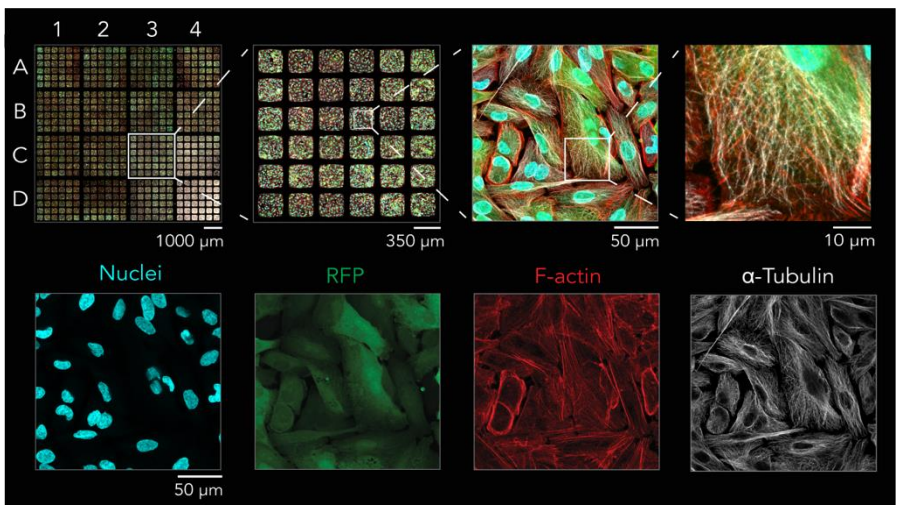

Figure 5.8: Screening and high-resolution imaging of tubulin staining. First row: composite images with increasing zoom and magnification. From left to right: mosaic image of the entire multichambered microwell chip, followed by a closer view of the entire C3 chamber (both acquired at 10x magnification), corresponding

to the best staining index. A single well of the C3 chamber imaged at higher magnification (40x objective) showing filaments and nuclei at the cellular level, followed by a cropped and enlarged view to visualize the same structures at the subcellular level. Second row: each fluorescence channel presented separately with nuclei (cyan), F-actin (red), RFP (green) and α-tubulin (grey).

High-quality imaging comes at the cost of slow acquisition and data processing. Combining fast-screening to select the sample to use for high-resolution imaging to gather detailed information dramatically decreases the duration of the assay and the amount of data. Large data set are usually generated by 3D imaging, so we tested whether the same image quality could be achieved with tumor spheroids.

In paper I, we performed high-resolution imaging of USW-induced renal carcinoma spheroids. After being cultured for 48 hours, the spheroids were fixed, permeabilized and incubated with anti-integrin β1 primary antibody for 20 hours. After extensive washing, the spheroids were exposed to the secondary antibody for 4 hours, followed by DAPI counterstaining for 1 hours. Staining buffer was replaced with the refractive index matching solution (Omnipaque 350, RI = 1.46) to make the spheroids optically transparent and minimize the refractive index mismatch with an oil-immersion objective (RI = 1.51). High-resolution visualization of integrin β1 across the entire spheroid volume was achieved by combining sample preparation for 3D imaging with confocal microscopy (Fig.5.9). The physical confinement facilitated rapid localization of optically transparent spheroids, thereby reducing the duration of the assay. It also prevented spheroid displacement during the acquisition, contributing to the final image quality.

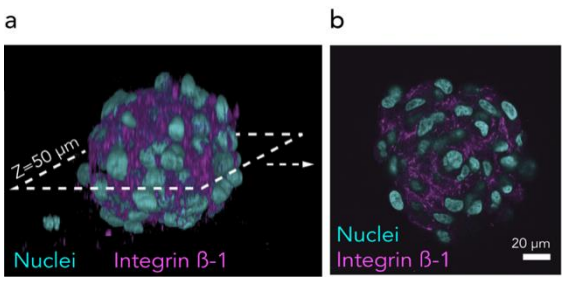

Figure 5.9: a. 3D composite image of the A498 spheroid stained with anti-integrin β-1 antibody (in magenta) and DAPI (in cyan). **b.** Visualization of integrin β-1 and nuclei in a single focal plane at the core of the A498 spheroid.

The sample preparation for deep-tissue imaging was further improved in paper II. Methanol-induced spheroid dehydration was introduced prior to permeabilization, to remove the lipid components and facilitate the antibody diffusion into the spheroid core. Such addition accelerated the immunostaining phase, decreasing both primary and secondary antibody incubation to 1 hour without compromising the image quality (Fig.10). This modified protocol was also used in paper III and paper IV.

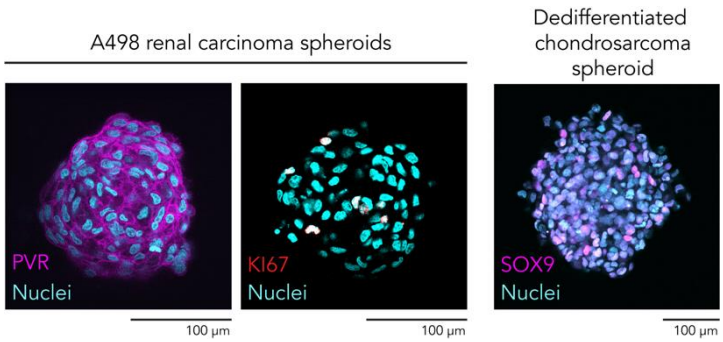

Figure 5.10: Examples of optimized staining protocol. Left panel: A498 spheroid stained for PVR (in magenta). Middle panel: A498 spheroid stained for KI67 (in red). Right panel: SOX9 (in magenta) in patient-derived dedifferentiated chondrosarcoma spheroid. In cyan: DAPI (nuclei).

5.4.2 Drug screening assays

In paper II we demonstrated that the multichambered microwell chip design is suitable for drug screening assays *in vitro*. The response of tumor cells to drug treatments was analyzed by live cell imaging, measuring the levels of TMRM (viability marker) and BioTracker NucView Caspase-3/7 (apoptotic marker) over time (Fig.5.11a).

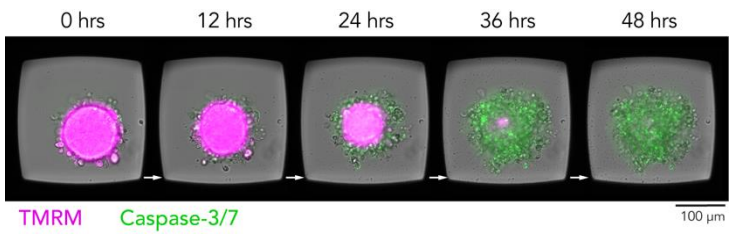

Figure 5.11: USW-induced HCC827 lung carcer spheroids were treated with gefitinib (10 µM) for 48 hours and the response was measured by live cell imaging, recording one image every 4 hours. Five representative timepoints are shown here. The response was measured as loss of viability dye (TMRM, in magenta) and acquisition of apoptotic marker (BioTracker NucView Caspase-3/7, in green).

For each microwell, we calculated the sample viability and the specific sample viability as follows:

$$Viability\ [\%] = \frac{TMRM_{\ t}}{TMRM_{\ t0}}$$

where $TMRM_t$ is the total intensity of TMRM in each microwell at timepoint (t), and $TMRM_{t0}$ is the total intensity of TMRM from the same microwell before the addition of the treatment. The viability is used to calculate the specific viability as follows:

$$Specific\ viability\ [\%] = \frac{Viability\ [\%]_{sample}}{Viability\ [\%]_{control}}$$

where the $Viability\ [\%]_{sample}$ (drug treatment) is the viability calculated in the chamber of interest and $Viability\ [\%]_{control}$ is the viability of the control chamber (DMSO). This equation is used to normalize the viability of the sample for the control (no treatment) at each timepoint.

Similarly, the apoptotic index was calculated as:

$$Apoptotic\ index\ [A.U.] = \frac{Caspase\text{-}3/7_t}{TMRM_{t0}}$$

where $Caspase\text{-}3/7_t$ is the total intensity of BioTracker NucView Caspase-3/7 in each microwell at timepoint (t), and $TMRM_{t0}$ is the total intensity of TMRM from the same microwell before the addition of the treatment. This equation is used to normalize the apoptotic index of the sample to the control (no treatment) at each timepoint as follows:

$$Specific\ apoptotic\ index\ [A.U.] = Apoptotic\ index\ [A.U.]_{sample} - Apoptotic\ index\ [A.U.]_{control}$$

where the $apoptotic\ index\ [A.U.]_{sample}$ is the apoptotic index calculated in the sample chamber of interest and the $apoptotic\ index\ [A.U.]_{control}$ is the apoptotic index of the control chamber.

We performed the first drug screening assay using cell monolayers. We exposed OVCAR8 ovarian cancer cells to increasing concentrations of paclitaxel for 72 hours, and we tracked the response by imaging the sample every 4 hours. Analysis of both specific viability and specific apoptosis analysis indicated that OVCAR8 cell death occurred at paclitaxel concentrations $\geq 1 \cdot 10^{-7}$ M (Fig.5.12a, 5.12b). The concentration response curve of the specific viability at 72 hours gave an inhibitory concentration (IC50) of $1 \cdot 10^{-7.8}$ M (Fig.5.12c). These results were in line with a control experiment performed with a standard CellTiter-Glo assay and previous publications.

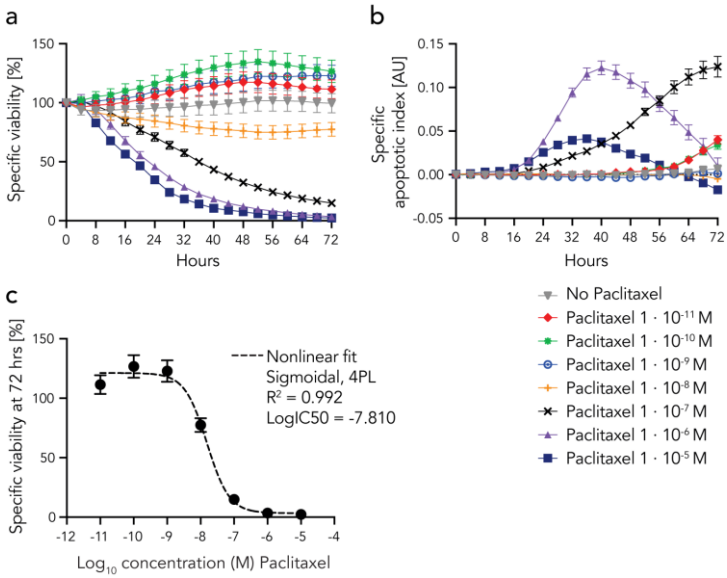

Figure 5.12: **a.** Time-course of specific viability of OVCAR8 cells exposed to different paclitaxel concentrations for 72 hours. **b.** Time course of the specific apoptotic index (arbitrary unit, A.U.). **c.** Specific viability after 72 hours for OVCAR8 cells treated with paclitaxel at increasing concentration fitted with the Hill equation to evaluate IC50. Dotted line represents the predicted curve with R^2 = 0.99, LogIC50 = -7.77 and H-value = 1.34.

To confirm the specificity of paclitaxel, we performed high-resolution imaging to visualize chromosome mis-segregation, which is a typical phenotypic abnormality induced by paclitaxel. Cells undergoing chromosome mis-segregation shows multiple microtubules spindle poles positioning in different directions (Fig.5.13a), instead of the classical bi-polar configuration occurring in a normal cell division (Fig.5.13b). Paclitaxel-treated cells showed up to five spindle poles, whereas control cells maintained the classical conformation (Fig.5.13c). The highest proportion of multipolar cells were observed for paclitaxel concentrations $\geq 1 \cdot 10^{-7}$ M (Fig.5.13d). These data confirmed the specificity of paclitaxel and further validated the live cell imaging assay.

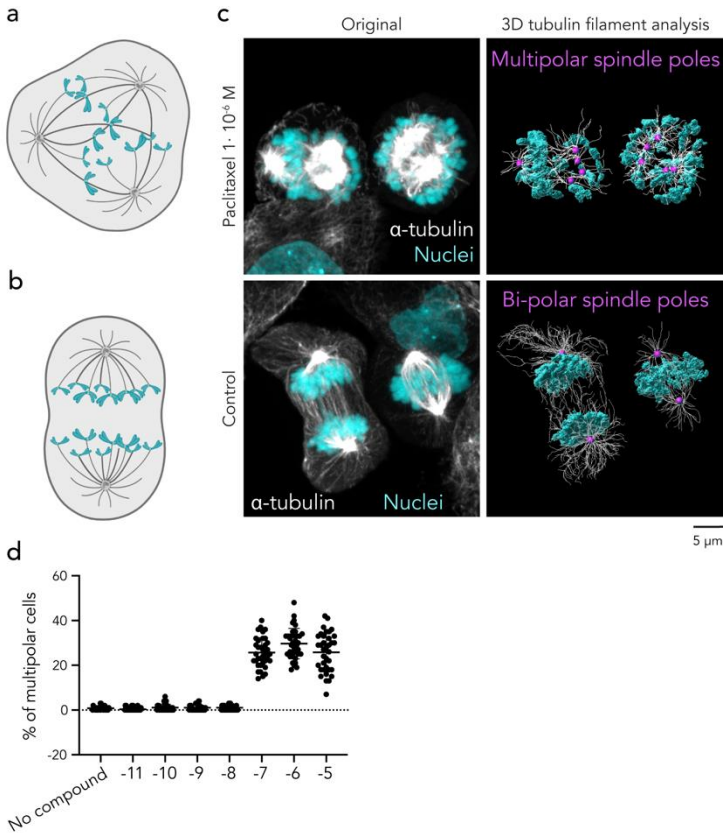

Figure 5.13: a. Representation of chromosome mis-segregation with multiple mitotic spindles forming in a single dividing cell. **b.** Representation of a normal cell division with bi-polar mitotic spindles. **c.** Confocal images of OVCAR8 cells cultured for 8 hours with $1 \cdot 10^{-6}$ M paclitaxel (upper panels) or without drug (lower panels). 3D rendering was performed in Imaris using conventional settings (left panel) showing microtubules (a-tubulin, gray) and nuclei (DAPI, cyan) or surface rendering with filament analysis (right panel) to visualize the poles of the mitotic spindles (dots in magenta). **d.** Fraction of multipolar OVCAR8 cell after 8 hours cell culture in increasing concentrations of paclitaxel (n=36 per concentration).

We used the same analysis for a multiplexed drug screening assay. Here, we exposed USW-induced spheroids to multiple anticancer treatments. Data from 2D drug screening and literature research were used to choose the combinations of cell lines and drugs, and as controls to validate our method. We picked four cell lines (HCC827, NCIH-1975, Kuramochi and OVCAR8) and three drugs (gefitinib, A-1155463 and paclitaxel) based on the following information: Kuramochi and OVCAR8 cells should respond to A-1155463 and paclitaxel, respectively, while HCC827 and NCIH-1975 cells to gefitinib. The sensitivity to gefitinib was predicted to be higher for HCC827 cells compared to

NCIH-1975 cells. DMSO was used as control (Fig.5.14a). The results of the live imaging assay performed in the multichambered microwell chip were in line with the predicted outcomes. In addition, other successful combinations of anticancer drug with cancer cell type were observed (Fig.5.14b). HCC827 spheroids were highly sensitive to gefitinib, whereas partial cell death was observed in NCIH-1975 treated with gefitinib. Kuramochi responded to A-1155463, whereas OVCAR8 responded to paclitaxel. In addition, NCIH-1975 and OVCAR8 showed sensitivity to A-1155463, whereas Kuramochi responded also to gefitinib.

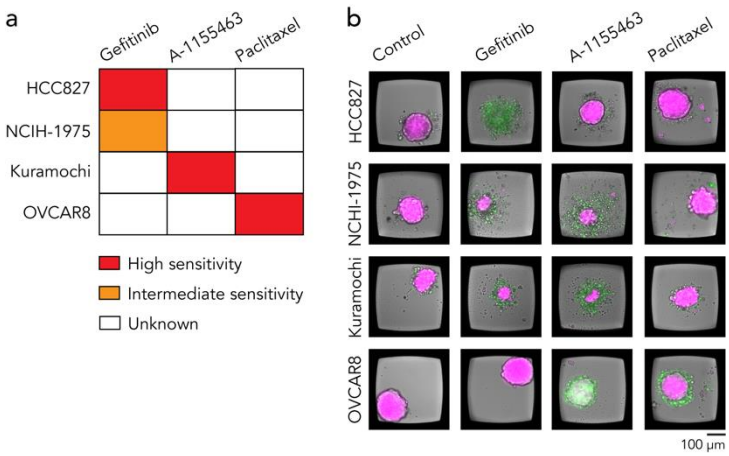

Figure 5.14: a. Schematic representation of the expected response of cell lines to drugs based on literature research and data from 2D drug toxicity assays. **b.** Images of representative wells showing spheroid viability after 48 hours from the addition of the drugs.

We evaluated the drug penetration by performing high-resolution imaging of optically cleared OVCAR8 spheroids after A-1155463 treatment. We observed homogenous caspase signals, indicating homogenous drug diffusion throughout the spheroid volume. These data showed how to apply the multichambered microwell chip to follow the dynamics of drug responses by live imaging. Moreover, we demonstrated that high-throughput analysis can be complemented with high-resolution deep-tissue imaging to obtain further information on drug efficacy and mechanisms of action.

5.4.3 NK cell-mediated spheroid killing assays

The cytolytic activity of NK cells against tumor cells was proven 47 years ago[38,39]. However, NK cell activity in the solid tumors is far from being well understood. In paper II, we performed an NK cell-mediated spheroid killing assay using the multichambered

microwell chip as both 3D culture system and live cell imaging platform. We cultured USW-induced A498 spheroids for 48 hours and we exposed them to IL-15 activated primary human NK cells for an additional 64 hours (Fig.5.15a). NK cells killed most of the tumor spheroids, as indicated by the loss of spheroid viability and increased apoptotic index over time (Fig.5.15b). Most of the tumor death occurred within the first 24 hours of the assay. However, the spheroid viability varied greatly across the 36 wells analyzed, with few spheroids almost unaffected by NK cell activity (around 70% of spheroid viability), and others almost completely dead (around 6-10% viability) (Fig.5.15c). Since NK cells were isolated from a single donor, such heterogeneity could be ascribed to intra-donor variability.

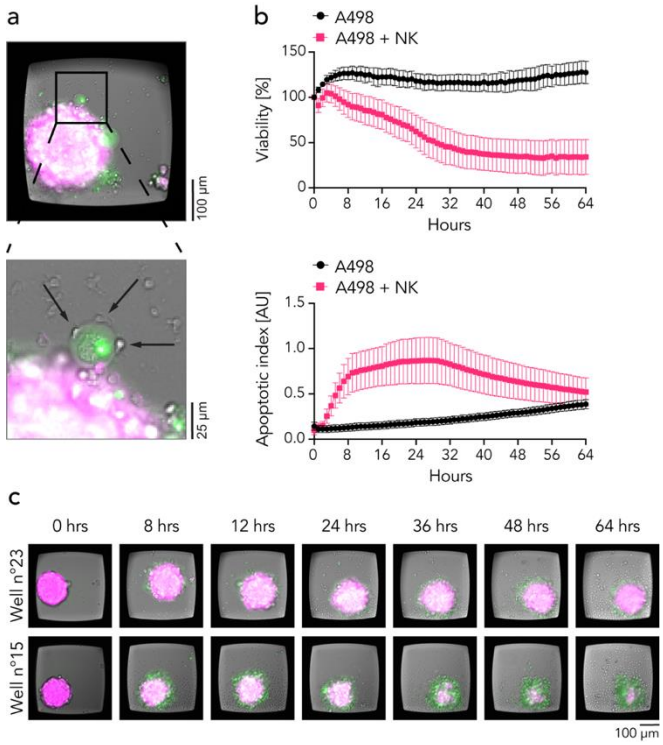

Figure 5.15: a. An example of NK cell interaction and killing at the periphery of A498 spheroid. **b.** Viability (upper panel) and apoptotic index (lower panel) plotted over time for A498 spheroids alone (black) or A498 spheroids co-cultured with NK cells (pink) (n=36). **c.** Time lapse sequences from two representative wells showing low NK cell-mediated killing (well n°23, upper panel) and high NK cell-mediated killing (well n°15, lower panel).

Combinatorial therapy is emerging as an effective strategy against cancer. In paper II, we applied the microwell chip to test combinatorial therapy *in vitro*. USW-induced OVCAR8

spheroids were exposed to IL-15 activated primary NK cells obtained from different donors, either in presence or in absence of A-1155463, cetuximab or paclitaxel. The efficacy was superior when NK cells were combined with the drugs compared to alone (Fig.5.16). Heterogeneity within the same donor (intra-donor variability) and between different donors (inter-donor viability) was detected, as we already observed with A498 spheroids. Inter-donor variability was reduced when combining NK cells with cetuximab.

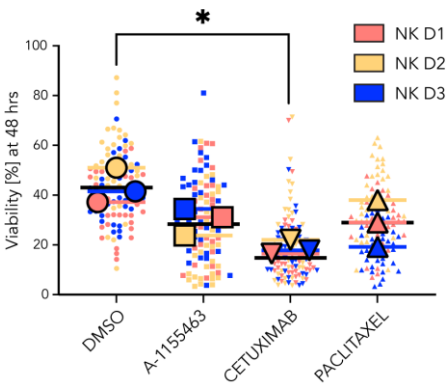

Figure 5.16: Dot plot showing the viability of each OVCAR8 spheroid (small dots) and the mean values for each donor (big dots and colored bars) after 48 hours from the addition of DMSO (circles), A1155463 (squares), cetuximab (inverted triangles) and paclitaxel (triangles) in the presence of NK cells from donor 1 (orange), donor 2 (yellow) and 3 (blue). Mean values from all donors are shown as black bars.

Nowadays, a lot of effort is focused in combining traditional treatments (radio-, chemo-, target therapy) with immunotherapy, to improve its efficacy in donors with innate or acquired resistance. Our experiments demonstrated the possibility to test the efficacy and to investigate the dynamics of cellular immunotherapy *in vitro*, either as a single agent or in combination with multiple drugs.

5.4.4 NK cell infiltration in tumor spheroids

The natural application of tumor spheroids in immunology is to analyse of immune cell infiltration. Compatibility with high-resolution imaging is still the main limiting factor for the use of spheroids for this purpose. In paper III, we used the microwell chip to quantify NK cell infiltration in tumor spheroids. We stained IL-15-activated primary human NK cells with CellTrace Yellow, a cytoplasmatic viability dye, and incubated them with USW-induced A498 spheroids for 3 hours. Then, spheroids were fixed, permeabilized and stained with the nuclear dye DAPI. These steps were followed by tissue clearing and confocal imaging (fig.5.17a). We recorded the position of NK cells throughout the spheroid volume, analyzing multiple spheroids for each donor. Image segmentation was performed during post-processing to divide the spheroid volume in three regions: spheroid surface, periphery, and core (Fig.517b). The periphery corresponded to the outer spheroid layer,

comprising cells located <15 μm from the spheroid surface. The spheroid core included the inner layer of cells located >15 μm from the spheroid surface. Data collected form three different donors showed that >50% of the NK cells were located at the spheroid surface (Fig.5.17c), strongly suggesting the need of strategies to improve NK cell infiltration in solid tumors.

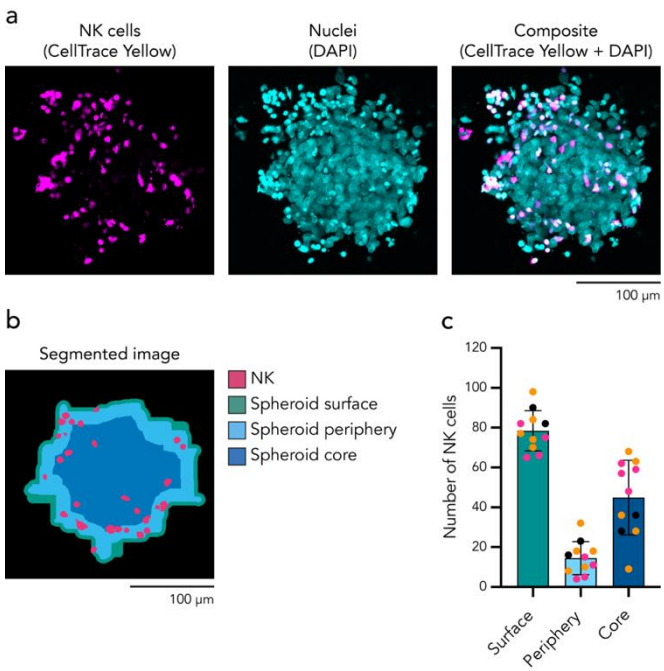

Figure 5.17: a. A representative image of IL-15 activated NK cells infiltrating A498 wt spheroids. After 3 hours co-culture, the samples were fixed and permeabilized before proceeding with staining and clearing. 3D maximum intensity projections of NK cells (left panel, in magenta), nuclei (central panel, in cyan) and the composite image showing both NK cells and A498 wt cells (right panel). **b. E**xample of image segmentation: the spheroid was divided in three regions: the surface (in teal), the spheroid periphery (<15 μm from the surface, in light blue) and the spheroid core (>15 μm from the surface, in blue). In magenta: NK cells. **c)** Number of NK cells residing in each spheroid region. Data obtained from 2 to 5 spheroids were averaged for each of the three donors (NK donors are indicated with different spot colors).

The method showed in paper III is useful for quantitative and qualitative analysis of NK cell infiltration into tumor spheroids. However, high-resolution imaging of the inner core of the spheroids is limited by the objective working distance. When the spheroid diameter goes beyond the limit, and long-working distance objectives are not available, other methods are needed to visualize NK cells activity in samples. Light sheet microscopy is particularly suitable for high-resolution volumetric imaging. In paper V, we proposed the combination

of light sheet microscopy and tissue expansion as an alternative option to achieve detailed visualization of spheroid-infiltrating NK cells. RFP$^+$ A498 spheroids were incubated with GFP$^+$ NK92 cells for 2 hours before undergoing tissue expansion. Immunostaining with anti-GFP antibody was performed after proteinase K digestion, to counteract the loss of GFP signal during the procedure. The sample were expanded in deionized water and imaged in light sheet microscopy The method allowed visualization of NK92 cells infiltrating the inner layers of the spheroid (Fig.5.18).

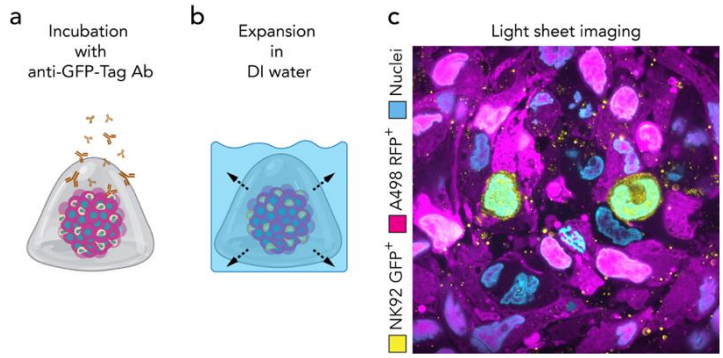

Figure 5.18: a. A498 RFP$^+$-NK92 GFP$^+$ co-cultures were incubated with anti-GFP-Tag antibodies after being embedded in hydrogel and treated with proteinase K, to increase the signal-to-noise ratio. **b, c.** Following the previous steps, samples were expanded in deionized water (**b.**) and imaging was performed by light sheet microscopy (**c.**). In yellow: NK92 GFP$^+$. In magenta: A498 RFP$^+$. In cyan: nuclei (DAPI staining).

This technique is suitable for imaging the details of NK cell interactions with tumor cells in thick samples, for instance to obtain snapshots of killing mechanisms, metabolic activity, or receptor modulation. However, the protocol is quite laborious and not compatible with high-throughput analysis.

5.4.5 Primary spheroid culture

Individuals respond differently to treatment. Assessing and understanding patient susceptibility requires experimental platforms that can reproduce the original tissue microenvironment *in vitro*. In paper IV, we cultured spheroid models of primary sarcoma in the microwell chip. Sarcomas obtained from surgical excisions underwent tissue dissociation and filtration to remove aggregates, debris, and necrotic tissue. Sarcoma cells were subsequently cultured in standard cell culture plates, to recover from the tissue treatment (Fig.5.19a). Tumor cells were identified by the formation of proliferating colonies with a standard transmitted light microscope. Sarcoma cells from culture passage 1 or 2 were then transferred in the microwell chip and exposed to USWs to obtain primary sarcoma

spheroids (Fig.5.19a). We obtained sarcoma spheroids from different subtypes and grades, such as leiomyosarcoma, cellular angiomyofibroma, low grade chondrosarcoma, dedifferentiated chondrosarcoma, undifferentiated pleiomorphic sarcoma, and an un-identified sarcoma subtype (Fig.5.19a, 5.19b). The morphology of the spheroids varied across different sarcomas, according to the different tissue origin and tumor stage (Fig.5.19a, 5.19b). Sarcoma spheroids were subsequently used to test cellular immunotherapy *in vitro*, either as single agent or in combination with drugs.

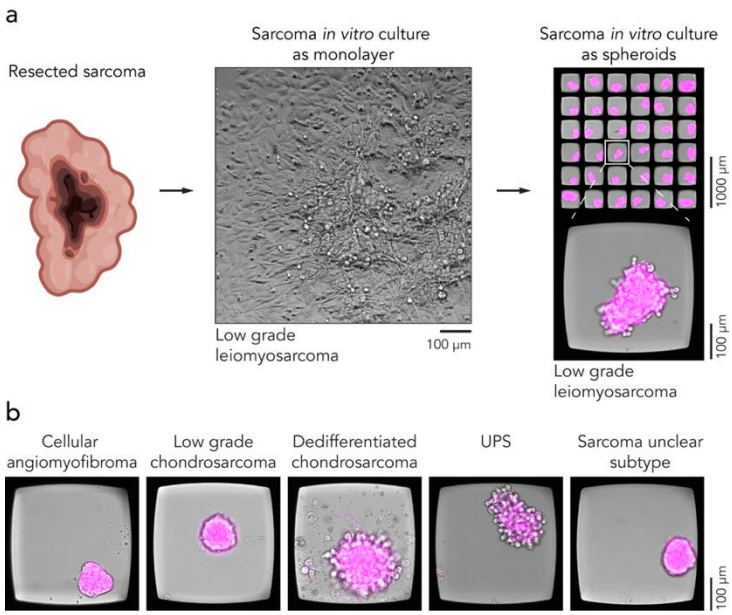

Figure 5.19: a. Schematic illustration of the workflow followed to obtain patient-derived sarcoma spheroids. From left to right: resected saromas were obtained from Karolinska Hospital within a few hours from surgery, sarcoma cells were obtained and cultured as monolayers before being used for USW-induced spheroid formation. Bright-field images of leiomyosarcoma cells cultured as monolayers (central panel) or as spheroids (right panel) are provided. **b.** Patient-derived sarcoma spheroids obtained from different subtypes and grades. UPS= undifferentiated pleiomorphic sarcoma In magenta: TMRM viability dye.

5.4.6 Multi-parametric flow cytometry analysis of tumor spheroids

The anti-adherence polymer surface coating allows the collection of spheroids from the microwell chip for further processing. We developed a method to perform flow cytometry on USW-induced spheroids retrieved from the microwell chip, which was used in paper I and III. A498 spheroids were collected from the single chambered chip and transferred to a FACS tube simply using a standard 200 µl pipet. Spheroids were treated with accumax for

one hour to obtain single cell suspension. Accumax is a tissue dissociation solution containing proteolytic enzymes and EDTA, which disrupts cell-to-cell and cell-to-substrate interactions. It was chosen over trypsin and EDTA alone due to high cell recovery and post-treatment preservation of protein expression. Following immunostaining, cells were analyzed by flow cytometry. Standard 2D cultures and miniaturized agarose-induced 3D cultures were used for comparison. Miniaturized agarose-induced 3D cultures allow the simultaneous production of 256 spheroids in agarose microwell plates (Fig.5.20a), where each agarose plate fits a 12-well plate well, and multiple batches can be used when many spheroids are needed. The agarose microwells have a diameter of 400 μm, which is close to the silicon microwells (350 μm). The size of agarose-induced and USW-induced spheroids was comparable (Fig.5.20a; 5.20b). Flow cytometry analysis following enzymatic dissociation showed that the viability of the USW-induced spheroids was not significantly different from standard 2D cultures and miniaturized agarose-induced 3D cultures (Fig.5.20c). Multi-parametric analysis was performed in paper III to quantify the expression of NK cell ligands on A498 spheroids. We observed lower expression of PVR and ULBP-2, 5, 6 in both agarose-induced and USW-induced A498 spheroids compared to A498 monolayers, showing that the influence of the 3D environment leads to modulation of PVR and ULBP-2, 5, 6 expressions (Fig.5.20d). No other ligands were modulated in the USW or agarose 3D cultures. These data also demonstrated that USWs do not induce changes in the spheroid phenotype in terms of NK ligands expression, further confirming that the platform is suitable for immunological studies.

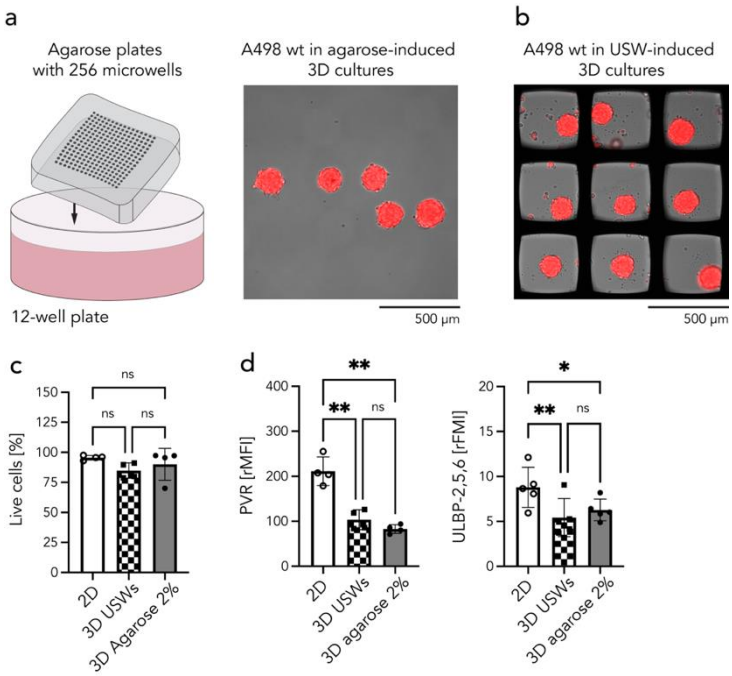

Figure 5.20; a. Left panel: illustration showing the agarose plates containing 256 wells used as control method for spheroid culture. Right panel: wide-field microscopy image representative of agarose-induced spheroids obtained from A498-RFP$^+$ cells. As hydrogels interfere with the image quality, the agarose-induced spheroids were transferred into a glass-bottom dish before imaging. **b.** Wide-field microscopy image of USW-induced spheroids obtained from A498-RFP$^+$ cells in the microwell chip. **c, d.** Analysis of cell viability (**c.**) and expression of PVR and ULBPs on A498 wt cells obtained from standard monolayer cultures (2D), USW-induced (3D USWs) or agarose-induced (3D agarose 2%) spheroids (**d.**).

Flow cytometry provides fast multi-parametric analysis, while imaging is suited for longitudinal studies of spheroid dynamics and morphology. Thus, by combining the two methods we could increase the information retrieved from the experiments. Single cell RNA sequencing, proteomics and metabolomics are other examples of analyses that could potentially be performed on spheroids that are collected from the microwell chip.

5.5 CURRENT LIMITATIONS AND FURTHER DEVELOPMENTS

In the previous sections, we described the advantages of the microwell chip in terms of biocompatibility and usefulness in a wide range of research applications. Here we report the current limitations of the platform, and solutions to overcome them. The number of conditions that can be tested simultaneously in the chip is restricted to the number of chambers. We developed the multichambered microwell chip from the single chambered

microwell chip to increase the number of conditions from 1 to 16. To test more than 16 treatments, multiple chips can be used at the same time. Currently, the USW method can only be used on one chip at the time, but new USW transducers and methods using frequency modulation are under development to allow simultaneous spheroid formation in multiple microwell chips.

Biological and technical replicates are needed in all investigations, and multiple experiments have been performed to reach the biological conclusions discussed in the next chapter. However, the presence of 36 replicates in each chamber could reduce the number of experiments needed to confirm biological findings, if proper internal controls are run simultaneously. Developing standard controls to validate the precision and ruggedness of the platform would help reducing the need for technical replicates. These considerations are particularly relevant in the field of precision medicine, where primary material is scarce, and the number of conditions should be maximized in as few experiments as possible.

For flow cytometry analysis of spheroids, useful information can be extrapolated only if enough cells are available for flow cytometry acquisition. As already mentioned, spheroids can currently be produced in only one chip at the time, and the number of cells available for flow cytometry is quite limited compared to many other 3D culture methods. Miniaturized 2% agarose hydrogels are more suitable for producing multiple spheroids simultaneously, as hydrogels can be produced in batches, and the main limiting factor is the number of cells available for setting up the tissue culture. For these reasons, flow cytometry analysis of USW-induced spheroids should be seen as a useful tool to complement imaging with multi-parametric analysis, but not as the main application of the method. Accordingly, miniaturized 2% agarose hydrogels were mostly used in paper III to characterize the phenotype of NK cells infiltrating tumor spheroids.

The current method of spheroid culture in the microwell chip from patient material presents some limitations. Patient-derived sarcoma cells underwent standard monolayer culture for one or two passages before being used for spheroid formation. A faster assembly of spheroids right after tissue dissociation would potentially provide a better representation of the original tumor.

Significant power would be given to the microchip method if single spheroids could be obtained from each well and further analyzed following live cell imaging. This would be particularly important when using patient-derived material, where tumor cell clones might respond differently to treatments, and further characterization would be needed to link the response to a cell phenotype. Using the multichambered microwell chip, we observed heterogeneous NK cell killing across the 36 wells, both in terms of killing dynamics and

spheroid viability at the end of the assay. The source of this variation is still unclear, and the possibility of retrieving NK cells from single wells could also help understanding their contribution to such heterogeneity.

Finally, the microwell chip design is not compatible with light sheet microscopy. In light sheet microscopy, the orthogonal geometry of sample illumination and detection requires optically transparent walls, and each spheroid should be individually accessible for both objectives. These requirements do not meet the microwell chip design. Therefore, spheroids need to be collected and embedded in hydrogels prior to light sheet imaging, increasing the risk of sample loss and experimental artifacts.

Despite some limitations, the platform has been proven to be easy to use and extremely useful for a wide range of biological applications. It has also provided several biological findings, which are described in the following chapter.

6 BIOLOGICAL FINDINGS

We applied the methods previously described to investigate the role of PVR in modulating NK cell activity in solid tumors. In paper III, we studied the expression of TIGIT, DNAM-1, CD96 and KIR2DL5 and their hierarchy in regulating NK cell degranulation, building a model of NK-mediated PVR recognition. Next, we evaluated the implications of PVR recognition on NK cell surveillance of renal carcinoma spheroids. In paper IV, we extended these findings to primary tumors, analyzing PVR recognition in patient-derived sarcomas. Our findings further confirm the importance of PVR in modulating TIGIT and KIR2DL5 signaling in solid tumors, but also reveal the presence of PVR-independent mechanisms regulating DNAM-1 functions. Better understanding of the role and the dynamics of PVR receptors is essential to build therapies that efficiently restore NK cell-mediated surveillance of PVR-expressing tumors.

6.1 EXPRESSION OF PVR RECEPTORS ON NK CELLS

Most IL-15 activated NK cells express the activating receptor DNAM-1, while the expression of PVR inhibitory receptors varies across NK cell subsets (Fig.6.1a) CD96 is expressed at low levels, and predominantly on $CD56^{Bright}$ NK cells (Fig.6.1a). The expressions of TIGIT and KIR2DL5 are bimodal, with both $TIGIT^{+}$ and $KIR2DL5^{+}$ cells expressed in $CD56^{Dim}$ NK subsets (Fig.6.1a). Higher expression of TIGIT was detected in $KIR2DL5^{-}$ cells compared to $KIR2DL5^{+}$, suggesting the presence of regulatory mechanisms to balance PVR-mediated inhibitory signals in $KIR2DL5^{+}$ donors (Fig.6.1b, 6.1c). Therefore, PVR recognition is mediated by a balance of activating and inhibitory receptors broadly distributed in both $CD56^{Bright}$ and $CD56^{Dim}$ NK cells.

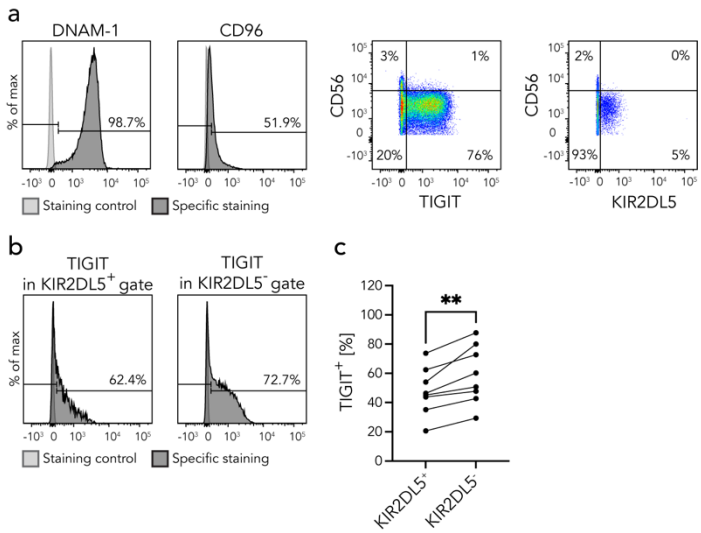

Figure 6.1: a) A representative example of DNAM-1, CD96, TIGIT and KIR2DL5 expression on NK cells after overnight activation with IL-15 (10 ng/ml). The numbers represent the percentage of positive cells. **b)** Expression of TIGIT in KIR2DL5^{+} (left panel) and KIR2DL5^{-} (right panel) NK cells isolated from a KIR2LD5^{+} donor. Light grey: unstained control; dark grey: specific staining. **c)** Pairwise comparison indicating the percentage of TIGIT^{+} NK cells in the KIR2DL5^{+} and KIR2DL5^{-} gates in KIR2LD5^{+} donors.

6.2 TIGIT AND KIR2DL5-MEDIATED INHIBITION DOMINATES OVER DNAM-1-ACTIVATION

Removing a protein from its context is a strategy to understand its function. In paper III, we applied this method to investigate the role of each PVR receptor. Specifically, we measured the response of NK cells against PVR knock-out A498 renal carcinoma cells (Fig.6.2a), both in the presence or in the absence of PVR receptor blocking. TIGIT^{+} KIR2DL5$^{+/-}$ NK cells degranulated more when exposed to A498 PVR KO compared to A498 wt cells (Fig.6.2b-d), while the opposite trend was observed in TIGIT^{-} KIR2DL5^{-} NK cells (Fig.6.2e), where DNAM-1 was the sole receptor responding to PVR modulation. No involvement of CD96 was observed in our system. Our data strongly suggested that TIGIT- and KIR2DL5-mediated inhibition was stronger than DNAM-1-mediated activation upon PVR recognition.

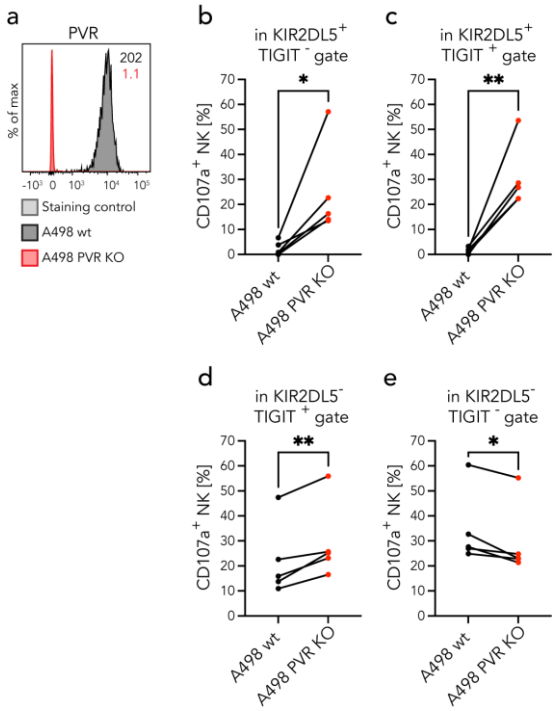

Figure 6.2: a. PVR expression on A498 wt (dark grey histogram) and A498 PVR KO (red histogram). Light gray: unstained control. **b-e.** Pairwise comparison of degranulating NK cells in response to A498 wt (black dots) or A498 PVR KO (red dots) gating on KIR2DL5$^+$ TIGIT$^-$ (**b**), KIR2DL5$^+$ TIGIT$^+$ (**c**), KIR2DL5$^-$ TIGIT$^+$ (**d**), or KIR2DL5$^-$ TIGIT$^-$ (**e**) NK cells. NK cells were activated overnight with IL-15.

To confirm this hypothesis, we needed to demonstrate the direct involvement of PVR inhibitory receptors in counterbalancing DNAM-1-PVR interaction. We performed NK cell degranulation against both A498 PVR KO and A498 wt cells in the presence of combinatorial PVR receptor blocking (Fig.6.3). Specifically, we were going after the receptor-ligand interaction inducing NK cell degranulation in response to PVR loss. KIR2DL5 was not considered, as the KIR2DL5$^+$ population was generally small and its contribution to NK degranulation minimal. DNAM-1 blockade, alone or in combination with CD96, inhibited NK cell degranulation overall, but it maintained the increase of NK cell response against A498 PVR KO compared to A498 wt. The increase disappeared by blocking TIGIT, both alone or in combination with anti-DNAM-1 or anti-CD96. CD96 blockade alone had no effects on NK cell degranulation. These data confirmed that TIGIT was responsible for increased NK cell degranulation in response to PVR loss. In other words, the absence of PVR prevented TIGIT to signal, unleashing NK cell degranulation

also in the absence of DNAM-1-PVR interaction. In fact, TIGIT and DNAM-1 co-blockade still increased NK cell degranulation compared to DNAM-1 blockade alone, indicating that TIGIT could turn off activating pathways that are independent of DNAM-1. Thus, TIGIT is the main driver of NK cell inhibition during the interaction with PVR-expressing target cells, and its inhibitory function is broader than directly counteracting activating signals from DNAM-1.

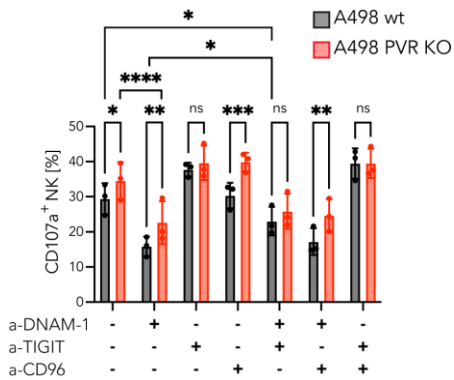

Figure 6.3: Percentage of degranulating NK cells after to 2 hours incubation with A498 wt (black bars) or A498 PVR KO (red bar) in the presence of DNAM-1, TIGIT and CD96 neutralizing antibodies, either alone or in combination. Isotype control antibody was used as control.

6.3 DNAM-1 ACTIVATION IS DOMINATED BY PVR-INDEPENDENT MECHANISMS

While performing combinatorial blocking, we noticed that DNAM-1 blockade affected NK cell degranulation even in response to A498 PVR KO, indicating that DNAM-1 has both PVR-dependent and PVR-independent mechanisms of activation. We measured the contribution of the two mechanisms in TIGIT$^-$ gates, to exclude the effect of TIGIT (Fig. 6.4). PVR-independent signaling was responsible for approximately 80% of the total DNAM-1 contribution to NK cell degranulation in our system. PVR-independent DNAM-1 activation could not be ascribed to Nectin-2, as Nectin-2 blockade on A498 PVR KO had a small effect on NK cell degranulation compared to DNAM-1 blockade. Therefore, DNAM-1 positively contributes to NK cell degranulation mainly via PVR- and Nectin-2-independent signaling pathways in our system.

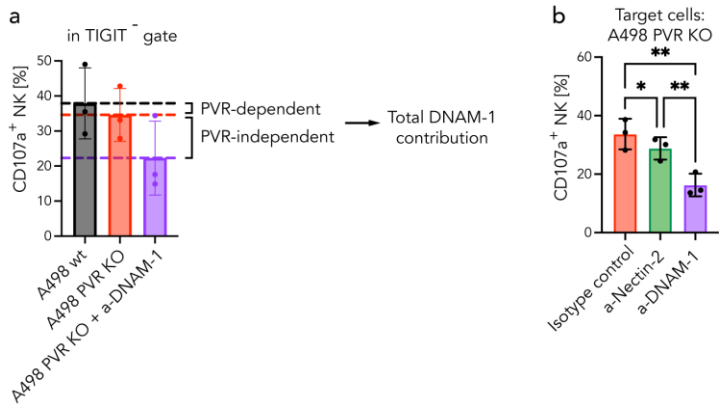

Figure 6.4: a. Percentage of degranulating NK cells in TIGIT$^-$ gate after to 2 hours incubation with A498 wt (black bars) or A498 PVR KO (red bar) or A498 PVR KO + anti-DNAM-1 (purple bar). **b.** Percentage of total NK cells degranulating in response to A498 PVR KO in the presence of isotype control (red bar), anti-Nectin-2 (green bar) or anti-DNAM-1 (purple bar).

6.4 TIGIT AND KIR2DL5 ARE SENSITIVE TO PVR MODULATION

Next, we investigated how NK cells reacted to partial PVR down-regulation, instead of complete loss. We obtained a wide range of PVR expression performing siRNA-mediated PVR knockdown on A498 wt cells for different time periods (24-96 hours) (Fig.6.5a) and we measured NK cell response in a CD107a release assay. A498 wt cells treated with scramble siRNA were used as control. NK cell degranulation inversely correlated with PVR expression (Fig.6.5b). The increase was maintained when blocking DNAM-1(Fig.6.5b). Increased degranulation was driven by TIGIT$^+$ NK cells (Fig.6.5c, 6.5d). In KIR2DL5$^+$ donors, KIR2DL5$^+$ TIGIT$^-$ NK cells increased degranulation correlating with the amount of PVR loss (Fig.6.6e). Therefore, TIGIT and KIR2DL5 signaling senses a wide range of PVR alterations, which directly affect NK degranulation capacity.

Next, we looked specifically at TIGIT$^-$ NK cells to understand how DNAM-1 senses PVR fluctuations, excluding any effect of TIGIT. However, PVR si-RNA down-modulation did not decrease NK cell degranulation in the TIGIT$^-$ gates (Fig.6.5d), indicating that the sensitivity of DNAM-1 to PVR variations was weak or non-existing. This insensitivity was not due to lack of DNAM-1-PVR interaction, as PVR induced DNAM-1 down-regulation on NK cells (Fig.6.5f). The levels of DNAM-1 down-regulation were dependent on the amount of PVR expressed on the surface of PVR-siRNA-treated A498 wt cells, indicating that interaction occurred in the full range of PVR expressions tested. These data confirmed

that wide ranges of PVR alteration in a wide range was primarily sensed by TIGIT and KIR2DL5 rather than DNAM-1.

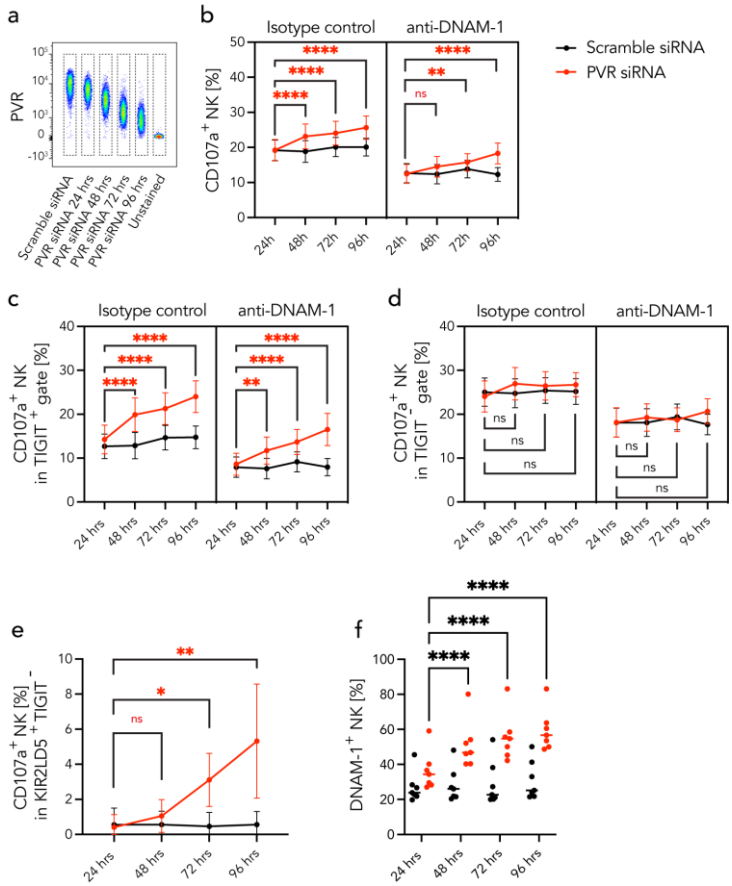

Figure 6.5: a. Representative dot-plot showing the PVR expression on A498 wt cells incubated with either scramble siRNA or PVR siRNA for 24, 48, 72 or 96 hours. **b-e.** Three-way plots showing the percentage of $CD107a^+$ NK cells in response to A498 wt treated with scramble siRNA (black dots) or PVR si-RNA (red dots) for 24, 48, 72 or 96 hours, in the presence of isotype control antibody (left panel) or anti-DNAM-1 blocking antibody (right panel). Gating: $CD45^+$ (**b.**), $TIGIT^+$ (**c.**), $TIGIT^-$ (**d.**), $KIR2DL5^+TIGIT^-$ (**e.**). **f.** Flow cytometry analysis of DNAM-1 expression in response to 2 hours incubation with A498 wt cells treated with PVR si-RNA for 24, 48, 72 or 96 hours.

6.5 VARIATION OF DNAM-1 AND TIGIT EXPRESSION IN TUMOR SPHEROIDS

To study the effect of the tumor microenvironment on TIGIT and DNAM-1 expression, we performed flow cytometry analysis on NK cells co-cultured with A498 renal carcinoma spheroids for 48 hours, both in the presence or in the absence of IL-15 (Fig.6.6). A substantial DNAM-1 down-regulation was observed in NK-A498 spheroid cocultures compared to NK cells alone. Resting NK cells down-regulated DNAM-1 in a PVR-dependent manner (Fig.6.6a), while additional PVR-independent mechanisms caused DNAM-1 loss in IL-15-activated NK cells (Fig.6.6b). In fact, removing PVR from A498 spheroids completely restored DNAM-1 expression in resting NK cells, and only partially in IL-15 activated NK cells (Fig.6.6a, 6.6b).

Resting NK cells are characterized by low TIGIT expression, while bi-modal TIGIT expression is observed in IL-15-activated NK cells. The exposure to A498 spheroids induced a slight TIGIT upregulation on resting NK cells (Fig.6.6c). The opposite trend was observed in IL-15 activated NK cells (Fig.6.6d). TIGIT up-regulation in resting NK cells was not induced by PVR (Fig.6.6c). On the other hand, TIGIT down-modulation on IL-15 activated NK cells was PVR-dependent (Fig.6.6d). Thus, substantial differences between resting and IL-15 activated NK cells were observed in the regulation of both DNAM-1 and TIGIT in the tumor microenvironment.

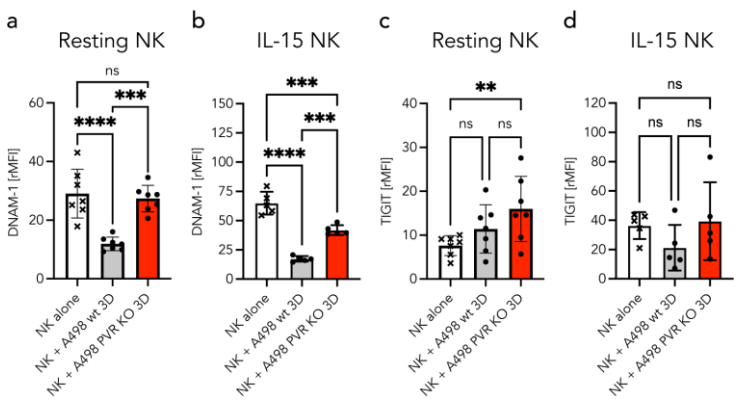

Figure 6.6: a-d. Flow cytometry analysis of NK cells cultured either alone (white bar), with A498 wt spheroids (grey bar) or with A498 PVR KO spheroids (red bar) in absence (**a, c**.) or in presence (**b, d**.) of IL-15.

6.6 EXTENT OF TIGIT INHIBITION AMONG DONORS

Since PVR induced a strong TIGIT-mediated NK cell inhibition, we tested whether TIGIT blockade could improve NK cell cytotoxicity against renal carcinoma spheroids. On average, TIGIT blockade significantly enhanced the ability of IL-15 activated NK cells to kill A498 wt spheroids (Fig.6.7a, 6.7b). Heterogeneous response was observed between donors, correlating with TIGIT expression (Fig.6.7b, 6.7c). Specifically, NK donors characterized by high TIGIT MFI at the beginning of the assay, such as donors 1 and 2 (Fig.6.7c, in green and in orange), showed low basal anti-tumoral activity, and TIGIT blockade had a positive effect on NK cell killing (Fig.6.7b, in green and in orange). On the other hand, TIGIT blockade did not change the outcome of NK activity for donors 3 and 4, both characterized by low TIGIT expression and high basal activity (Fig.6.7b, 6.7c, in blue and in grey). Thus, TIGIT is associated to heterogeneous response to NK cell activity, and TIGIT blockade selectively improves the outcome of NK cell treatment in donors expressing high levels of TIGIT.

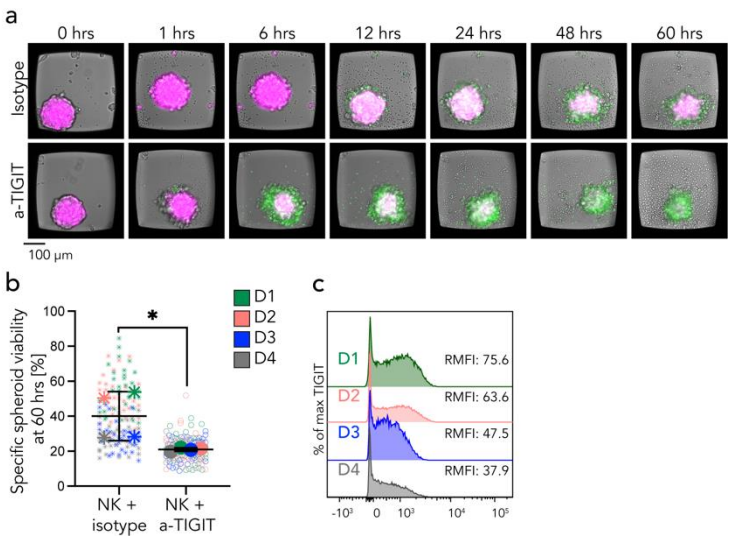

Figure 6.7: a. Time-lapse sequences from representative microwells showing NK cell-mediated killing of A498 wt spheroids in presence of an isotype control antibody (upper panel) or anti-TIGIT antibody (bottom panel). In magenta: TMRM viability dye. In green: Caspase-3/7 apoptotic marker. NK cells were activated with IL-15 overnight. **b.** Dot-plot showing viability of individual A498 wt spheroids (small dots, n=36) after 60 hours treatment with NK cells isolated from donor 1 (D1, green), donor 2 (D2, orange), donor 3 (D3, blue) and donor 4 (D4, grey), in the presence of isotype control antibody (stars) or anti-TIGIT antibody (circles). Black bars: mean values from the 36 spheroids. **c.** Flow cytometry analysis of TIGIT expression on NK cells from the four different donors (D1-4) used in the live cell imaging assay.

Heterogenous response was not observed in resting NK cells co-incubated with A498 spheroids, either in the presence of isotype control or anti-TIGIT antibody (Fig.6.8a). Resting NK cells are characterized by low TIGIT expression, which increases in the spheroid microenvironment (Fig.6.6c). Accordingly, the effect of TIGIT blockade was more evident at late timepoints of the assay (Fig.6.8b). In both resting NK cells and IL-15 activated NK cells, TIGIT blockade enhanced NK cell activity despite DNAM-1 down-regulation, in line with our previous experiments showing the efficacy of TIGIT blockade in the absence of DNAM-1 signaling.

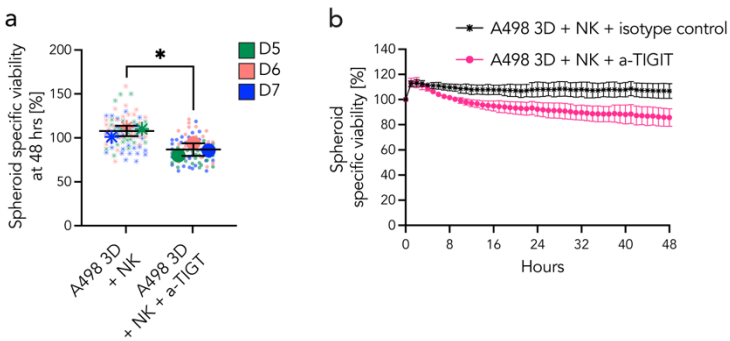

Figure 6.8: a. Dot-plot showing spheroid viability of individual A498 wt spheroids (small dots, n=36) after 60 hours treatment with NK cells isolated from donor 5 (D5, green), donor 6 (D6, orange), donor 8 (D8, blue) in the presence of isotype control antibody (stars) or anti-TIGIT antibody (circles). Black bars: mean values from 3 donors. **b.** Time course of specific spheroid viability of A498 wt spheroids exposed to resting NK cells in the presence of isotype control (black stars) or anti-TIGIT (magenta-filled dots) for 48 hours.

6.7 SUPERIOR EFFECT OF TIGIT BLOCKADE IN COMBINATION WITH CETUXIMAB

Cetuximab is a chimeric monoclonal antibody targeting EGFR. It exerts antitumoral activity by blocking EGFR signaling and promoting antibody-dependent cellular cytotoxicity (ADCC)[426,427]. Since A498 cells express EGFR, we tested whether cetuximab could further improve the efficacy of anti-TIGIT blockade. Cetuximab as single agent reduced the spheroid viability to 21.0% from the 40.0% observed for NK cell treatment alone (Fig.6.9a). Adding TIGIT neutralizing antibody further decreased the spheroid viability to 11.8% (Fig.6.9a, 6.9b). This effect was still dependent on the levels of TIGIT expression on the NK cells. the combination of cetuximab with TIGIT blockade improves NK cell antitumoral activity in donors with high TIGIT expression.

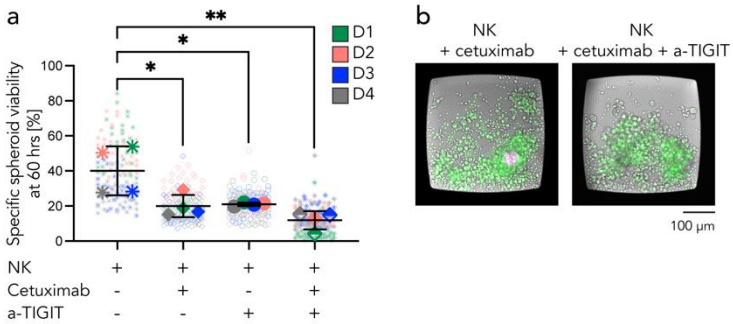

Figure 6.9: a. Dot-plot showing the specific spheroid viability of A498 wt spheroids (small symbols, n=36) after 60 hours treatment with NK cells isolated from donor 1-4 (D1-4), in presence of isotype control antibody (stars), cetuximab (rhombuses), anti-TIGIT antibody (filled dots) or the combination of cetuximab and anti-TIGIT (half-empty rhombuses). The black bars show the mean value and SD of the four donors. **b.** NK-cell mediated killing of A498 wt spheroids in the presence of cetuximab alone (left panel) or in combination with anti-TIGIT (right panel). Timepoint: 60 hours. In magenta: TMRM; in green: caspase-3/7.

6.8 AXITINIB AND LENALIDOMIDE REDUCE TIGIT EXPRESSION

Two additional drugs were tested in combination with TIGIT blockade for the treatment of A498 renal carcinoma spheroids: axitinib and lenalidomide. Axitinib is a second-generation vascular endothelial growth factor receptors (VEGF-R) tyrosine kinase inhibitor (TKI) used for treatment of advanced renal carcinoma. Lenalidomide is an immunomodulatory drug recently proposed for treatment of refractory metastatic renal carcinoma[428]. Combining axitinib and lenalidomide with NK cells significantly reduced the spheroid viability compared to single treatments. However, the addition of anti-TIGIT antibodies did not increase cytotoxicity further. We noticed that treating NK cells with IL-15 in presence of axitinib or lenalidomide reduced TIGIT expression (Fig.6.10). No effects were observed for cetuximab (Fig.6.10). Thus, axitinib- and lenalidomide-induced TIGIT down-regulation could possibility explain the inefficacy of TIGIT blockade when combined with these two drugs.

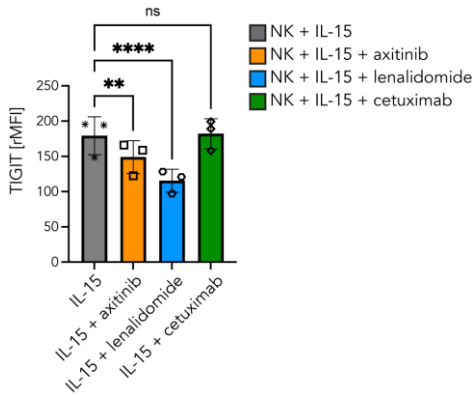

Figure 6.10: TIGIT expression on NK cells cultured alone for 48 hours in the presence of IL-15 (grey bar) together with axinitib (orange bar), lenalidomide (light blue bar) or cetuximab (green bar).

6.9 DNAM-1 PROMOTES NK CELL INFILTRATION

NK cell infiltration in A498 spheroids relies on DNAM-1 activity. In fact, NK cell incubation with anti-DNAM-1 antibody decreased the percentage of NK cells reaching the spheroid core compared to the isotype control (Fig.6.11). No differences were observed in the presence of anti-TIGIT antibody, suggesting no involvement of TIGIT in NK cell infiltration.

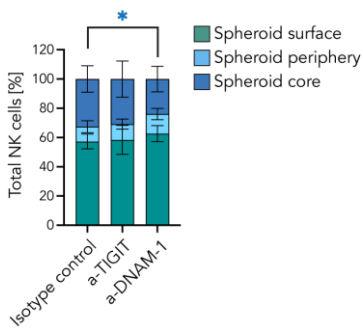

Figure 6.11: Number of NK cells residing in each spheroid region normalized for the total number of NK cells counted in the three spheroid regions.

6.10 TIGIT HETEROGENEITY AND DNAM-1 DOWN-REGULATION ARE RECAPITULATED IN SARCOMA PATIENTS

We obtained tumor tissue and peripheral blood from sarcoma patients undergoing surgery. We characterized the immune cell composition in the peripheral tumor, central tumor and peripheral blood by flow cytometry, particularly focusing on TIGIT and DNAM-1 expression on NK cells (Fig.6.12a). The percentage of $TIGIT^+$ NK cells in the peripheral blood was highly heterogeneous among individuals, and such heterogeneity was maintained in the sarcoma tissue. On the other hand, the percentage of $DNAM\text{-}1^+$ NK cells was high

and quite homogeneous in peripheral blood, but drastically decreased in the central and peripheral sarcoma tissue. Therefore, sarcoma patients maintain the heterogeneous TIGIT expression that also characterizes healthy donors in both tumor tissues and peripheral blood. On the other hand, DNAM-1 down-regulation in the sarcomas could undermine NK cell migration and cytotoxicity.

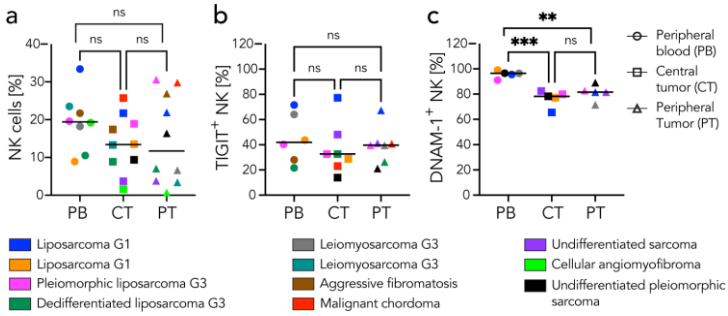

Figure 6.12: a. Flow cytometry analysis of the percentage of NK cells in peripheral blood (PB, dots) and tumor-infiltrating lymphocytes obtained from the central tumor (CT, squares) or peripheral tumor regions (PT, triangles). Each color represents a patient diagnosed with the sarcoma subtype and grade indicated in the figure legend. **b, c.** Percentage of TIGIT$^+$ (**b.**) and DNAM-1$^+$ (**c.**) NK cells in sarcoma patients.

6.11 CASE STUDY 1: DEDIFFERETIATED CHONDROSARCOMA ASSOCIATED WITH HIGH PVR AND NECTIN-2 EXPRESSION

We analyzed the expression of NK cell ligands in primary chondrosarcoma spheroids (Fig.6.13a). Higher expression of PVR, Nectin-2 and HLA class I was observed in dedifferentiated chondrosarcoma (patient 1) compared to low grade chondrosarcomas (patients 02 to 04) (Fig.6.13a). This phenotype was associated with low cytotoxic activity of allogeneic NK cells (Fig.6.13b, lower panel). TIGIT blockade improved NK cell killing against dedifferentiated chondrosarcoma spheroids (Fig.6.13b, upper panel). These data suggest that NK cell therapy combined with TIGIT blockade could be a valid treatment option for dedifferentiated chondrosarcoma patients expressing high levels of TIGIT ligands.

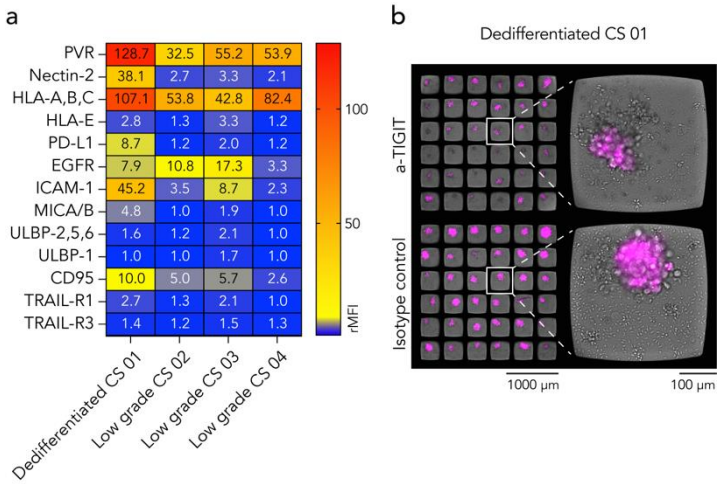

Figure 6.13: a. Expression of NK cell ligands on patient-derived chondrosarcoma (CS) spheroids. **b.** Representative chambers and wells showing patient-derived chondrosarcoma grade 4 spheroids exposed to IL-15 activated NK cells for 24 hours in presence (upper panel) or in absence (lower panel) of TIGIT blockade. In magenta: TMRM viability dye marker.

6.12 CASE STUDY 2: EVALUATION OF COMBINATORIAL TREATMENT FOR NK-RESISTANT CELLULAR ANGIOMYOFIBROMA

We obtained primary spheroids from a case of cellular angiomyofibroma. Low percentage of NK cells (Fig.6.12b, in spring green) combined with high percentage of PD-1^+ $CD8^+$ T were observed in the original sarcoma tissue compared to the peripheral blood, suggesting a highly immunosuppressive tumor microenvironment. Flow cytometry analysis revealed high levels of inhibitory NK ligands in cellular angiomyofibroma spheroids, such as PVR, Nectin-2, HLA class I and PD-L1, together with EGFR. Accordingly, the spheroids were resistant to allogeneic NK cell-mediated killing. Thus, the immunosuppressive phenotype was maintained *in vitro*. We evaluated the efficacy of anti-TIGIT, anti-PVR, anti-PD-L1 (atezolizumab) and anti-EGFR (cetuximab) in improving NK cell activity. Anti-TIGIT and anti-PVR antibodies slightly decreased the specific spheroid viability. The responses of anti-TIGIT and anti-PVR were similar, further suggesting the marginal role of PVR-dependent DNAM-1 recognition in this model. More effective was the activity of NK cells in combination with atezolizumab and cetuximab. The addition of anti-TIGIT to cetuximab treatment further decreased the spheroid viability, while no further improvements were observed combining anti-PD-L1 with anti-TIGIT. In conclusion, the most effective treatments were atezolizumab alone and the combination of anti-TIGIT with cetuximab. Even if residual cellular angiomyofibroma cells resistant to NK cells could be

still observed in the microwells, the treatments significantly improved NK cell-mediated cytotoxicity.

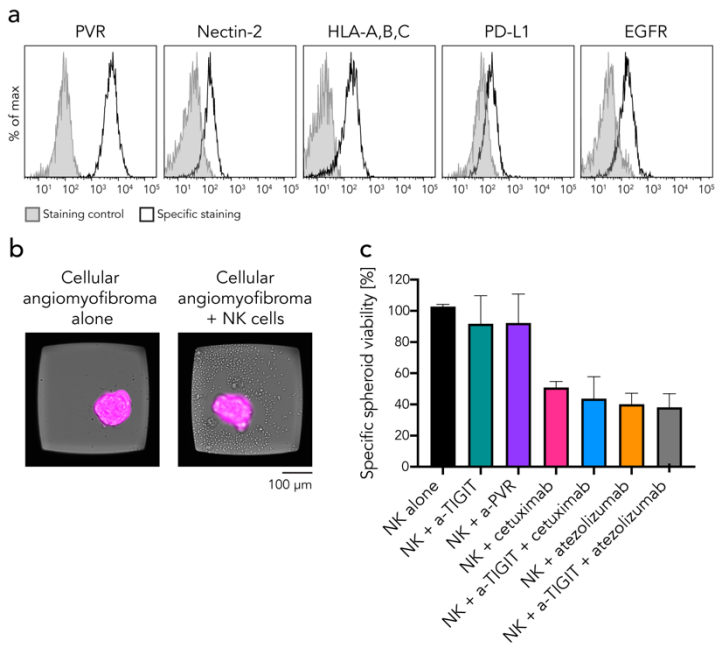

Figure 6.14: a. Flow cytometry analysis of NK cell inhibitory ligands and EGFR on patient-derived angiomyofibroma spheroids. **b.** Patient-derived cellular angiomyofibroma maintained for 24 hours alone (left panel) or with NK cells (right panel). **c.** Specific spheroid viability of patient-derived cellular angiomyofibroma spheroids after 24 hours treatment with NK cells alone (in black) or combined with anti-TIGIT (teal green), anti-PVR (purple), cetuximab (magenta), cetuximab + anti-TIGIT (blue), atezolizumab (orange) and atezolizumab + anti-TIGIT (grey).

7 CONCLUSIONS

This doctoral work has led to new biological insights about how NK cells interact with tumor cells. The findings can be summarized in a few key observations. The overall response of NK cell to PVR is mainly inhibitory and dominated by TIGIT. The inhibitory function of TIGIT is broader than simply counteracting PVR-dependent activation of DNAM-1, as the effect of TIGIT blockade could be observed even when DNAM-1 activation was prevented. Nevertheless, DNAM-1 contributes strongly to NK immunosurveillance, but mainly through PVR-independent mechanisms. We hypothesize two possible PVR-independent mechanisms of DNAM-1 activation: 1) the presence of a hitherto unknown DNAM-1 ligand, or 2) DNAM-1 is stabilizing the LFA-1 ^{open} conformation, implicating direct involvement of DNAM-1 in immune synapse formation

Based on our data, we suggest a schematic model of the role of PVR receptors in degranulation response of IL-15 activated NK cell (Fig. 7.1)

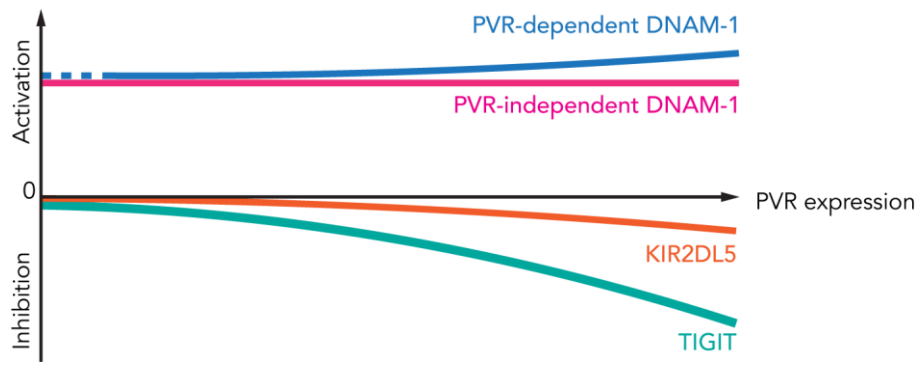

Figure 7.1: Model of PVR receptor influence on NK cell responsiveness

In this model, NK cells sense variations of PVR-expression mainly through TIGIT and KIR2DL5. The PVR-dependent DNAM-1 contribution to NK cell responsiveness is small and not particularly sensitive to variations in PVR expression, while the PVR-independent DNAM-1 function contributes strongly to NK cell response. No involvement of CD96 was detected in our experiments. This model is in line with previous observations in both mouse and human models[150,216,232].

Our model predicts that TIGIT blockade should efficiently improve NK cell immunosurveillance. However, this prediction is under the assumption that activating mechanisms and expression of TIGIT are maintained in the tumor microenvironment.

However, TIGIT and DNAM-1 expression was modulated in renal carcinoma spheroids, both by PVR-dependent and PVR-independent mechanisms. In line with our *in vitro* observations, DNAM-1 expression was drastically decreased in central and peripheral tumor regions compared to peripheral blood in sarcoma patients. In addition, long exposure to the tumor microenvironment could affect the overall ability of NK cells to perform cytotoxicity, reducing the ability of NK cells to respond to antibody therapy.

To take all these aspects into consideration, we evaluated the efficacy of TIGIT blockade, alone or in combination with other drugs, in a more natural environment, such as in renal carcinoma spheroids and patient-derived sarcoma spheroids. In renal carcinoma spheroids, $TIGIT^{high}$ NK donors showed lower cytotoxic activity compared to $TIGIT^{low}$ NK donors. TIGIT blockade improved the activity of $TIGIT^{high}$ NK donors, suggesting that TIGIT expression might be associated with the efficacy of NK cell therapy. Thus, anti-TIGIT therapy could be a valid complementary treatment for cancer patients characterized by high TIGIT expression. These data further demonstrate that $TIGIT^{high}$ NK cells NK are not exhausted, but have a strong cytotoxic potential that can be unleashed by blocking TIGIT signaling. Axitinib and lenalidomide induced TIGIT down-regulation. Decreasing TIGIT-mediated NK cell inhibition might be an indirect mechanism of action of these drugs, and further experiments are needed to confirm this hypothesis.

We evaluated TIGIT blockade in patient-derived sarcoma spheroids resistant to NK therapy. In dedifferentiated chondrosarcomas, high levels of PVR correlated with resistance to NK cell therapy, which was partially reverted by TIGIT blockade. Similarly, NK-resistant cellular angiomyofibroma spheroids expressed high levels of PVR. Treating cellular angiomyofibroma spheroids with anti-TIGIT or anti-PVR led to similar improvements. Correlation of PVR expression with sarcomas resistance to NK cell therapy, combined with similar effects obtained by anti-TIGIT and anti-PVR treatments, further confirmed the predominant role of TIGIT over DNAM-1 in PVR-mediated tumor recognition. The efficacy of anti-TIGIT treatment on NK killing was not comparable to the effects of cetuximab or atezolizumab. Therefore, the use of TIGIT blockade in combinatorial therapy might be a better option to reach clinically relevant responses in sarcoma patients.

Our results suggest that PVR should be considered a negative prognostic marker of NK-based cellular immunotherapy. In case of high PVR expression, anti-TIGIT and anti-PVR antibody therapy, as well as drugs reducing TIGIT levels, should be considered to complement NK cell therapy. However, the heterogeneity of TIGIT expression among individuals suggests that strategies to target TIGIT should be carefully evaluated for each patient. TIGIT expression was modulated by the tumor microenvironment, but not

drastically. Thus, defining a TIGIT expression cut-off in circulating NK cells as a predictive factor might be a simple and effective way to select patients responsive to anti-TIGIT therapy.

In conclusion, this doctoral work describes the development of USW-based spheroid formation in a microwell chip compatible with a wide range of biological applications (**Paper I**). The described work of the role of PVR and its receptors in shaping NK cell responses shows that the chip platform is a valuable research tools for making fundamental immunological discoveries (**Paper III**). The high-throughput drug screening and assessment of drug- and antibody-mediated NK cell cytotoxicity shows that the platform can be used to directly evaluated treatments which could be valuable for validating hypotheses generated in precision medicine (**Paper II**). The use of tumor spheroids from patient-derived sarcoma combined with drug-assisted NK cell cytotoxicity lay the foundation for the chip platform to be used in personalized medicine where treatments are tested directly using patients' own tumor and immune cells (**Paper IV**). Finally, we showed how continuous improvement of sample preparation could further increase our ability to describe biological mechanisms within thick specimens (**Paper V**). In a broader perspective, the work presented here outlines how new technical developments, in this case a miniaturized platform for 3D cell culture and imaging, can be used to shed new light on fundamental questions in life science and provide valuable preclinical data that, in the future, could support clinical decisions.

8 POINTS OF PERSPECTIVE

The presented research has two main questions to follow-up: understanding the PVR-independent mechanisms of DNAM-1 activation and implementing the culture of patient material in the microwell chip.

PVR-independent DNAM-1 activation significantly contributes to immunosurveillance. Activated NK cells lost DNAM-1 expression in renal carcinoma spheroids with mechanisms independent of PVR, suggesting that unknown processes regulate both DNAM-1 signaling and its stability at the cell membrane. Uncovering these processes could provide better understanding of immunotherapy resistance, and lead to the development of new therapeutic strategies. PVR-independent DNAM-1 activation could rely on the physical interaction with LFA-1. According with this theory, LFA-1 and DNAM-1 are physically associated on NK cells, and DNAM-1 colocalizes at the immune synapse with LFA-1 ^{open} even in the absence of PVR ligation[216,220]. In these settings, DNAM-1 could stabilize the LFA-1 ^{open} conformation, contributing to synapse formation and stability. To test this hypothesis, one could measure DNAM-1 phosphorylation upon interaction with ICAM-1 coated beads. The phosphorylation of DNAM-1 and its downstream signaling pathway would prove the synergistic activity between LFA-1 and DNAM-1 in the absence of PVR interaction. Those experiments should be followed by live cell imaging to assess the dynamics of immune synapse formation. Another approach would be to perform immunoprecipitation with DNAM-1-Fc followed by deep proteomic analysis to explore the existence of a putative DNAM-1 ligand. Still, the two hypotheses might not be mutually exclusive.

In Paper IV, we used patient-derived sarcoma spheroids to test the efficacy of NK cell therapy alone or in combinatorial settings. We observed high levels of PVR in dedifferentiated chondrosarcoma and cellular angiomyofibroma, associated with resistance to NK cell treatment. Likely, additional mechanisms are related to NK cell resistance. Our observations would benefit from a larger set of experiments to enable statistical analysis to validate the hypothesis. In addition, our current workflow should be implemented with the use of broader multi-parametric analyses. We are currently working on the analyzing proteomic data from plasma from sarcoma patients. Our colleagues are performing genetic analysis on a larger cohort of sarcoma patients. In addition, we have collected the peripheral blood of patients to perform imaging-based cytotoxicity using patient-derived spheroid and autologous lymphocytes. Genetic, proteomic, and functional analysis could generate new hypothesis to be tested in our microwell chip, further demonstrating the feasibility of our platform for therapy testing and precision medicine.

We believe that these improvements, combined with an upgraded set-up as described in section 5.5, would lead to a broader use of our platform for imaging-based precision immunotherapy.

9 ACKNOWLEDGEMENTS

A few weeks ago, someone asked me: “So Valentina, did you enjoy your PhD?”. For once, I gave a short and straight answer, and a positive one. That answer finds its place in all the experiences I had the opportunity to share with amazing people, that made my journey great.

First and foremost, I would like to express my deepest gratitude to my supervisor **Björn**. You gave me countless opportunities to learn, to pursue scientific questions and share our work. I am immensely grateful for that. When I started the PhD, my favorite cell shape was a single dot on what I used to define a “colorful” FACS-plot. I still like it though. But you taught me how to really look at things, and the importance of collecting and assembling information from multiple perspectives. Working in your group opened a whole world of new techniques and analysis that could be performed. If I would try to summarize what I learnt in these years, the main message would probably be: *Do not settle for what you have but develop more when you need*. But most of all, thanks for never stopping my enthusiasm, and for being always available and supportive.

I would like to thank my co-supervisor **Martin** for the great discussions and the human support. I am amazed by the ideas that are constantly being developed in your group. Thanks for always being there when I needed some help.

I would like to express my greatest appreciation to my co-supervisor **Andreas** for following all the NK- and sarcoma-related projects, for always being ready to discuss new data and for the support during the final stages of the PhD. Thanks for giving me the opportunity to collaborate with your group, it has been a great personal and scientific experience.

A big thank goes to my supervisor **Niklas**, for your kindness and scientific inspiration. You always put an extra attention to the human part of the work, and that helped me during the last year of intense work we both experienced. At the same time, it has been so inspirational to see how new platforms can be so quickly and easily developed out of your drawings, and how much one could improve already existing methods.

A deep thank goes to **Klas** for accepting me as visiting student and letting me begin my journey in KI. I had a wonderful time in your group, thanks for the great discussions we had and for giving me the opportunity to work on such inspiring projects.

There are no appropriate words to express all my gratitude to the two colleagues and friends with who I worked so closely with during these years, **Kalle** and **Steve**. Thanks for sharing with me so many hours of tireless lab work, for bearing with all my working plans changing from one day to another, and for being patient when straightforward projects became huge

and extremely complicated. Thanks for flowing in so many ideas that became shared projects, for all the suggestions and help. But most importantly, thanks for all the fun, both within and outside Scilife, and for amazing New Year's Eves and great bike rides.

A warm thanks goes to my friend and desk mate **Hanna** for always being there, for the fun times and for being supportive in troubled times. For all the pic-nicks, BBQs, dinners and adventures in the Swedish wilderness. For showing me how to be methodic and precise at work.

Thank you, **Quentin**, for the passion we share for music and live concerts, for having that critical mind that improved so many projects, presentations, and manuscripts. For always being ready for new adventures and being an amazing jump diver.

Thanks, **Patrick**, for sharing the passion of lab work and the tendency to always add a new condition in already huge assays. Thanks for all the support and great suggestions for the future. Thanks, **Laura**, for being such a good friend and kind person to have around, for bringing the Mediterranean vibe in the lab. Thanks, **Ludde** for the fun, and all the help with the microscopes, and for providing a great extra desk panel to add all my lab notes. Thanks, **Chiara**, for making me feel at home, for our discussions on Repubblica news, Morgana episodes and books. Thanks for being the artistic soul of the group. Thanks, **Karolin**, for cheering up the group chats with crazy and extremely fun stories, and for all the team building activities you organized in these years, both inside and outside the lab. Thanks, **Kyra**, for your sarcasm that makes me laugh a lot in the lab, and for taking care of projects when I did not know where to fit them. Thanks, **Damien**, for keeping the lab running so smoothly and for always being available and such an enthusiastic colleague. Thanks, **Björn** for always bringing new creative ideas. Thanks, **Elina,** for being a fun colleague to have around. Thanks to **Per** for the chats on Gomorra. Thanks **Jacopo**, for bringing more Liguria to the lab, for being so open-minded and extremely fun. Thanks for all the help with my project and for the support. Thank to **Aline**, for sharing so many views of science and life. Thanks for the great time spent together in retreats and conferences, and for still making me feel connected despite the distance. A big thank goes to the students **Grace**, **Lorenzo**, **Birte** and **Natalia**, for filling my working days with your enthusiasm, for always being ready for new challenges and for providing unvaluable help in all the projects.

A big thanks goes to the current and past members of **Gamma 3 Lab**, for creating such a comfortable and fun working environment. A special thanks goes to **Testa lab**, for sharing late working nights and pizza in SciLifeLab, and for supporting me during the final stretches of the thesis. Thanks, **Marta**, for your contagious laugh and for your thousand interests, it

is always so fun to talk to you, making it so hard to stop and go back to work. Thanks to the current and former members of Kärre group, for the great time I had as a visiting student.

I had the luck to meet two amazing people when I arrived in Stockholm, **Arnika** and **Rosa**. You both have been a great source of inspiration, the two big sisters to look up to. You smoothened the path from master student to PhD student. You help me in so many ways, that I would probably need another thesis to write them all. I have always been so thrilled to meet you again in conferences, and I cannot wait to spend more time together again.

Un ringraziamento speciale va al mio amico **Mauricio**. Non dimenticheró mai la prima sera che ci siamo conosciuti, per le risate che ci siamo fatti, e che non sono mai cambiate da allora. Grazie per la tua simpatia, per conoscermi cosí bene, e per sopportarmi. Grazie per condividere una passione per la musica, per tutti i concerti e per le ore passate a mandarci link di canzoni. Grazie al mio amico **Alex**, per tutte le incredibili serate pre-pandemia, per essere cosí aperto ad ascoltare tutte le mie storie incredibili, per insegrarmi a come vestirmi bene, per essere un amico cosí attento e vero. A big thank goes to my dear friend **Shady**, a travelling soul always ready for new countries and new experiences. I still miss your voice around the lab, despite it has been already 5 years since I moved from MTC. Thanks for sharing with me so many adventures and great time, and for being such a good friend. Thanks to **Sandra** for all the laughs and fun late nights, for being an amazing scientist, for being so committed and a source of inspiration. Un ringraziamento speciale va a **Clarissa** ed **Elisa**, per rimanere sempre la mie fedeli amiche di Vara e di Genova, nonostante i km di distanza. Per riportarmi in valle o al mare quando torno, e per tutte le chiaccherate. Per esserci sempre, non importa dove e quando. Un grazie alla **Benni**, a **Emi** e a **Willi**, per le chiamate, i viaggi, ma soprattutto le risate che han fatto volare via cinque anni di liceo e sono rimaste sempre le stesse.

Come non ringraziare le "Pains are back", il piú bel gruppo di studentesse di Biotecnologie di Genova. Grazie per sopportarmi, anche quando sono riluttante a normali forme di comunicazione tramite social media. Grazie **Fra**, per capirmi sempre, anche quando entro in totale paranoia a Capodanno. Per essere super paziente e per esserci sempre. Grazie **Sara**, perché niente sembra esser cambiato quando ci rivediamo, per farmi ridere solo al pensarti, per essere cosí intrapredente e fonte di ispirazione. Grazie **Ele**, per essere al tempo stesso svampi e tostistissima, per avere mille idee, per saper combinare una miriade interessi allo stesso tempo. Grazie **Guenda**, per la tua simpatia e le tue risate. Per dare un ulteriore pizzico di pazzia al gruppo. Ma ti prego di tenere i gatti distanti da queste pagine, anche la tesi potrebbe iniziare a starnutire.

I deeply thank all **Bodén** family for your warmness and kindness, for involving me in so many adventures and fun family events. Thanks, **Henrik**, for always creating such interesting conversations, for being supportive and for all the laughs. Thanks **Richard**, **Ulrika** and **Lucas**, for organizing so many activities and always involving me, from teaching me cross-countries ski, going mountain biking and exploring different parts of Sweden. Most importantly, thanks for sharing with me all the fun. Thanks **Karin**, for being so kind and always supportive, and for sharing your cooking and planting expertise, which are amazing.

Ma il piú grande ringraziamento di tutti va alla mia famiglia, quell'insieme di progressive rock, musica dance anni ´80, passione politica e duro lavoro che mi ha formato e mi fa portato fin qui, rendendo ogni passo della mia vita entusiasmante. Grazie a **mamma** e **papá**, per avermi trasmesso l'arte dell'impegno, per avermi insegnato che per raggiungere traguardi bisogna metterci tutta la passione ma anche prendersi le proprie responsabilitá, senza mai dimenticarsi di divertirsi. Per essere voi la mia primaria fonte di ispirazione. Per accompagnarmi ovunque la vita mi porti. Per avermi sempre supportato, ma mai forzato. Grazie allo **zio Lino**, per portare un po´ di sana filosofia nella famiglia, per le tue riflessioni che mi riportano sul piano umano quando quello scientifico prende il sopravvento. Grazie alla **zia Laura**, per i tuoi sorrisi e le risate, per portare cosí tanto calore in famiglia. Grazie allo **zio Roberto** e alla passione politica, per essere una fonte di ispirazione. Grazie alla **zia Simona**, l'anima artistica della famiglia. A **Paola**, per essere sempre positiva e pronta ad affrontare nuove avventure. Grazie alla **nonna Luisa**, che con i tuoi racconti, cosí veri ed incredibili a pensarci, mi hai insegnato che nella vita, a volte, bisogna pur saper improvvisare. Grazie alle vecchie generazioni, non avermi mai lasciato. Questo traguardo non é altro che il risultato del vostro impegno e delle vostre lotte.

Un ringraziamento speciale va al mio cuginetto **Pietro** per la grande persona che sei sempre stato. Grazie per la tua sensibilitá, per ispirarmi con le tue passioni e le nuove avventure, e il tuo entusiasmo verso il futuro.

Finally, I want to express my deepest love and gratitude to **Andreas**, the sailor that adjusts the route when I drift away, the peaceful song that calms my soul, the upbeat rhythm that cheers me up, the feeling that keeps me smiling. I cannot not imagine a funnier and more supportive person to share my days with.

10 REFERENCES

1. Sung, H. *et al.* Global Cancer Statistics 2020: GLOBOCAN Estimates of Incidence and Mortality Worldwide for 36 Cancers in 185 Countries. *CA: A Cancer Journal for Clinicians* **71**, 209–249 (2021).
2. World Health Organization. *Global Health Estimates 2020: Deaths by Cause, Age, Sex, by Country and by Region, 2000-2019.* (2020).
3. Mbeunkui, F. & Johann, D. J. Cancer and the tumor microenvironment: A review of an essential relationship. *Cancer Chemotherapy and Pharmacology* **63**, 571–582 (2009).
4. Wild, C. P., Weiderpass, E. & Stewart, B. W. *World Cancer Report 2020*. *International Agency for Research on Cancer 2020* https://linkinghub.elsevier.com/retrieve/pii/S004578251000068X (2020).
5. Brambilla, E. & Travis, W. D. *World Cancer Report 2014*. *Geneva: WHO* (2014). doi:9283204298.
6. Dunn, G. P., Old, L. J. & Schreiber, R. D. The Three Es of Cancer Immunoediting. *Annual Review of Immunology* **22**, 329–360 (2004).
7. Dunn, G. P., Bruce, A. T., Ikeda, H., Old, L. J. & Schreiber, R. D. Cancer immunoediting: from immunosurveillance to tumor escape. *Nature Immunology* **3**, 991–998 (2002).
8. COLEY, W. B. CONTRIBUTION TO THE KNOWLEDGE OF SARCOMA. *Annals of Surgery* **14**, 199–220 (1891).
9. McCarthy, E. F. The toxins of William B. Coley and the treatment of bone and soft-tissue sarcomas. *The Iowa orthopaedic journal* **26**, 154–8 (2006).
10. Grünewald, T. G. *et al.* Sarcoma treatment in the era of molecular medicine. *EMBO Molecular Medicine* **12**, (2020).
11. Bruns, P. von. Die Heilwirkung des Erysipelas auf Geschwülste. *Berliner Klinische Wochenschrift* **3**, (1888).
12. Fehleisen, F. Die Aetiologie des Erysipels. *Deutsche Medizinische Wochenschrift* **9**, 237–238 (1883).
13. Busch, W. Aus der Sitzung der medicinischen Section vom 13 November 1867. *Berliner Klinische Wochenschrift* **5**, (1867).
14. COLEY, W. B. THE TREATMENT OF INOPERABLE SARCOMA WITH THE ’MIXED TOXINS OF ERYSIPELAS AND BACILLUS PRODIGIOSUS. *Journal of the American Medical Association* **XXXI**, 456 (1898).
15. Shrady, G. F. & Stedman, T. L. *Medical Record*. (W. Wood., 1902).
16. Grubbé, E. H. Priority in the Therapeutic Use of X-rays. *Radiology* **21**, 156–162 (1933).
17. Lederman, M. The early history of radiotherapy: 1895-1939. *International Journal of Radiation Oncology, Biology, Physics* **7**, 639–648 (1981).

18. Giesel, F. Ueber radioactive stoffe. *Berichte der deutschen chemischen Gesellschaft* **33**, 3569–3571 (1900).

19. Curie, P. & Curie, M. Sur la radioactivité provoquée par les rayons de Becquerel. *Comptes rendus des séances de l'académie des sciences* **129**, 714–716 (1899).

20. Curie, M. *Pierre Curie*. (The Machmillan Company, 1923).

21. Becquerel, H. & Curie, P. Action physiologique des rayons du radium. *Compt. Rend. Acad. Sci* **132**, 1289–1291 (1901).

22. Mould, R. F. Pierre Curie, 1859–1906. *Current Oncology* **14**, 74–82 (2007).

23. Calmette, A. L'Infection Bacillaire et la Tuberculose chez l'Homme et chez les Animaux. *JAMA: The Journal of the American Medical Association* **80**, 1265 (1936).

24. OLD, L. J., CLARKE, D. A. & BENACERRAF, B. Effect of Bacillus Calmette-Guérin Infection on Transplanted Tumours in the Mouse. *Nature* **184**, 291–292 (1959).

25. Gutterman, J., Mavligit, G., McBride, C., Iii, E. F. & Hersh, E. M. BCG stimulation of immune responsiveness in patients with malignant melanoma. Preliminary report. *Cancer* **32**, 321–327 (1973).

26. Grant, R. M. *et al.* RESULTS OF ADMINISTERING B.C.G. TO PATIENTS WITH MELANOMA. *The Lancet* **304**, 1096–1100 (1974).

27. Donaldson, R. C. Chemoimmunotherapy for cancer of the head and neck. *The American Journal of Surgery* **126**, 507–512 (1973).

28. Morales, A. & Eidinger, D. Bacillus calmette guerin in the treatment of adenocarcinoma of the kidney. *Journal of Urology* **115**, 377–380 (1976).

29. Morales, A., Eidinger, D. & Bruce, A. W. Intracavitary Bacillus Calmette-Guerin in the Treatment of Superficial Bladder Tumors. *Journal of Urology* **116**, 180–186 (1976).

30. Dobosz, P. & Dzieciątkowski, T. The Intriguing History of Cancer Immunotherapy. *Frontiers in Immunology* **10**, (2019).

31. Ehrlich, P. Ueber den jetzigen stand der Karzinomforschung. *Nederlands Tijdschrift voor Geneeskunde* **5**, 273–290 (1909).

32. Murphy, J. B. & Morton, J. J. The Lymphocyte as a Factor in Natural and Induced Resistance to Transplanted Cancer. *Proceedings of the National Academy of Sciences* **1**, 435–437 (1915).

33. Burnet, M. Cancer-A Biological Approach* Iii. Viruses Associated With Neoplastic Conditions. *British Medical Journal* **1**, 841 (1957).

34. Burnet, F. M. Immunological Surveillance in Neoplasia. *Immunological Reviews* **7**, 3–25 (1971).

35. Thomas, L. On immunosurveillance in human cancer. *Yale Journal of Biology and Medicine* **55**, 329–333 (1982).

36. Golstein, P., Wigzell, H., Blomgren, H. & Svedmyr, E. A. J. Cells mediating specific in vitro cytotoxicity. II. Probable autonomy of thymus-processed lymphocytes (T cells) for the killing of allogeneic target cells. *Journal of Experimental Medicine* **135**, 890–906 (1972).

37. Golstein, P. & Blomgren, H. Further evidence for autonomy of T cells mediating specific in vitro cytotoxicity: Efficiency of very small amounts of highly purified T cells. *Cellular Immunology* **9**, 127–141 (1973).

38. Kiessling, R., Klein, E., Pross, H. & Wigzell, H. „Natural" killer cells in the mouse. II. Cytotoxic cells with specificity for mouse Moloney leukemia cells. Characteristics of the killer cell. *European Journal of Immunology* **5**, 117–121 (1975).

39. Kiessling, R., Klein, E. & Wigzell, H. „Natural" killer cells in the mouse. I. Cytotoxic cells with specificity for mouse Moloney leukemia cells. Specificity and distribution according to genotype. *European Journal of Immunology* **5**, 112–117 (1975).

40. Rosenberg, S. A. *et al.* Biological Activity of Recombinant Human Interleukin-2 Produced in Escherichia coli. *Science* **223**, 1412–1415 (1984).

41. Shankaran, V. *et al.* IFNγ and lymphocytes prevent primary tumour development and shape tumour immunogenicity. *Nature* **410**, 1107–1111 (2001).

42. Dighe, A. S., Richards, E., Old, L. J. & Schreiber, R. D. Enhanced in vivo growth and resistance to rejection of tumor cells expressing dominant negative IFNγ receptors. *Immunity* **1**, 447–456 (1994).

43. Kaplan, D. H. *et al.* Demonstration of an interferon γ-dependent tumor surveillance system in immunocompetent mice. *Proceedings of the National Academy of Sciences* **95**, 7556–7561 (1998).

44. Ishida, Y., Agata, Y., Shibahara, K. & Honjo, T. Induced expression of PD-1, a novel member of the immunoglobulin gene superfamily, upon programmed cell death. *EMBO Journal* **11**, 3887–3895 (1992).

45. Leach, D. R., Krummel, M. F. & Allison, J. P. Enhancement of antitumor immunity by CTLA-4 blockade. *Science* **271**, 1734–1736 (1996).

46. Falzone, L., Salomone, S. & Libra, M. Evolution of cancer pharmacological treatments at the turn of the third millennium. *Frontiers in Pharmacology* **9**, (2018).

47. Chen, D. S. & Mellman, I. Oncology Meets Immunology: The Cancer-Immunity Cycle. *Immunity* **39**, 1–10 (2013).

48. Dunn, G. P., Old, L. J. & Schreiber, R. D. The three Es of cancer immunoediting. *Annual Review of Immunology* **22**, 329–360 (2004).

49. Binnewies, M. *et al.* Understanding the tumor immune microenvironment (TIME) for effective therapy. *Nature Medicine* **24**, 541–550 (2018).

50. Balkwill, F. R., Capasso, M. & Hagemann, T. The tumor microenvironment at a glance. *Journal of Cell Science* **125**, 5591–5596 (2012).

51. Yu, Y. & Cui, J. Present and future of cancer immunotherapy: A tumor microenvironmental perspective. *Oncology Letters* **16**, 4105–4113 (2018).

52. Beatty, G. L. & Gladney, W. L. Immune escape mechanisms as a guide for cancer immunotherapy. *Clinical Cancer Research* **21**, 687–692 (2015).

53. Pardoll, D. M. The blockade of immune checkpoints in cancer immunotherapy. *Nature Reviews Cancer* **12**, 252–264 (2012).

54. Lozano, E., Dominguez-Villar, M., Kuchroo, V. & Hafler, D. A. The TIGIT/CD226 Axis Regulates Human T Cell Function. *The Journal of Immunology* **188**, 3869–3875 (2012).

55. Wei, S. C., Duffy, C. R. & Allison, J. P. Fundamental mechanisms of immune checkpoint blockade therapy. *Cancer Discovery* **8**, 1069–1086 (2018).

56. Vaddepally, R. K., Kharel, P., Pandey, R., Garje, R. & Chandra, A. B. Review of Indications of FDA-Approved Immune Checkpoint Inhibitors per NCCN Guidelines with the Level of Evidence. *Cancers* **12**, (2020).

57. Ljunggren, H.-G. & Kärre, K. In search of the 'missing self': MHC molecules and NK cell recognition. *Immunology Today* **11**, 237–244 (1990).

58. Krneta, T., Gillgrass, A., Chew, M. & Ashkar, A. A. The breast tumor microenvironment alters the phenotype and function of natural killer cells. *Cellular & Molecular Immunology* **13**, 628–639 (2016).

59. Artis, D. & Spits, H. The biology of innate lymphoid cells. *Nature* **517**, (2015).

60. Seillet, C., Belz, G. T. & Huntington, N. D. Development, homeostasis, and heterogeneity of NK cells and ILC1. *Current Topics in Microbiology and Immunology* (2016) doi:10.1007/82_2015_474.

61. Mak, T. W. & Saunders, M. E. 14 - T Cell Activation. in *The Immune Response* (eds. Mak, T. W. & Saunders, M. E.) 373–401 (Academic Press, 2006). doi:https://doi.org/10.1016/B978-012088451-3.50016-8.

62. Vivier, E. Functions of natural killer cells. *Nature immunology* **9**, 503–10 (2008).

63. Robertson, M. J. & Ritz, J. Biology and clinical relevance of human natural killer cells. *Blood* **76**, 2421 LP – 2438 (1990).

64. Hashemi, E. & Malarkannan, S. Tissue-Resident NK Cells: Development, Maturation, and Clinical Relevance. *Cancers* **12**, 1553 (2020).

65. Santoli, D., Trinchieri, G., Moretta, L., Zmijewski, C. M. & Koprowski, H. Spontaneous cell-mediated cytotoxicity in humans. Distribution and characterization of the effector cell. *Clinical and experimental immunology* **33**, 309–18 (1978).

66. Carrega, P. & Ferlazzo, G. Natural killer cell distribution and trafficking in human tissues. *Frontiers in Immunology* **3**, (2012).

67. Cooper, M. A., Fehniger, T. A. & Caligiuri, M. A. The biology of human natural killer-cell subsets. *Trends in Immunology* **22**, 633–640 (2001).

68. Robertson, M. J. *et al.* Response of human natural killer (NK) cells to NK cell stimulatory factor (NKSF): cytolytic activity and proliferation of NK cells are differentially regulated by NKSF. *The Journal of experimental medicine* (1992) doi:10.1084/jem.175.3.779.

69. Seillet, C. & Belz, G. T. Differentiation and diversity of subsets in group 1 innate lymphoid cells. *International immunology* **28**, 3–11 (2016).

70. Cooper, M. A. *et al.* Human natural killer cells: a unique innate immunoregulatory role for the CD56(bright) subset. *Blood* **97**, 3146–51 (2001).

71. Robertson, M. J. Role of chemokines in the biology of natural killer cells. *Journal of Leukocyte Biology* **71**, 173–183 (2002).

72. Vivier, E. *et al.* Innate or Adaptive Immunity? The Example of Natural Killer Cells. *Science* **331**, 44–49 (2011).

73. Vacca, P., Mingari, M. C. & Moretta, L. Natural killer cells in human pregnancy. *Journal of Reproductive Immunology* (2013) doi:10.1016/j.jri.2012.10.008.

74. Kalkunte, S. S. *et al.* Vascular Endothelial Growth Factor C Facilitates Immune Tolerance and Endovascular Activity of Human Uterine NK Cells at the Maternal-Fetal Interface. *The Journal of Immunology* **182**, 4085–4092 (2009).

75. Hanna, J. *et al.* Decidual NK cells regulate key developmental processes at the human fetal-maternal interface. *Nature Medicine* (2006) doi:10.1038/nm1452.

76. le Bouteiller, P. Human decidual NK cells: Unique and tightly regulated effector functions in healthy and pathogen-infected pregnancies. *Frontiers in Immunology* **4**, 1–5 (2013).

77. Tosello-Trampont, A., Surette, F. A., Ewald, S. E. & Hahn, Y. S. Immunoregulatory Role of NK Cells in Tissue Inflammation and Regeneration. *Frontiers in Immunology* **8**, 1–10 (2017).

78. Kohrt, H. E. *et al.* Anti-KIR antibody enhancement of anti-lymphoma activity of natural killer cells as monotherapy and in combination with anti-CD20 antibodies. *Blood* **123**, 678–686 (2014).

79. O'Sullivan, T. E. *et al.* Adipose-Resident Group 1 Innate Lymphoid Cells Promote Obesity-Associated Insulin Resistance. *Immunity* **45**, 428–441 (2016).

80. Fernandez, N. C. *et al.* Dendritic cells (DC) promote natural killer (NK) cell functions: Dynamics of the human DC/NK cell cross talk. *European Cytokine Network* (2002).

81. Nielsen, N., Ødum, N., Ursø, B., Lanier, L. L. & Spee, P. Cytotoxicity of CD56bright NK cells towards autologous activated CD4+ T cells is mediated through NKG2D, LFA-1 and TRAIL and dampened via CD94/NKG2A. *PloS one* **7**, e31959 (2012).

82. Cerboni, C. *et al.* Antigen-activated human T lymphocytes express cell-surface NKG2D ligands via an ATM/ATR-dependent mechanism and become susceptible to autologous NK-cell lysis. *Blood, The Journal of the American Society of Hematology* **110**, 606–615 (2007).

83. Mayol, K., Biajoux, V., Marvel, J., Balabanian, K. & Walzer, T. Sequential desensitization of CXCR4 and S1P5 controls natural killer cell trafficking. *Blood* **118**, 4863–4871 (2011).

84. Broxmeyer, H. E. *et al.* Rapid mobilization of murine and human hematopoietic stem and progenitor cells with AMD3100, a CXCR4 antagonist. *The Journal of Experimental Medicine* **201**, 1307–1318 (2005).

85. Bernardini, G. *et al.* CCL3 and CXCL12 regulate trafficking of mouse bone marrow NK cell subsets. *Blood* **111**, 3626–3634 (2008).

86. Zhang, Y. *et al.* In vivo kinetics of human natural killer cells: The effects of ageing and acute and chronic viral infection. *Immunology* **121**, 258–265 (2007).

87. Baekkevold, E. S. *et al.* The ccr7 ligand elc (ccl19) is transcytosed in high endothelial venules and mediates t cell recruitment. *J Exp Med* (2001) doi:10.1084/jem.193.9.1105.

88. Gregoire, C. *et al.* The trafficking of natural killer cells. *Immunol Rev* **220**, 169–182 (2007).

89. Campbell, J. J. *et al.* Unique Subpopulations of CD56+ NK and NK-T Peripheral Blood Lymphocytes Identified by Chemokine Receptor Expression Repertoire. *The Journal of Immunology* **166**, 6477–6482 (2001).

90. Juelke, K. *et al.* CD62L expression identifies a unique subset of polyfunctional CD56dimNK cells. *Blood* **116**, 1299–1307 (2010).

91. Parolini, S. *et al.* The role of chemerin in the colocalization of NK and dendritic cell subsets into inflamed tissues. (2007) doi:10.1182/blood-2006-08-038844.

92. Martín-Fontecha, A. *et al.* Induced recruitment of NK cells to lymph nodes provides IFN-γ for TH1 priming. *Nature Immunology* (2004) doi:10.1038/ni1138.

93. Platonova, S. *et al.* Profound coordinated alterations of intratumoral NK cell phenotype and function in lung carcinoma. *Cancer Research* **71**, 5412–5422 (2011).

94. Carrega, P. *et al.* Natural killer cells infiltrating human nonsmall-cell lung cancer are enriched in CD56brightCD16-cells and display an impaired capability to kill tumor cells. *Cancer* **112**, 863–875 (2008).

95. Sconocchia, G. *et al.* Melanoma cells inhibit NK cell functions - Letter. *Cancer Research* **72**, 5428–5429 (2012).

96. Remark, R. *et al.* Characteristics and clinical impacts of the immune environments in colorectal and renal cell carcinoma lung metastases: Influence of tumor origin. *Clinical Cancer Research* **19**, 4079–4091 (2013).

97. Platonova, S. *et al.* Profound coordinated alterations of intratumoral NK cell phenotype and function in lung carcinoma. *Cancer Research* **71**, 5412–5422 (2011).

98. Mamessier, E. *et al.* Human breast cancer cells enhance self tolerance by promoting evasion from NK cell antitumor immunity. *Journal of Clinical Investigation* **121**, 3609–3622 (2011).

99. Carlsten, M. *et al.* Primary Human Tumor Cells Expressing CD155 Impair Tumor Targeting by Down-Regulating DNAM-1 on NK Cells. *The Journal of Immunology* **183**, 4921–4930 (2009).

100. Erdag, G. *et al*. Immunotype and immunohistologic characteristics of tumor-infiltrating immune cells are associated with clinical outcome in metastatic melanoma. *Cancer Research* **72**, 1070–1080 (2012).

101. Sconocchia, G. *et al*. Tumor infiltration by FcIγRIII (CD16)+ myeloid cells is associated with improved survival in patients with colorectal carcinoma. *International Journal of Cancer* **128**, 2663–2672 (2011).

102. Sconocchia, G. *et al.* Defective Infiltration of Natural Killer Cells in MICA/B-Positive Renal Cell Carcinoma Involves β2-Integrin-Mediated Interaction. *Neoplasia* **11**, 662–671 (2009).

103. Halama, N. *et al.* Natural killer cells are scarce in colorectal carcinoma tissue despite high levels of chemokines and cytokines. *Clinical Cancer Research* **17**, 678–689 (2011).

104. Pachynski, R. K. *et al.* The chemoattractant chemerin suppresses melanoma by recruiting natural killer cell antitumor defenses. *The Journal of Experimental Medicine* **209**, 1427–1435 (2012).

105. Xie, K. Interleukin-8 and human cancer biology. *Cytokine and Growth Factor Reviews* **12**, 375–391 (2001).

106. Sun, H., Sun, C. & Xiao, W. Expression regulation of co-inhibitory molecules on human natural killer cells in response to cytokine stimulations. *Cytokine* **65**, 33–41 (2014).

107. Moretta, A., Bottino, C., Mingari, M. C., Biassoni, R. & Moretta, L. What is a natural killer cell? *Nature Immunology* **3**, 6–8 (2002).

108. Bryceson, Y. T., March, M. E., Ljunggren, H.-G. & Long, E. O. Synergy among receptors on resting NK cells for the activation of natural cytotoxicity and cytokine secretion. *Blood* **107**, 159–66 (2006).

109. Bryceson, Y. T., Ljunggren, H.-G. & Long, E. O. Minimal requirement for induction of natural cytotoxicity and intersection of activation signals by inhibitory receptors. *Blood* **114**, 2657–66 (2009).

110. Fauriat, C., Long, E. O., Ljunggren, H.-G. & Bryceson, Y. T. Regulation of human NK-cell cytokine and chemokine production by target cell recognition. *Blood* **115**, 2167–2176 (2010).

111. Bryceson, Y. T., March, M. E., Barber, D. F., Ljunggren, H.-G. & Long, E. O. Cytolytic granule polarization and degranulation controlled by different receptors in resting NK cells. *The Journal of Experimental Medicine ARTICLE 1001 JEM* **202**, (2005).

112. Smith, M. A. *et al.* PRDM1/Blimp-1 Controls Effector Cytokine Production in Human NK Cells. *The Journal of Immunology* **185**, 6058–6067 (2010).

113. Vivier, E., Nunès, J. A. & Vély, F. Natural killer cell signaling pathways. *Science* **306**, 1517–1519 (2004).

114. Stanietsky, N. *et al.* The interaction of TIGIT with PVR and PVRL2 inhibits human NK cell cytotoxicity. *Proceedings of the National Academy of Sciences of the United States of America* **106**, 17858–63 (2009).

115. Yu, X. *et al.* The surface protein TIGIT suppresses T cell activation by promoting the generation of mature immunoregulatory dendritic cells. *Nature Immunology* **10**, 48–57 (2009).

116. Parham, P., Norman, P. J., Abi-Rached, L. & Guethlein, L. A. Human-specific evolution of killer cell immunoglobulin-like receptor recognition of major histocompatibility complex class I molecules. *Philosophical Transactions of the Royal Society B: Biological Sciences* (2012) doi:10.1098/rstb.2011.0266.

117. Husain, B. *et al.* A platform for extracellular interactome discovery identifies novel functional binding partners for the immune receptors B7-H3/CD276 and PVR/CD155. *Molecular and Cellular Proteomics* **18**, 2310–2323 (2019).

118. Braud, V. M. *et al.* HLA-E binds to natural killer cell receptors CD94/NKG2A, B and C. *Nature* **391**, 795–799 (1998).

119. Bjorkman, P. J. & Parham, P. Structure, Function, and Diversity of Class I Major Histocompatibility Complex Molecules. *Annual Review of Biochemistry* **59**, 253–288 (1990).

120. Borrego, F., Ulbrecht, M., Weiss, E. H., Coligan, J. E. & Brooks, A. G. Recognition of Human Histocompatibility Leukocyte Antigen (HLA)-E Complexed with HLA Class I Signal Sequence–derived Peptides by CD94/NKG2 Confers Protection from Natural Killer Cell–mediated Lysis. *The Journal of Experimental Medicine* **187**, 813–818 (1998).

121. Parham, P. MHC class I molecules and KIRS in human history, health and survival. *Nature Reviews Immunology* **5**, 201–214 (2005).

122. Kärre, K., Ljunggren, H. G., Piontek, G. & Kiessling, R. Selective rejection of H–2-deficient lymphoma variants suggests alternative immune defence strategy. *Nature* **319**, 675–678 (1986).

123. Kadri, N. *et al.* Dynamic Regulation of NK Cell Responsiveness. in *Current Topics in Microbiology and Immunology* 95–114 (2015). doi:10.1007/82_2015_485.

124. Brodin, P., Kärre, K. & Höglund, P. NK cell education: not an on-off switch but a tunable rheostat. *Trends in Immunology* **30**, 143–149 (2009).

125. Boudreau, J. E. & Hsu, K. C. Natural Killer Cell Education and the Response to Infection and Cancer Therapy: Stay Tuned. *Trends in Immunology* **39**, 222–239 (2018).

126. Goodridge, J. P., Önfelt, B. & Malmberg, K. J. Newtonian cell interactions shape natural killer cell education. *Immunological Reviews* **267**, 197–213 (2015).

127. Anfossi, N. *et al.* Human NK Cell Education by Inhibitory Receptors for MHC Class I. *Immunity* **25**, 331–342 (2006).

128. He, Y. & Tian, Z. NK cell education via nonclassical MHC and non-MHC ligands. *Cellular and Molecular Immunology* **14**, 321–330 (2017).

129. He, Y. *et al.* Contribution of inhibitory receptor TIGIT to NK cell education. *Journal of Autoimmunity* **81**, 1–12 (2017).

130. Petrova, V., Annicchiarico-Petruzzelli, M., Melino, G. & Amelio, I. The hypoxic tumour microenvironment. *Oncogenesis* **7**, (2018).

131. Wang, J. X. *et al.* Lactic acid and an acidic tumor microenvironment suppress anticancer immunity. *International Journal of Molecular Sciences* **21**, 1–14 (2020).

132. Harmon, C. *et al.* Lactate-mediated acidification of tumor microenvironment induces apoptosis of liver-resident NK cells in colorectal liver metastasis. *Cancer Immunology Research* **7**, 335–346 (2019).

133. Brand, A. *et al.* LDHA-Associated Lactic Acid Production Blunts Tumor Immunosurveillance by T and NK Cells. *Cell Metabolism* **24**, 657–671 (2016).

134. Ni, J. *et al.* Single-Cell RNA Sequencing of Tumor-Infiltrating NK Cells Reveals that Inhibition of Transcription Factor HIF-1α Unleashes NK Cell Activity. *Immunity* **52**, 1075-1087.e8 (2020).

135. Solocinski, K. *et al.* Overcoming hypoxia-induced functional suppression of NK cells. *Journal for ImmunoTherapy of Cancer* **8**, (2020).

136. Balsamo, M. *et al.* Hypoxia downregulates the expression of activating receptors involved in NK-cell-mediated target cell killing without affecting ADCC. *European Journal of Immunology* (2013) doi:10.1002/eji.201343448.

137. Ghiringhelli, F. *et al.* CD4 + CD25 + regulatory T cells inhibit natural killer cell functions in a transforming growth factor–β–dependent manner. *The Journal of Experimental Medicine* **202**, 1075–1085 (2005).

138. Li, T. *et al.* Hepatocellular carcinoma-associated fibroblasts trigger NK cell dysfunction via PGE2 and IDO. *Cancer Letters* (2012) doi:10.1016/j.canlet.2011.12.020.

139. Balsamo, M. *et al.* Melanoma-associated fibroblasts modulate NK cell phenotype and antitumor cytotoxicity. *Proceedings of the National Academy of Sciences* (2009) doi:10.1073/pnas.0906481106.

140. Pietra, G. *et al.* Melanoma cells inhibit natural killer cell function by modulating the expression of activating receptors and cytolytic activity. *Cancer Research* (2012) doi:10.1158/0008-5472.CAN-11-2544.

141. El-Gazzar, A., Groh, V. & Spies, T. Immunobiology and conflicting roles of the human NKG2D lymphocyte receptor and its ligands in cancer. *Journal of immunology (Baltimore, Md. : 1950)* **191**, 1509–15 (2013).

142. Tarazona, R. *et al.* Natural Killer Cell immunomodulation: Targeting Activating, inhibitory, and Co-stimulatory Receptor Signaling for Cancer immunotherapy. **6**, 601 (2015).

143. Nakai, R. *et al.* Overexpression of Necl-5 correlates with unfavorable prognosis in patients with lung adenocarcinoma. *Cancer Science* **101**, 1326–1330 (2010).

144. Stamm, H. *et al.* Immune checkpoints PVR and PVRL2 are prognostic markers in AML and their blockade represents a new therapeutic option. *Oncogene* **37**, 5269–5280 (2018).

145. Masson, D. *et al.* Overexpression of the CD155 gene in human colorectal carcinoma. *Gut* **49**, 236–240 (2001).

146. Sloan, K. E. *et al.* CD155/PVR plays a key role in cell motility during tumor cell invasion and migration. *BMC Cancer* **4**, 73 (2004).

147. Chandramohan, V. *et al.* Validation of an immunohistochemistry assay for detection of CD155, the poliovirus receptor, in malignant gliomas. *Archives of Pathology and Laboratory Medicine* **141**, 1697–1704 (2017).

148. Sho, M. *et al.* Clinical significance of CD155 expression in human pancreatic cancer. *Anticancer Research* **35**, 2287–2297 (2015).

149. Bevelacqua, V. *et al.* Nectin like-5 overexpression correlates with the malignant phenotype in cutaneous melanoma. *Oncotarget* **3**, 1–6 (2012).

150. Shibuya, A. *et al.* DNAM-1, A Novel Adhesion Molecule Involved in the Cytolytic Function of T Lymphocytes. *Immunity* **4**, 573–581 (1996).

151. Bottino, C. *et al.* Identification of PVR (CD155) and Nectin-2 (CD112) as Cell Surface Ligands for the Human DNAM-1 (CD226) Activating Molecule. *The Journal of Experimental Medicine* **198**, 557–567 (2003).

152. Wang, P. L., Farrell, S. O., Clayberger, C. & Krensky, A. M. Identification and molecular cloning of tactile. A novel human T cell activation antigen that is a member of the Ig gene superfamily. *The Journal of Immunology* **148**, 2600 LP – 2608 (1992).

153. Fuchs, A., Cella, M., Giurisato, E., Shaw, A. S. & Colonna, M. Cutting edge: CD96 (tactile) promotes NK cell-target cell adhesion by interacting with the poliovirus receptor (CD155). *Journal of immunology (Baltimore, Md. : 1950)* **172**, 3994–8 (2004).

154. Vilches, C. *et al.* KIR2DL5, a Novel Killer-Cell Receptor with a D0-D2 Configuration of Ig-Like Domains. *The Journal of Immunology* **164**, 5797–5804 (2000).

155. Estefanía, E. *et al.* Human KIR2DL5 Is an Inhibitory Receptor Expressed on the Surface of NK and T Lymphocyte Subsets. *The Journal of Immunology* **178**, 4402–4410 (2007).

156. Ikeda, W. *et al.* Tage4/nectin-like molecule-5 heterophilically trans-interacts with cell adhesion molecule nectin-3 and enhances cell migration. *Journal of Biological Chemistry* **278**, 28167–28172 (2003).

157. Freistadt, M. S. & Eberle, K. E. Physical association between CD155 and CD44 in human monocytes. *Molecular Immunology* **34**, 1247–1257 (1997).

158. Siddique, T. *et al.* The poliovirus sensitivity (PVS) gene is on chromosome 19q12→q13.2. *Genomics* **3**, 156–160 (1988).

159. Chadéneau, C., Lecabellec, M., Lemoullac, B., Meflah, K. & Denis, M. G. Over-expression of a novel member of the immunoglobulin superfamily in Min mouse intestinal adenomas. *International Journal of Cancer* **68**, 817–821 (1996).

160. Nobis, P. *et al.* Production of a monoclonal antibody against an epitope on HeLa cells that is the functional poliovirus binding site. *J. gen. Virol* **66**, 2563–2569 (1985).

161. Mendelsohn, C. L., Wimmer, E. & Racaniello', V. R. Cellular Receptor for Poliovirus: Molecular Cloning,Nucleotide Sequence, and the Expression of a New Member of the lmmunoglobulin Superfamily. *Cell* **56**, 855–865 (1989).

162. Koike, S. *et al.* The poliovirus receptor protein is produced both as membrane-bound and secreted forms. *The EMBO journal* **9**, 3217–24 (1990).

163. Baury, B. *et al.* Identification of secreted CD155 isoforms. *Biochemical and Biophysical Research Communications* **309**, 175–182 (2003).

164. Iguchi-Manaka, A. *et al.* Increased Soluble CD155 in the Serum of Cancer Patients. (2016) doi:10.1371/journal.pone.0152982.

165. Ohka, S., Ohno, H., Tohyama, K. & Nomoto, A. Basolateral sorting of human poliovirus receptor α involves an interaction with the μ1B subunit of the clathrin adaptor complex in polarized epithelial cells. *Biochemical and Biophysical Research Communications* **287**, 941–948 (2001).

166. Fujito, T. *et al.* Inhibition of cell movement and proliferation by cell–cell contact-induced interaction of Necl-5 with nectin-3. *The Journal of Cell Biology* **171**, 165–173 (2005).

167. Mueller, S. & Wimmer, E. Recruitment of Nectin-3 to Cell-Cell Junctions through trans - Heterophilic Interaction with CD155, a Vitronectin and Poliovirus Receptor That Localizes to α v β 3 Integrin-containing Membrane Microdomains. *Journal of Biological Chemistry* **278**, 31251–31260 (2003).

168. Kajita, M., Ikeda, W., Tamaru, Y. & Takai, Y. *Regulation of platelet-derived growth factor-induced Ras signaling by poliovirus receptor Necl-5 and negative growth regulator Sprouty2*. *Genes to Cells* vol. 12 (2007).

169. Masoumi-Moghaddam, S., Amini, A. & Morris, D. L. The developing story of Sprouty and cancer. *Cancer and Metastasis Reviews* vol. 33 695–720 (2014).

170. Oda, T., Ohka, S. & Nomoto, A. Ligand stimulation of CD155α inhibits cell adhesion and enhances cell migration in fibroblasts. *Biochemical and Biophysical Research Communications* **319**, 1253–1264 (2004).

171. Amano, H. *et al.* Interaction and localization of Necl-5 and PDGF receptor β at the leading edges of moving NIH3T3 cells: Implications for directional cell movement. *Genes to Cells* **13**, 269–284 (2008).

172. Minami, A. *et al.* Necl-5/PVR enhances PDGF-induced attraction of growing microtubules to the plasma membrane of the leading edge of moving NIH3T3 cells. *Genes to Cells* **15**, 1123–1135 (2010).

173. Reymond, N. *et al.* DNAM-1 and PVR Regulate Monocyte Migration through Endothelial Junctions. *Journal of Experimental Medicine* **199**, 1331–1341 (2004).

174. Sullivan, D. P., Seidman, M. A. & Muller, W. A. Poliovirus receptor (CD155) regulates a step in transendothelial migration between PECAM and CD99. *American Journal of Pathology* **182**, 1031–1042 (2013).

175. Quail, D. F. & Joyce, J. A. Microenvironmental regulation of tumor progression and metastasis. *Nature Medicine* vol. 19 1423–1437 (2013).

176. Tane, S. *et al.* The role of Necl-5 in the invasive activity of lung adenocarcinoma. *Experimental and Molecular Pathology* **94**, 330–335 (2013).

177. Merrill, M. K. *et al.* Poliovirus receptor CD155-targeted oncolysis of glioma. *Neuro-Oncology* **6**, 208–217 (2004).

178. Casado, J. G. *et al.* Expression of adhesion molecules and ligands for activating and costimulatory receptors involved in cell-mediated cytotoxicity in a large panel of human melanoma cell lines. *Cancer Immunology, Immunotherapy* **58**, 1517–1526 (2009).

179. Peng, Y.-P. *et al.* Altered expression of CD226 and CD96 on natural killer cells in patients with pancreatic cancer. *Oncotarget* **7**, (2016).

180. Lepletier, A. *et al.* Tumor CD155 Expression Is Associated with Resistance to Anti-PD1 Immunotherapy in Metastatic Melanoma. *Clinical Cancer Research* **26**, 3671–3681 (2020).

181. Braun, M. *et al*. CD155 on Tumor Cells Drives Resistance to Immunotherapy by Inducing the Degradation of the Activating Receptor CD226 in CD8+ T Cells. *Immunity* **53**, 805-823.e15 (2020).

182. Qu, P. *et al*. Loss of CD155 expression predicts poor prognosis in hepatocellular carcinoma. *Histopathology* **66**, 706–14 (2015).

183. Gong, J. *et al.* UPR decreases CD226 ligand CD155 expression and sensitivity to NK cell-mediated cytotoxicity in hepatoma cells. *European Journal of Immunology* **44**, 3758–3767 (2014).

184. Brandetti, E. *et al.* MYCN is an immunosuppressive oncogene dampening the expression of ligands for NK-cell-activating receptors in human high-risk neuroblastoma. *OncoImmunology* **6**, e1316439 (2017).

185. Chen, B., Lee, J. B., Kang, H., Minden, M. D. & Zhang, L. Targeting chemotherapy-resistant leukemia by combining DNT cellular therapy with conventional chemotherapy. *Journal of Experimental & Clinical Cancer Research* **37**, 88 (2018).

186. Soriani, A. *et al.* ATM-ATR–dependent up-regulation of DNAM-1 and NKG2D ligands on multiple myeloma cells by therapeutic agents results in enhanced NK-cell susceptibility and is associated with a senescent phenotype. doi:10.1182/blood-2008-08.

187. Niu, C. *et al.* Low-dose bortezomib increases the expression of NKG2D and DNAM-1 ligands and enhances induced NK and γδ T cell-mediated lysis in multiple myeloma. *Oncotarget* **8**, 5954–5964 (2017).

188. Soriani, A. *et al.* p38 MAPK differentially controls NK activating ligands at transcriptional and post-transcriptional level on multiple myeloma cells. *OncoImmunology* **6**, e1264564 (2017).

189. Vassena, L., Giuliani, E., Matusali, G., Cohen, E. A. & Doria, M. The human immunodeficiency virus type 1 Vpr protein upregulates PVR via activation of the ATR-mediated DNA damage response pathway. *Journal of General Virology* **94**, 2664–2669 (2013).

190. Bachelet, I., Munitz, A., Mankutad, D. & Levi-Schaffer, F. Mast cell costimulation by CD226/CD112 (DNAM-1/Nectin-2): A novel interface in the allergic process. *Journal of Biological Chemistry* **281**, 27190–27196 (2006).

191. Burns, G. F., Triglia, T., Werkmeister, J. A., CG, B. & AW, B. TLiSA1, a human T lineage-specific activation antigen involved in the differentiation of cytotoxic T lymphocytes and anomalous killer cells from their precursors. *J Exp Med* **161**, 1063–78 (1985).

192. Scott, J. L. *et al.* Characterization of a novel membrane glycoprotein involved in platelet activation. *Journal of Biological Chemistry* **264**, 13475–13482 (1989).

193. Chan, C. J. *et al.* DNAM-1/CD155 Interactions Promote Cytokine and NK Cell-Mediated Suppression of Poorly Immunogenic Melanoma Metastases. *The Journal of Immunology* **184**, 902–911 (2010).

194. Lakshmikanth, T. *et al.* NCRs and DNAM-1 mediate NK cell recognition and lysis of human and mouse melanoma cell lines in vitro and in vivo. *Journal of Clinical Investigation* **119**, 1251–1263 (2009).

195. Cho, D. *et al.* Cytotoxicity of activated natural killer cells against pediatric solid tumors. *Clinical Cancer Research* **16**, 3901–3909 (2010).

196. Verhoeven, D. H. J. *et al.* NK cells recognize and lyse Ewing sarcoma cells through NKG2D and DNAM-1 receptor dependent pathways. *Molecular Immunology* **45**, 3917–3925 (2008).

197. Toutirais, O. *et al.* DNAX accessory molecule-1 (CD226) promotes human hepatocellular carcinoma cell lysis by Vγ9Vδ2 T cells. *European Journal of Immunology* **39**, 1361–1368 (2009).

198. Carlsten, M. *et al.* Primary Human Tumor Cells Expressing CD155 Impair Tumor Targeting by Down-Regulating DNAM-1 on NK Cells. *The Journal of Immunology* **183**, 4921–4930 (2009).

199. Carlsten, M. *et al.* DNAX accessory molecule-1 mediated recognition of freshly isolated ovarian carcinoma by resting natural killer cells. *Cancer Research* **67**, 1317–1325 (2007).

200. Rocca, Y. S. *et al.* Phenotypic and functional dysregulated blood NK cells in colorectal cancer patients can be activated by cetuximab plus IL-2 or IL-15. *Frontiers in Immunology* **7**, 413 (2016).

201. Castriconi, R. *et al.* Natural Killer Cell-Mediated Killing of Freshly Isolated Neuroblastoma Cells. *Cancer Research* **64**, 9180–9184 (2004).

202. Tran, H. C. *et al.* TGFβR1 blockade with galunisertib (LY2157299) enhances anti-neuroblastoma activity of the anti-GD2 antibody dinutuximab (ch14.18) with natural killer cells. *Clinical Cancer Research* **23**, 804–813 (2017).

203. El-Sherbiny, Y. M. *et al.* The requirement for DNAM-1, NKG2D, and NKp46 in the natural killer cell-mediated killing of myeloma cells. *Cancer Research* **67**, 8444–8449 (2007).

204. Pende, D. *et al.* Expression of the DNAM-1 ligands, Nectin-2 (CD112) and poliovirus receptor (CD155), on dendritic cells: Relevance for natural killer-dendritic cell interaction. *Blood* **107**, 2030–2036 (2006).

205. Magri, G. *et al.* NKp46 and DNAM-1 NK-cell receptors drive the response to human cytomegalovirus-infected myeloid dendritic cells overcoming viral immune evasion strategies. (2011) doi:10.1182/blood-2010.

206. Tahara-Hanaoka, S. Functional characterization of DNAM-1 (CD226) interaction with its ligands PVR (CD155) and nectin-2 (PRR-2/CD112). *International Immunology* **16**, 533–538 (2004).

207. Wang, H. *et al.* Binding mode of the side-by-side two-IgV molecule CD226/DNAM-1 to its ligand CD155/Necl-5. doi:10.1073/pnas.1815716116.

208. de Andrade, L. F., Smyth, M. J. & Martinet, L. DNAM-1 control of natural killer cells functions through nectin and nectin-like proteins. *Immunology and cell biology* **92**, 237–44 (2014).

209. Zhang, Z. *et al.* DNAM-1 controls NK cell activation via an ITT-like motif. *The Journal of Experimental Medicine* **212**, 2165–2182 (2015).

210. Shibuya, A., Lanier, L. L. & Phillips, J. H. Protein kinase C is involved in the regulation of both signaling and adhesion mediated by DNAX accessory molecule-1 receptor. *Journal of immunology (Baltimore, Md. : 1950)* **161**, 1671–6 (1998).

211. Du, X. *et al.* CD226 regulates natural killer cell antitumor responses via phosphorylation-mediated inactivation of transcription factor FOXO1. *Proceedings of the National Academy of Sciences* 201814052 (2018) doi:10.1073/pnas.1814052115.

212. Hara, H. *et al.* The MAGUK family protein CARD11 is essential for lymphocyte activation. *Immunity* **18**, 763–775 (2003).

213. Hanada, T., Lin, L., Tibaldi, E. v, Reinherz, E. L. & Chishti, A. H. GAKIN, a novel kinesin-like protein associates with the human homologue of the Drosophila Discs large tumor suppressor in T lymphocytes. *Journal of Biological Chemistry* **275**, 28774–28784 (2000).

214. Bryceson, Y. T., March, M. E., Ljunggren, H. G. & Long, E. O. Synergy among receptors on resting NK cells for the activation of natural cytotoxicity and cytokine secretion. *Blood* **107**, 159–166 (2006).

215. Kim, H. S. & Long, E. O. Complementary phosphorylation sites in the adaptor protein SLP-76 promote synergistic activation of natural killer cells. *Science signaling* **5**, ra49 (2012).

216. Shibuya, K. *et al.* Physical and functional association of LFA-1 with DNAM-1 adhesion molecule. *Immunity* **11**, 615–623 (1999).

217. Grakoui, A. *et al.* The immunological synapse: A molecular machine controlling T cell activation. *Science* **285**, 221–227 (1999).

218. Springer, T. A. Adhesion receptors of the immune system. *Nature* **346**, 425–434 (1990).

219. Kim, M., Carman, C. v. & Springer, T. A. Bidirectional transmembrane signaling by cytoplasmic domain separation in integrins. *Science* **301**, 1720–1725 (2003).

220. Enqvist, M. *et al.* Coordinated Expression of DNAM-1 and LFA-1 in Educated NK Cells. *The Journal of Immunology* **194**, 4518–4527 (2015).

221. Anfossi, N. *et al.* Human NK Cell Education by Inhibitory Receptors for MHC Class I. *Immunity* **25**, 331–342 (2006).

222. Enqvist, M. *et al.* Coordinated Expression of DNAM-1 and LFA-1 in Educated NK Cells. *Journal of immunology (Baltimore, Md. : 1950)* **194**, 4518–27 (2015).

223. Thomas, L. M., Peterson, M. E. & Long, E. O. Cutting Edge: NK Cell Licensing Modulates Adhesion to Target Cells. *The Journal of Immunology* **191**, 3981–3985 (2013).

224. Wagner, A. K. *et al.* Expression of CD226 is associated to but not required for NK cell education. *Nature Communications* **8**, 15627 (2017).

225. Carlsten, M. *et al.* Primary human tumor cells expressing CD155 impair tumor targeting by down-regulating DNAM-1 on NK cells. *Journal of immunology (Baltimore, Md. : 1950)* **183**, 4921–30 (2009).

226. Chauvin, J. M. *et al.* IL15 stimulation with TIGIT blockade reverses CD155-mediated NK-Cell dysfunction in Melanoma. *Clinical Cancer Research* **26**, 5520–5533 (2020).

227. Sanchez-Correa, B. *et al.* Decreased expression of DNAM-1 on NK cells from acute myeloid leukemia patients. *Immunology and Cell Biology* **90**, 109–115 (2012).

228. Han, B. *et al.* Altered NKp30, NKp46, NKG2D, and DNAM-1 Expression on Circulating NK Cells Is Associated with Tumor Progression in Human Gastric Cancer. *Journal of Immunology Research* **2018**, 1–9 (2018).

229. Iguchi-Manaka, A. *et al.* Increased soluble CD155 in the serum of cancer patients. *PLoS ONE* **11**, e0152982 (2016).

230. Jin, H. S. *et al.* CD226hiCD8+T cells are a prerequisite for anti-TIGIT immunotherapy. *Cancer Immunology Research* **8**, 912–925 (2020).

231. Weulersse, M. *et al.* Eomes-Dependent Loss of the Co-activating Receptor CD226 Restrains CD8+ T Cell Anti-tumor Functions and Limits the Efficacy of Cancer Immunotherapy. *Immunity* **53**, 824-839.e10 (2020).

232. Li, X. Y. *et al.* CD155 loss enhances tumor suppression via combined host and tumor-intrinsic mechanisms. *Journal of Clinical Investigation* **128**, 2613–2625 (2018).

233. Du, Y. *et al.* The CD226 gene in susceptibility of rheumatoid arthritis in the Chinese Han population. *Rheumatology International* **32**, 1299–1304 (2012).

234. Mosaad, Y. M. *et al.* Association between CD226 polymorphism and soluble levels in rheumatoid arthritis: Relationship with clinical activity. *Immunological Investigations* **47**, 264–278 (2018).

235. Hashemi, M. *et al.* CD226 rs763361 (Gly307ser) polymorphism is associated with susceptibility to rheumatoid arthritis in Zahedan, southeast Iran. *Iranian Biomedical Journal* **17**, 194–199 (2013).

236. Piédavent-Salomon, M. *et al.* Multiple sclerosis associated genetic variants of CD226 impair regulatory T cell function. *Brain* **138**, 3263–3274 (2015).

237. Du, Y. *et al.* Association of the CD226 single nucleotide polymorphism with systemic lupus erythematosus in the Chinese Han population. *Tissue Antigens* **77**, 65–67 (2011).

238. Douroudis, K. *et al.* The CD226 Gly307Ser gene polymorphism is associated with severity of psoriasis. *Journal of Dermatological Science* **58**, 160–161 (2010).

239. Dieudé, P. *et al.* Association of the CD226 Ser307 variant with systemic sclerosis. *Arthritis and Rheumatism* **63**, 1097–1105 (2011).

240. Todd, J. A. *et al.* Robust associations of four new chromosome regions from genome-wide analyses of type 1 diabetes. *Nature Genetics* **39**, 857–864 (2007).

241. Abu El-Ella, S. S., Khattab, E. S. A. E. H., El-Mekkawy, M. S. & El-Shamy, A. A. CD226 gene polymorphism (rs763361 C>T) is associated with susceptibility to type 1 diabetes mellitus among Egyptian children. *Archives de Pediatrie* **25**, 378–382 (2018).

242. Boles, K. S. *et al.* A novel molecular interaction for the adhesion of follicular CD4 T cells to follicular DC. *European Journal of Immunology* **39**, 695–703 (2009).

243. Li, M. *et al.* T-cell Immunoglobulin and ITIM Domain (TIGIT) Receptor/Poliovirus Receptor (PVR) Ligand Engagement Suppresses Interferon-γ Production of Natural Killer Cells via β-Arrestin 2-mediated Negative Signaling. *Journal of Biological Chemistry* **289**, 17647–17657 (2014).

244. Liu, S. *et al.* Recruitment of Grb2 and SHIP1 by the ITT-like motif of TIGIT suppresses granule polarization and cytotoxicity of NK cells. *Cell Death and Differentiation* **20**, 456–464 (2013).

245. Joller, N. *et al.* Cutting Edge: TIGIT Has T Cell-Intrinsic Inhibitory Functions. *The Journal of Immunology* **186**, 1338–1342 (2011).

246. Reches, A. *et al.* Nectin4 is a novel TIGIT ligand which combines checkpoint inhibition and tumor specificity. *J Immunother Cancer* **8**, 266 (2020).

247. Ge, Z., Peppelenbosch, M. P., Sprengers, D. & Kwekkeboom, J. TIGIT, the Next Step Towards Successful Combination Immune Checkpoint Therapy in Cancer. doi:10.3389/fimmu.2021.699895.

248. Li, M. *et al.* T-cell immunoglobulin and ITIM domain (TIGIT) receptor/poliovirus receptor (PVR) ligand engagement suppresses interferon-γ production of natural killer cells via β-arrestin 2-mediated negative signaling. *Journal of Biological Chemistry* **289**, 17647–17657 (2014).

249. Gao, H. *et al.* Identification of β-arrestin2 as a G protein-coupled receptor-stimulated regulator of NF-κB pathways. *Molecular Cell* **14**, 303–317 (2004).

250. Ebner, P., Versteeg, G. A. & Ikeda, F. Ubiquitin enzymes in the regulation of immune responses. *Critical Reviews in Biochemistry and Molecular Biology* vol. 52 425–460 (2017).

251. Sun, S.-C. Deubiquitylation and regulation of the immune response. *Nature Reviews Immunology* **8**, 501–511 (2008).

252. Wang, F. *et al.* TIGIT expression levels on human NK cells correlate with functional heterogeneity among healthy individuals. *Eur. J. Immunol* **45**, 2886–2897 (2015).

253. Freed-Pastor, W. A. *et al.* The CD155/TIGIT axis promotes and maintains immune evasion in neoantigen-expressing pancreatic cancer. *Cancer Cell* **39**, 1342-1360.e14 (2021).

254. Johnston, R. J. *et al.* The Immunoreceptor TIGIT Regulates Antitumor and Antiviral CD8+T Cell Effector Function. *Cancer Cell* **26**, 923–937 (2014).

255. He, W. *et al.* CD155T/TIGIT Signaling Regulates CD8 + T-cell Metabolism and Promotes Tumor Progression in Human Gastric Cancer. *Cancer Research* **77**, 6375–6388 (2017).

256. Josefsson, S. E. *et al.* T cells expressing checkpoint receptor TIGIT are enriched in follicular lymphoma tumors and characterized by reversible suppression of T-cell receptor signaling. *Clinical Cancer Research* (2018) doi:10.1158/1078-0432.CCR-17-2337.

257. Chauvin, J. M. *et al.* TIGIT and PD-1 impair tumor antigen-specific CD8+ T cells in melanoma patients. *Journal of Clinical Investigation* **125**, 2046–2058 (2015).

258. Fourcade, J. *et al.* CD226 opposes TIGIT to disrupt Tregs in melanoma. *JCI Insight* **3**, (2018).

259. Kong, Y. *et al.* T-cell immunoglobulin and ITIM domain (TIGIT) associates with CD8+T-cell exhaustion and poor clinical outcome in AML patients. *Clinical Cancer Research* **22**, 3057–3066 (2016).

260. Wang, M. *et al.* CD8 + T cells expressing both PD-1 and TIGIT but not CD226 are dysfunctional in acute myeloid leukemia (AML) patients. *Clinical Immunology* **190**, 64–73 (2018).

261. Catakovic, K. *et al.* TIGIT expressing CD4+T cells represent a tumor-supportive T cell subset in chronic lymphocytic leukemia. *OncoImmunology* **7**, e1371399 (2018).

262. Fourcade, J. *et al.* CD226 opposes TIGIT to disrupt Tregs in melanoma. *JCI Insight* **3**, (2018).

263. Kurtulus, S. *et al.* TIGIT predominantly regulates the immune response via regulatory T cells. *Journal of Clinical Investigation* **125**, 4053–4062 (2015).

264. Zhang, Q. *et al.* Blockade of the checkpoint receptor TIGIT prevents NK cell exhaustion and elicits potent anti-tumor immunity. *Nature Immunology* **19**, 723–732 (2018).

265. Sun, H. *et al.* Human CD96 Correlates to Natural Killer Cell Exhaustion and Predicts the Prognosis of Human Hepatocellular Carcinoma. *Hepatology* **70**, 168–183 (2019).

266. Gur, C. *et al.* Binding of the Fap2 Protein of Fusobacterium nucleatum to Human Inhibitory Receptor TIGIT Protects Tumors from Immune Cell Attack. *Immunity* **42**, 344–355 (2015).

267. Sarhan, D. *et al.* Adaptive NK cells with low TIGIT expression are inherently resistant to myeloid-derived suppressor cells. *Cancer Research* **76**, 5696–5706 (2016).

268. Niu, J. *et al.* First-in-human phase 1 study of the anti–TIGIT antibody vibostolimab as monotherapy or with pembrolizumab for advanced solid tumors, including non–small cell lung cancer. *Annals of Oncology* (2021) doi:10.1016/j.annonc.2021.11.002.

269. Alteber, Z. *et al.* Therapeutic targeting of checkpoint receptors within the DNAM1 axis. *Cancer Discovery* vol. 11 1040–1051 (2021).

270. Jin, H. S. *et al.* CD226hiCD8+T cells are a prerequisite for anti-TIGIT immunotherapy. *Cancer Immunology Research* **8**, 912–925 (2020).

271. Rodriguez-Abreu, D. *et al.* Primary analysis of a randomized, double-blind, phase II study of the anti-TIGIT antibody tiragolumab (tira) plus atezolizumab (atezo) versus placebo plus atezo as first-line (1L) treatment in patients with PD-L1-selected NSCLC (CITYSCAPE). *https://doi.org/10.1200/JCO.2020.38.15_suppl.9503* **38**, 9503–9503 (2020).

272. Rodriguez-Abreu, D. *et al.* Primary analysis of a randomized, double-blind, phase II study of the anti-TIGIT antibody tiragolumab (tira) plus atezolizumab (atezo) versus placebo plus atezo as first-line (1L) treatment in patients with PD-L1-selected NSCLC (CITYSCAPE). *Journal of Clinical Oncology* **38**, 9503–9503 (2020).

273. Meyer, D. *et al.* CD96 interaction with CD155 via its first Ig-like domain is modulated by alternative splicing or mutations in distal Ig-like domains. *Journal of Biological Chemistry* **284**, 2235–2244 (2009).

274. Holmes, V. M. *et al.* Interaction between nectin-1 and the human natural killer cell receptor CD96. *PLOS ONE* **14**, e0212443 (2019).

275. Kaname, T. *et al.* Mutations in CD96, a Member of the Immunoglobulin Superfamily, Cause a Form of the C (Opitz Trigonocephaly) Syndrome. *The American Journal of Human Genetics* **81**, 835–841 (2007).

276. Garg, S., Madkaikar, M. & Ghosh, K. Investigating cell surface markers on normal hematopoietic stem cells in three different niche conditions. *International Journal of Stem Cells* **6**, 129–133 (2013).

277. Zhang, W. *et al.* Expressions of CD96 and CD123 in bone marrow cells of patients with myelodysplastic syndromes. *Clinical Laboratory* (2015) doi:10.7754/Clin.Lab.2015.141240.

278. Chan, C. J. *et al.* The receptors CD96 and CD226 oppose each other in the regulation of natural killer cell functions. *Nature Immunology* **15**, 431–438 (2014).

279. Blake, S. J. *et al.* Suppression of metastases using a new lymphocyte checkpoint target for cancer immunotherapy. *Cancer Discovery* **6**, 446–459 (2016).

280. Harjunpää, H. *et al.* Deficiency of host CD96 and PD-1 or TIGIT enhances tumor immunity without significantly compromising immune homeostasis. *OncoImmunology* **7**, e1445949 (2018).

281. Roman Aguilera, A. *et al.* CD96 targeted antibodies need not block CD96-CD155 interactions to promote NK cell anti-metastatic activity. *OncoImmunology* **7**, e1424677 (2018).

282. Georgiev, H., Ravens, I., Papadogianni, G. & Bernhardt, G. Coming of age: CD96 emerges as modulator of immune responses. *Frontiers in Immunology* **9**, 1–10 (2018).

283. Cisneros, E., Moraru, M., Gómez-Lozano, N., López-Botet, M. & Vilches, C. KIR2DL5: An orphan inhibitory receptor displaying complex patterns of polymorphism and expression. *Frontiers in Immunology* **3**, 1–8 (2012).

284. Cisneros, E., Estefanía, E. & Vilches, C. Allelic polymorphism determines surface expression or intracellular retention of the human NK cell receptor KIR2DL5A (CD158f). *Frontiers in Immunology* **7**, 1–11 (2017).

285. Mulrooney, T. J. *et al.* Promoter variants of KIR2DL5 add to diversity and may impact gene expression. *Immunogenetics* **60**, 287–294 (2008).

286. Gómez-Lozano, N. *et al.* Epigenetic silencing of potentially functional KIR2DL5 alleles: Implications for the acquisition of KIR repertoires by NK cells. *European Journal of Immunology* **37**, 1954–1965 (2007).

287. Yusa, S., Catina, T. L. & Campbell, K. S. KIR2DL5 Can Inhibit Human NK Cell Activation Via Recruitment of Src Homology Region 2-Containing Protein Tyrosine Phosphatase-2 (SHP-2). *The Journal of Immunology* **172**, 7385–7392 (2004).

288. Yusa, S.-I., Catina, T. L. & Campbell, K. S. Phosphatase-2 (SHP-2) Region 2-Containing Protein Tyrosine Activation Via Recruitment of Src Homology KIR2DL5 Can Inhibit Human NK Cell. *J Immunol References* **172**, 7385–7392 (2004).

289. Jiao, Y.-L. *et al.* Polymorphisms of KIRs gene and HLA-C alleles in patients with ankylosing spondylitis: Possible association with susceptibility to the disease. *Journal of Clinical Immunology* **28**, 343–349 (2008).

290. Jiao, Y.-L. *et al*. Polymorphisms of KIR gene and HLA-C alleles: Possible association with susceptibility to HLA-B27-positive patients with ankylosing spondylitis. *Journal of Clinical Immunology* **30**, 840–844 (2010).

291. Díaz-Peña, R. *et al.* Activating KIR genes are associated with ankylosing spondylitis in Asian populations. *Human Immunology* **69**, 437–442 (2008).

292. Kimoto, Y. *et al.* Association of killer cell immunoglobulin-like receptor 2DL5 with systemic lupus erythematosus and accompanying infections. *Rheumatology* **49**, 1346–1353 (2010).

293. Anastasaki, C., Dahiya, S. & Gutmann, D. H. KIR2DL5 mutation and loss underlies sporadic dermal neurofibroma pathogenesis and growth. *Oncotarget* **8**, 47574–47585 (2017).

294. Greenlee, R. T. *et al*. The occurrence of rare cancers in U.S. adults, 1995-2004. *Public Health Reports* **125**, 28–43 (2010).

295. Gatta, G. *et al*. Burden and centralised treatment in Europe of rare tumours: results of RARECAREnet—a population-based study. *The Lancet Oncology* **18**, 1022–1039 (2017).

296. DeSantis, C. E., Kramer, J. L. & Jemal, A. The burden of rare cancers in the United States. *CA: A Cancer Journal for Clinicians* **67**, 261–272 (2017).

297. Siegel, R. L., Miller, K. D. & Jemal, A. Cancer statistics, 2019. *CA: a cancer journal for clinicians* **69**, 7–34 (2019).

298. Hattori, E., Oyama, R. & Kondo, T. Systematic Review of the Current Status of Human Sarcoma Cell Lines. *Cells* **8**, 157 (2019).

299. Muff, R. *et al*. Explant culture of sarcoma patients' tissue. **96**, (2016).

300. Parham, D. M., Barr, F. G., Montgomery, E. A. & Nascimento, A. F. *WHO classification of tumours of soft tissue and bone. Lyon, France: IARC* (2013). doi:10.1097/PAT.0000000000000050.

301. Fletcher, C. D. M. The evolving classification of soft tissue tumours - an update based on the new 2013 WHO classification. *Histopathology* **64**, 2–11 (2014).

302. Sbaraglia, M., Bellan, E. & Dei Tos, A. P. The 2020 WHO Classification of Soft Tissue Tumours: News and perspectives. *Pathologica* **113**, 70–84 (2021).

303. Yamamoto, N. *et al*. Therapeutic Targets for Bone and Soft-Tissue Sarcomas. *International Journal of Molecular Sciences* **20**, 170 (2019).

304. Casali, P. G. *et al*. Bone sarcomas: ESMO–PaedCan–EURACAN Clinical Practice Guidelines for diagnosis, treatment and follow-up. *Annals of Oncology* **29**, iv79–iv95 (2018).

305. Meyer, M. & Seetharam, M. First-Line Therapy for Metastatic Soft Tissue Sarcoma. *Current Treatment Options in Oncology* **20**, 6 (2019).

306. Gronchi, A. *et al.* Soft tissue and visceral sarcomas: ESMO–EURACAN–GENTURIS Clinical Practice Guidelines for diagnosis, treatment and follow-up☆. *Annals of Oncology* **32**, 1348–1365 (2021).

307. Druker, B. J. *et al.* Efficacy and safety of a specific inhibitor of the BCR-ABL tyrosine kinase in chronic myeloid leukemia. *New England Journal of Medicine* **344**, 1031–1037 (2001).

308. Casali, P. G. *et al.* Gastrointestinal stromal tumours: ESMO-EURACAN Clinical Practice Guidelines for diagnosis, treatment and follow-up. *Annals of Oncology* **29**, iv68–iv78 (2018).

309. Sonpavde, G., Hutson, T. E. & Sternberg, C. N. Pazopanib, a potent orally administered small-molecule multitargeted tyrosine kinase inhibitor for renal cell carcinoma. *Expert Opinion on Investigational Drugs* **17**, 253–261 (2008).

310. Li, X., Wang, G., Cai, Z. & Sun, W. Review Article Immunotherapeutic strategies for sarcoma: current perspectives. *Am J Transl Res* **12**, 7693–7701 (2020).

311. Zhu, M. M. T., Shenasa, E. & Nielsen, T. O. Sarcomas: Immune biomarker expression and checkpoint inhibitor trials. *Cancer Treatment Reviews* **91**, 102115 (2020).

312. Bonaventura, P. *et al.* Cold tumors: A therapeutic challenge for immunotherapy. *Frontiers in Immunology* **10**, (2019).

313. van Erp, A. E. M. *et al.* Expression and clinical association of programmed cell death-1, programmed death-ligand-1 and $CD8^+$ lymphocytes in primary sarcomas is subtype dependent. *Oncotarget* **8**, 71371–71384 (2017).

314. Dancsok, A. R. *et al.* Expression of lymphocyte immunoregulatory biomarkers in bone and soft-tissue sarcomas. *Modern Pathology* **32**, 1772–1785 (2019).

315. Pollack, S. M. *et al.* T-cell infiltration and clonality correlate with programmed cell death protein 1 and programmed death-ligand 1 expression in patients with soft tissue sarcomas. *Cancer* **123**, 3291–3304 (2017).

316. Birdi, H. K. *et al.* Immunotherapy for sarcomas: New frontiers and unveiled opportunities. *Journal for ImmunoTherapy of Cancer* **9**, 1–11 (2021).

317. Painter, C. A. *et al.* The Angiosarcoma Project: enabling genomic and clinical discoveries in a rare cancer through patient-partnered research. *Nature Medicine* **26**, 181–187 (2020).

318. Samstein, R. M. *et al.* Tumor mutational load predicts survival after immunotherapy across multiple cancer types. *Nature Genetics* vol. 51 202–206 (2019).

319. Tawbi, H. A. *et al.* Pembrolizumab in advanced soft-tissue sarcoma and bone sarcoma (SARC028): a multicentre, two-cohort, single-arm, open-label, phase 2 trial. *The Lancet. Oncology* **18**, 1493–1501 (2017).

320. Wagner, M. J. *et al.* Multicenter phase II trial (SWOG S1609, cohort 51) of ipilimumab and nivolumab in metastatic or unresectable angiosarcoma: a substudy of dual anti-CTLA-4 and anti-PD-1 blockade in rare tumors (DART). *Journal for immunotherapy of cancer* **9**, e002990 (2021).

321. Florou, V. *et al.* Angiosarcoma patients treated with immune checkpoint inhibitors: a case series of seven patients from a single institution. *Journal for immunotherapy of cancer* **7**, 213 (2019).

322. Wilky, B. A. *et al.* Axitinib plus pembrolizumab in patients with advanced sarcomas including alveolar soft-part sarcoma: a single-centre, single-arm, phase 2 trial. *The lancet oncology* **20**, 837–848 (2019).

323. Naqash, A. R. *et al.* Phase II study of atezolizumab in advanced alveolar soft part sarcoma (ASPS). *Journal of Clinical Oncology* **39**, 11519 (2021).

324. Tabata, M. M., Novoa, R. A., Bui, N. Q. & Zaba, L. C. Successful treatment of HIV-negative Kaposi sarcoma with ipilimumab and nivolumab and concurrent management of baseline psoriasis and bullous pemphigoid. *JAAD case reports* **6**, 447–449 (2020).

325. Migliorini, D. *et al.* First report of clinical responses to immunotherapy in 3 relapsing cases of chordoma after failure of standard therapies. *Oncoimmunology* **6**, e1338235–e1338235 (2017).

326. Davis, L. E., Nicholls, L. A., Babiker, H. M., Liau, J. & Mahadevan, D. PD-1 Inhibition Achieves a Complete Metabolic Response in a Patient with Malignant Peripheral Nerve Sheath Tumor. *Cancer Immunology Research* **7**, 1396 LP – 1400 (2019).

327. Hattori, E., Oyama, R. & Kondo, T. Systematic Review of the Current Status of Human Sarcoma Cell Lines. *Cells* **8**, 157 (2019).

328. Jacques, C. *et al.* Small animal models for the study of bone sarcoma pathogenesis:characteristics, therapeutic interests and limitations. *Journal of Bone Oncology* **12**, 7–13 (2018).

329. Castillo-Tandazo, W., Mutsaers, A. J. & Walkley, C. R. Osteosarcoma in the Post Genome Era: Preclinical Models and Approaches to Identify Tractable Therapeutic Targets. *Current Osteoporosis Reports* **17**, 343–352 (2019).

330. Jacks, T. *et al.* Tumor spectrum analysis in p53-mutant mice. *Current Biology* **4**, 1–7 (1994).

331. Walkley, C. R. *et al.* Conditional mouse osteosarcoma, dependent on p53 loss and potentiated by loss of Rb, mimics the human disease. *Genes and Development* (2008) doi:10.1101/gad.1656808.

332. Keller, C., Hansen, M. S., Coffin, C. M. & Capecchi, M. R. Pax3:Fkhr interferes with embryonic Pax3 and Pax7 function: Implications for alveolar rhabdomyosarcoma cell of origin. *Genes and Development* (2004) doi:10.1101/gad.1243904.

333. Kirsch, D. G. *et al.* A spatially and temporally restricted mouse model of soft tissue sarcoma. *Nature Medicine* (2007) doi:10.1038/nm1602.

334. Haldar, M., Hedberg, M. L., Hockin, M. F. & Capecchi, M. R. A CreER-based random induction strategy for modeling translocation- associated sarcomas in mice. *Cancer Research* (2009) doi:10.1158/0008-5472.CAN-08-4127.

335. Charytonowicz, E. *et al.* PPARγ agonists enhance ET-743 - Induced adipogenic differentiation in a transgenic mouse model of myxoid round cell liposarcoma. *Journal of Clinical Investigation* (2012) doi:10.1172/JCI60015.

336. Jacques, C. *et al.* Small animal models for the study of bone sarcoma pathogenesis:characteristics, therapeutic interests and limitations. *Journal of Bone Oncology* **12**, 7–13 (2018).

337. Crnalic, S., Håkansson, I., Boquist, L., Löfvenberg, R. & Broström, L. Å. A novel spontaneous metastasis model of human osteosarcoma developed using orthotopic transplantation of intact tumor tissue into tibia of nude mice. *Clinical and Experimental Metastasis* (1997) doi:10.1023/A:1018456911823.

338. Lu, W., Chao, T., Ruiqi, C., Juan, S. & Zhihong, L. Patient-derived xenograft models in musculoskeletal malignancies. *Journal of Translational Medicine* **16**, 1–16 (2018).

339. Igarashi, K. *et al.* Patient-derived orthotopic xenograft models of sarcoma. *Cancer Letters* **469**, 332–339 (2020).

340. Tsimberidou, A. M., Fountzilas, E., Nikanjam, M. & Kurzrock, R. Review of precision cancer medicine: Evolution of the treatment paradigm. *Cancer Treatment Reviews* **86**, 102019 (2020).

341. Carbone, M. *et al.* Tumour predisposition and cancer syndromes as models to study gene–environment interactions. *Nature Reviews Cancer* **20**, 533–549 (2020).

342. Murthy, V. H., Krumholz, H. M. & Gross, C. P. Participation in Cancer Clinical Trials. *JAMA* **291**, 2720 (2004).

343. Pisco, A. O. *et al.* Non-Darwinian dynamics in therapy-induced cancer drug resistance. *Nature Communications* **4**, 2467 (2013).

344. Gerlinger, M. & Swanton, C. How Darwinian models inform therapeutic failure initiated by clonal heterogeneity in cancer medicine. *British Journal of Cancer* **103**, 1139–1143 (2010).

345. National Research Council (US) Committee. *Toward precision medicine: Building a knowledge network for biomedical research and a new taxonomy of disease*. *Toward Precision Medicine: Building a Knowledge Network for Biomedical Research and a New Taxonomy of Disease* (2012). doi:10.17226/13284.

346. Planchard, D. *et al.* Metastatic non-small cell lung cancer: ESMO Clinical Practice Guidelines for diagnosis, treatment and follow-up. *Annals of Oncology* **30**, 863–870 (2019).

347. Butterfield, L. H. The Society for Immunotherapy of Cancer Biomarkers Task Force recommendations review. *Seminars in Cancer Biology* **52**, 12–15 (2018).

348. Ameratunga, M., Xu, W. & Lopez, J. Personalized Cancer Immunotherapy: Today's Challenge and Tomorrow's Promise. *Journal of Immunotherapy and Precision Oncology* **1**, 56–67 (2018).

349. Ashley, E. A. Towards precision medicine. *Nature Reviews Genetics* **17**, 507–522 (2016).

350. Schoenfeld, A. J. & Hellmann, M. D. Acquired Resistance to Immune Checkpoint Inhibitors. *Cancer Cell* **37**, 443–455 (2020).

351. Herbst Prof, R. S. *et al.* Pembrolizumab versus docetaxel for previously treated, PD-L1-positive, advanced non-small-cell lung cancer (KEYNOTE-010): a randomised controlled trial. *The Lancet (British edition)* **387**, 1540–1550 (2015).

352. Reck, M. *et al.* Pembrolizumab versus Chemotherapy for PD-L1–Positive Non–Small-Cell Lung Cancer. *The New England journal of medicine* **375**, 1823–1833 (2016).

353. Ferris, R. L. *et al.* Nivolumab vs investigator's choice in recurrent or metastatic squamous cell carcinoma of the head and neck: 2-year long-term survival update of CheckMate 141 with analyses by tumor PD-L1 expression. *Oral oncology* **81**, 45–51 (2018).

354. Davis, A. A. & Patel, V. G. The role of PD-L1 expression as a predictive biomarker: an analysis of all US Food and Drug Administration (FDA) approvals of immune checkpoint inhibitors. *Journal for immunotherapy of cancer* **7**, 278 (2019).

355. Robert, C. *et al.* Nivolumab in Previously Untreated Melanoma without BRAF Mutation. *New England Journal of Medicine* **372**, 320–330 (2014).

356. Alexandrov, L. B. *et al.* Signatures of mutational processes in human cancer. *Nature* **500**, 415–421 (2013).

357. McGranahan, N. *et al.* Clonal neoantigens elicit T cell immunoreactivity and sensitivity to immune checkpoint blockade. *Science* **351**, 1463–1469 (2016).

358. Marabelle, A. *et al.* Association of tumour mutational burden with outcomes in patients with advanced solid tumours treated with pembrolizumab: prospective biomarker analysis of the multicohort, open-label, phase 2 KEYNOTE-158 study. *The Lancet Oncology* **21**, 1353–1365 (2020).

359. Administration, U. S. F. and D. FDA approves pembrolizumab for adults and children with TMB-H solid tumors. *US Food and Drug Administration: Silver Spring, MD, USA* (2020).

360. Subbiah, V., Solit, D. B., Chan, T. A. & Kurzrock, R. The FDA approval of pembrolizumab for adult and pediatric patients with tumor mutational burden (TMB)≥ 10: a decision centered on empowering patients and their physicians. *Annals of oncology: official journal of the European Society for Medical Oncology* **31**, 1115–1118 (2020).

361. Prasad, V. & Addeo, A. The FDA approval of pembrolizumab for patients with TMB> 10 mut/Mb: was it a wise decision? No. *Annals of Oncology* **31**, 1112–1114 (2020).

362. McGrail, D. J. *et al.* High tumor mutation burden fails to predict immune checkpoint blockade response across all cancer types. *Annals of oncology* **32**, 661–672 (2021).

363. Overman, M. J. *et al.* Durable Clinical Benefit With Nivolumab Plus Ipilimumab in DNA Mismatch Repair–Deficient/Microsatellite Instability–High Metastatic Colorectal Cancer. *Journal of Clinical Oncology* **36**, 773–779 (2018).

364. Marabelle, A. *et al.* Efficacy of Pembrolizumab in Patients With Noncolorectal High Microsatellite Instability/Mismatch Repair–Deficient Cancer: Results From the Phase II KEYNOTE-158 Study. *Journal of Clinical Oncology* **38**, 1–10 (2019).

365. Schalper, K. A. *et al.* Objective measurement and clinical significance of TILs in non–small cell lung cancer. *Journal of the National Cancer Institute* **107**, dju435 (2015).

366. Bertrand, R. *et al.* Gut microbiome influences efficacy of PD-1–based immunotherapy against epithelial tumors. *Science* **359**, 91–97 (2018).

367. Gopalakrishnan, V. *et al.* Gut microbiome modulates response to anti-PD-1 immunotherapy in melanoma patients. *Science (New York, N.Y.)* **359**, 97–103 (2018).

368. Diana, M. *et al.* Genomic correlates of response to immune checkpoint therapies in clear cell renal cell carcinoma. *Science* **359**, 801–806 (2018).

369. Lee, J. N., Jiang, X., Ryan, D. & Whitesides, G. M. Compatibility of mammalian cells on surfaces of poly(dimethylsiloxane). *Langmuir* **20**, 11684–11691 (2004).

370. Su, X. *et al.* Microfluidic cell culture and its application in high-throughput drug screening: cardiotoxicity assay for hERG channels. *Journal of biomolecular screening* **16**, 101–111 (2011).

371. Wei, C.-W., Cheng, J.-Y. & Young, T.-H. Elucidating in vitro cell-cell interaction using a microfluidic coculture system. *Biomedical Microdevices* **8**, 65–71 (2006).

372. Chang, C.-W. *et al.* A polydimethylsiloxane–polycarbonate hybrid microfluidic device capable of generating perpendicular chemical and oxygen gradients for cell culture studies. *Lab on a Chip* **14**, 3762–3772 (2014).

373. Perez-Moreno, M., Jamora, C. & Fuchs, E. Sticky business: Orchestrating cellular signals at adherens junctions. *Cell* **112**, 535–548 (2003).

374. Kusindarta, D. L. The Role of Extracellular Matrix in Tissue Regeneration. in (ed. Kaoud, H. W. E.-H. A. hay E.-S.) Ch. 5 (IntechOpen, 2018). doi:10.5772/intechopen.75728.

375. Altman, G. H. *et al.* Cell differentiation by mechanical stress. *The FASEB journal : official publication of the Federation of American Societies for Experimental Biology* **16**, 270–272 (2002).

376. Poltavets, V., Kochetkova, M., Pitson, S. M. & Samuel, M. S. The role of the extracellular matrix and its molecular and cellular regulators in cancer cell plasticity. *Frontiers in Oncology* **8**, 1–19 (2018).

377. Koohestani, F. *et al.* Extracellular matrix collagen alters cell proliferation and cell cycle progression of human uterine leiomyoma smooth muscle cells. *PloS one* **8**, e75844–e75844 (2013).

378. López-Martínez, C., Huidobro, C., Albaiceta, G. M. & López-Alonso, I. Mechanical stretch modulates cell migration in the lungs. *Annals of translational medicine* **6**, 28 (2018).

379. Mason, E. F. & Rathmell, J. C. Cell metabolism: An essential link between cell growth and apoptosis. *Biochimica et Biophysica Acta (BBA) - Molecular Cell Research* **1813**, 645–654 (2011).

380. Clanton, T. L., Hogan, M. C. & Gladden, L. B. Regulation of Cellular Gas Exchange, Oxygen Sensing, and Metabolic Control. *Comprehensive Physiology* 1135–1190 (2013) doi:https://doi.org/10.1002/cphy.c120030.

381. Lin, X. *et al.* Oxygen-induced cell migration and on-line monitoring biomarkers modulation of cervical cancers on a microfluidic system. *Scientific Reports* **5**, 9643 (2015).

382. Petrie Aronin, C. E. *et al.* Migrating Myeloid Cells Sense Temporal Dynamics of Chemoattractant Concentrations. *Immunity* **47**, 862-874.e3 (2017).

383. Stojanovic, A., Correia, M. P. & Cerwenka, A. Shaping of NK cell responses by the tumor microenvironment. *Cancer microenvironment : official journal of the International Cancer Microenvironment Society* **6**, 135–46 (2013).

384. Costa, E. C. *et al.* 3D tumor spheroids: an overview on the tools and techniques used for their analysis. *Biotechnology Advances* **34**, 1427–1441 (2016).

385. Fennema, E., Rivron, N., Rouwkema, J., van Blitterswijk, C. & de Boer, J. Spheroid culture as a tool for creating 3D complex tissues. *Trends in Biotechnology* **31**, 108–115 (2013).

386. Zimmermann, M., Box, C. & Eccles, S. A. Two-Dimensional vs. Three-Dimensional In Vitro Tumor Migration and Invasion Assays. in *BMC Systems Biology* vol. 10 227–252 (Humana Press, Totowa, NJ, 2013).

387. Breslin, S. & O'Driscoll, L. Three-dimensional cell culture: the missing link in drug discovery. *Drug Discovery Today* **18**, 240–249 (2013).

388. Bergenheim, F. *et al.* A fully defined 3D matrix for ex vivo expansion of human colonic organoids from biopsy tissue. *Biomaterials* **262**, 120248 (2020).

389. Angres, B. M. & Wurst, H. 3-D Life biomimetic hydrogels. *Technology Platforms for 3D Cell Culture* 197–221 (2017) doi:https://doi.org/10.1002/9781118851647.ch9.

390. Kleinman, H. K. *et al.* Basement membrane complexes with biological activity. *Biochemistry* **25**, 312–318 (1986).

391. Kleinman, H. K. & Martin, G. R. Matrigel: basement membrane matrix with biological activity. in *Seminars in cancer biology* vol. 15 378–386 (Elsevier, 2005).

392. Caicedo-Carvajal, C. E., Liu, Q., Remache, Y., Goy, A. & Suh, K. S. Cancer Tissue Engineering: A Novel 3D Polystyrene Scaffold for In Vitro Isolation and Amplification of Lymphoma Cancer Cells from Heterogeneous Cell Mixtures. *Journal of tissue engineering* **2011**, 362326 (2011).

393. Zhao, X., Zhang, S. & Spirio, L. PuraMatrix. in *Scaffolding In Tissue Engineering* 217–238 (CRC Press, 2005). doi:10.1201/9781420027563.ch15.

394. Aisenbrey, E. A. & Murphy, W. L. Synthetic alternatives to Matrigel. *Nature Reviews Materials* **5**, 539–551 (2020).

395. Tibbitt, M. W. & Anseth, K. S. Hydrogels as extracellular matrix mimics for 3D cell culture. *Biotechnology and Bioengineering* (2009) doi:10.1002/bit.22361.

396. Langhans, S. A. Three-dimensional in vitro cell culture models in drug discovery and drug repositioning. *Frontiers in Pharmacology* **9**, 1–14 (2018).

397. Carletti, E., Motta, A. & Migliaresi, C. Scaffolds for Tissue Engineering and 3D Cell Culture BT - 3D Cell Culture: Methods and Protocols. in (ed. Haycock, J. W.) 17–39 (Humana Press, 2011). doi:10.1007/978-1-60761-984-0_2.

398. Friedrich, J., Seidel, C., Ebner, R. & Kunz-Schughart, L. A. Spheroid-based drug screen: considerations and practical approach. *Nature Protocols* **4**, 309–324 (2009).

399. Olofsson, K. *et al.* Acoustic formation of multicellular tumor spheroids enabling on-chip functional and structural imaging. *Lab on a Chip* **18**, 2466–2476 (2018).

400. Christakou, A. E., Ohlin, M., Önfelt, B. & Wiklund, M. Ultrasonic three-dimensional on-chip cell culture for dynamic studies of tumor immune surveillance by natural killer cells. *Lab on a Chip* **15**, 3222–3231 (2015).

401. Handschel, J. G. K. *et al.* Prospects of micromass culture technology in tissue engineering. *Head & face medicine* **3**, 4 (2007).

402. Fennema, E., Rivron, N., Rouwkema, J., van Blitterswijk, C. & de Boer, J. Spheroid culture as a tool for creating 3D complex tissues. *Trends in Biotechnology* **31**, 108–115 (2013).

403. Souza, G. R. *et al.* Three-dimensional tissue culture based on magnetic cell levitation. *Nature Nanotechnology* **5**, 291–296 (2010).

404. de Souza, N. Organoids. *Nature Methods* **15**, 23 (2018).

405. Lichtman, J. W. & Conchello, J. A. Fluorescence microscopy. *Nature Methods* **2**, 910–919 (2005).

406. Aswani, K., Jinadasa, T. & Brown, C. M. Fluorescence Microscopy Light Sources. *Microscopy Today* **20**, 22–28 (2012).

407. Wessels, J. T., Pliquett, U. & Wouters, F. S. Light-emitting diodes in modern microscopy-from David to Goliath? *Cytometry Part A* **81 A**, 188–197 (2012).

408. Shapiro, H. M. & Telford, W. G. Lasers for Flow Cytometry: Current and Future Trends. *Current Protocols in Cytometry* **83**, 1.9.1-1.9.21 (2018).

409. Schmit, T., Klomp, M. & Khan, M. N. An Overview of Flow Cytometry: Its Principles and Applications in Allergic Disease Research. *Methods in Molecular Biology* **2223**, 169–182 (2021).

410. Velden, V. H. J. van der & Scid, T.-. Modern Flow cytometry. *Erasmus* 1–6 (2015).

411. Hooke, R. *Micrographia, or, some physiological descriptions of minute bodies made by magnifying glasses :with observations and inquiries thereupon*. (Printed by Jo. Martyn and Ja. Allestry, printers to the Royal Society, 1665).

412. Goodwin, P. C. A primer on the fundamental principles of light microscopy: Optimizing magnification, resolution, and contrast. *Molecular Reproduction and Development* **82**, 502–507 (2015).

413. Weber, M., Mickoleit, M. & Huisken, J. *Light sheet microscopy*. *Methods in Cell Biology* vol. 123 (Elsevier Inc., 2014).

414. Reynaud, E. G., Kržič, U., Greger, K. & Stelzer, E. H. K. Light sheet-based fluorescence microscopy: More dimensions, more photons, and less photodamage. *HFSP Journal* **2**, 266–275 (2008).

415. Lorenzo, C. *et al.* Live cell division dynamics monitoring in 3D large spheroid tumor models using light sheet microscopy. *Cell Division* **6**, 22 (2011).

416. Jan, H., Jim, S., Filippo, D. B., Joachim, W. & K., S. E. H. Optical Sectioning Deep Inside Live Embryos by Selective Plane Illumination Microscopy. *Science* **305**, 1007–1009 (2004).

417. J., K. P., D., S. A., Joachim, W. & H.K., S. E. Reconstruction of Zebrafish Early Embryonic Development by Scanned Light Sheet Microscopy. *Science* **322**, 1065–1069 (2008).

418. Wu, Y. *et al.* Inverted selective plane illumination microscopy (iSPIM) enables coupled cell identity lineaging and neurodevelopmental imaging in Caenorhabditis elegans. *Proceedings of the National Academy of Sciences* **108**, 17708–17713 (2011).

419. Cossarizza, A. *et al.* Guidelines for the use of flow cytometry and cell sorting in immunological studies. *European Journal of Immunology* **47**, 1584–1797 (2017).

420. Richardson, D. S. & Lichtman, J. W. Clarifying Tissue Clearing. *Cell* **162**, 246–257 (2015).

421. Pawley, JB and Masters, B. R. Handbook of biological confocal microscopy. *Optical Engineering* vol. 35 11–17 (1996).

422. Chen, F., Tillberg, P. W. & Boyden, E. S. Expansion microscopy. *Science* **347**, 543–548 (2015).

423. Chang, J.-B. *et al.* Iterative expansion microscopy. *Nature methods* **14**, 593–599 (2017).

424. Gallagher, B. R. & Zhao, Y. Expansion microscopy: A powerful nanoscale imaging tool for neuroscientists. *Neurobiology of Disease* **154**, 105362 (2021).

425. Asano, S. M. *et al.* Expansion Microscopy: Protocols for Imaging Proteins and RNA in Cells and Tissues. *Current Protocols in Cell Biology* **80**, 1–41 (2018).

426. Pander, J. *et al*. Activation of tumor-promoting type 2 macrophages by EGFR-targeting antibody cetuximab. *Clinical Cancer Research* **17**, 5668–5673 (2011).

427. Baysal, H. *et al*. The Right Partner in Crime: Unlocking the Potential of the Anti-EGFR Antibody Cetuximab via Combination With Natural Killer Cell Chartering Immunotherapeutic Strategies. *Frontiers in Immunology* **12**, 1–24 (2021).

428. Amato, R. J., Hernandez-Mcclain, J., Saxena, S. & Khan, M. Lenalidomide therapy for metastatic renal cell carcinoma. *American Journal of Clinical Oncology: Cancer Clinical Trials* **31**, 244–249 (2008).